MEASUREMENT AND MODELING OF FURNITURE EFFECT IN AN INDOOR PROPAGATION CHANNEL

MYO MYINT MAW

A THESIS SUBMITTED IN FULFILLMENT
OF THE REQUIREMENT FOR THE DEGREE OF
DOCTOR OF ENGINEERING IN ELECTRICAL ENGINEERING
FACULTY OF ENGINEERING
KING MONGKUT'S INSTITUTE OF TECHNOLOGY LADKRABANG
2015

KMITL-2015-EN-D-018-061

MEASUREMENT AND MODELING OF FURNITURE EFFECT IN AN INDOOR PROPAGATION CHANNEL

MYO MYINT MAW

A THESIS SUBMITTED IN FULLFILLMENT
OF THE REQUIREMENT FOR THE DEGREE OF
DOCTOR OF ENGINEERING IN ELECTRICAL ENGINEERING
FACULTY OF ENGINEERING
KING MONGKUT'S INSTITUTE OF TECHNOLOGY LADKRABANG
2015

KMITL-2015-EN-D-018-061

หัวข้อวิทยานิพนธ์	การทำแบบจำลองและการวัดผลกระทบของเฟอร์นิเจอร์ของช่องสัญญาณการแพร่กระจายคลื่นภายในอาคาร
นักศึกษา	นางสาวเมียว มิ มอ
รหัสนักศึกษา	53601051
ปริญญา	วิศวกรรมศาสตรดุษฎีบัณฑิต
สาขาวิชา	วิศวกรรมไฟฟ้า
พ.ศ.	2558
อาจารย์ที่ปรึกษาวิทยานิพนธ์	ดร.สถาพร พรหมวงศ์

บทคัดย่อ

วิทยานิพนธ์ฉบับนี้ได้กล่าวถึงผลกระทบจากการกระจัดกระจายคลื่นของช่องสัญญาณการแพร่กระจายภายในอาคาร ในระบบการสื่อสารภายในอาคารมีผลกระทบมาจากหลายสภาวะแวดล้อมโดยรวม เช่น ผนังกำแพง มนุษย์ และเฟอร์นิเจอร์ ล้วนแล้วแต่ส่งผลการสะท้อนหรือการกระจัดกระจายของคลื่น ดังนั้น ภาคตัดของเรดาร์จึงเป็นส่วนที่สำคัญในการวิเคราะห์ของการกระจัดกระจายคลื่นภายในอาคารได้ศึกษาไว้ในวิทยานิพนธ์

ในวิทยานิพนธ์นี้ได้ทำการประยุกต์สมการของฟังก์ชันการถ่ายโอนช่องสัญญาณสำหรับเรดาร์แบบแถบกว้าง และได้แนะนำวิธีการสังเกตทางเวลามาใช้ในการแก้ปัญหาผลการกระจัดกระจายคลื่นหลายวิถีอันเนื่องมาจากสภาวะแวดล้อมภายในอาคารโดยวิธีการเกตทางเวลานี้เป็นการแปลงสัญญาณในโดเมนความถี่มาเป็นโดเมนเวลาและกรองช่วงเวลาพัลส์ด้วยหลักการกำหนดหน้าต่างของไกเซอร์ สำหรับการศึกษาทดลองวิจัยได้ทำการวัดคุณลักษณะของสัญญาณในช่วงความถี่ 3 กิกะเฮิรตซ์ถึง 7 กิกะเฮิรตซ์ โดยกำหนดวัตถุเป้าหมายคือ เก้าอี้ และโต๊ะสำนักงาน จากนั้นได้ทำการวัดคุณลักษณะฟังก์ชันการถ่ายโอนของช่องสัญญาณโดยใช้เครื่องวิเคราะห์โครงข่ายแบบเวกเตอร์ และใช้สายอากาศปากแตรในการประเมินผลการวัดทั้งระนาบแนวตั้งและระนาบแนวนอนหรือโพลาไรซ์ในแนวเดียวกัน

นอกจากนี้ยังได้นำเสนอแบบจำลองการกระจายแบบล็อกปกติเพื่ออธิบายคุณสมบัติการเปลี่ยนแปลงทางสถิติของภาคตัดขวางเรดาร์ ซึ่งมีการเปลี่ยนแปลงไปตามความถี่ การโพลาไรซ์ และมุมที่ได้ทำการศึกษาเส้นทางหลายวิถีที่สำคัญสามารถเกิดขึ้นได้จากการสะท้อนพื้นและรูปร่างของเป้าที่มีโครงสร้างซับซ้อน ในการพิจารณาให้ข้อมูลภาคตัดขวางของเรดาร์เป็นไปตามแบบจำลองการกระจายล็อกปกติ ได้ใช้กระบวนการทดสอบแบบโคมอนโกรอฟไซฟนอฟในการวิเคราะห์ข้อมูล ผลที่ได้นี้มีประโยชน์อย่างมากในการศึกษาวิทยุอิมพัลส์แถบกว้างยิ่งสำหรับระบบสื่อสารไร้สายภายในอาคาร

Thesis Title	Measurement and Modeling of Furniture Effect in an Indoor Propagation Channel
Student	Miss Myo Myint Maw
Student ID.	53601051
Degree	Doctoral of Engineering
Program	Electrical Engineering
Year	2015
Thesis Advisor	Dr. Sathaporn Promwong

ABSTRACT

This thesis describes the scattering effect in an indoor propagation channel. In indoor communication system, there are many effects from surrounding environments and types of obstacles such as walls, human body, furniture, complex targets or scatterers which are main scatterers which dominate the propagation characteristics. Thus, radar cross section (RCS) is one part of analysis of the scattering has been studied in this thesis.

In this thesis, the extension of the ultra wide band (UWB) radar equation which incorporates the channel transfer function is presented. Time gating method is also applied to remove multipath effect, a phenomenon which typically occurs in the indoor environment. The time gating method transforms the frequency domain response to time domain response and filter out the late time pulses, which are caused by the multipath effects by imposing gating window. The Kaiser-Bessel window is used in time domain to extract scattering from the target. In an experiment setup, the frequency range of 3 GHz to 7 GHz in frequency domain is used for indoor UWB radar application. Two furniture items such as an office chair and a steel desk are used as a sample target. Two double-ridged waveguide horn antennas for both vertical and horizontal polarizations were used to obtain the transfer function of scattering of the furniture prior to analysis in order to derive the bistatic RCS. The channel transfer function of scattering in UWB radar between transmitter and receiver antennas was measured using a vector network analyzer (VNA).

In addition, lognormal distribution model is proposed as the description of the characterization of the fluctuation statistics of RCS difference, whose sensitivity on frequency, polarization and angles are also studied. A significant multipath can occur

due to ground reflections and the irregularity of the complex target shape. In order to determine an acceptable fit between the RCS data and lognormal distribution model, Kolmogorov-Smirnov (K-S) non-parametric goodness of fit test procedures are applied to the data. These are very useful experimental result to study in UWB impulse radio for short range wireless indoor communication system.

ACKNOWLEDGEMENTS

Foremost, I would like to express my heartfelt gratitude to my advisor, Dr. Sathaporn Promwong; he has been a tremendous mentor for me. I would like to thank you for the continuous support of my Doctoral Degree study and research for his patience, motivation and immense knowledge. His guidance helped me in all the time of research and writing of this thesis. I would like to express my sincere gratitude to my co-researcher, Prof. Dr. Jun-ichi Takada, for his continuous guidance, support and wisdom throughout my study. Without his patient, valuable suggestions and comments, and invaluable time spent with me in this thesis, this thesis would not have been successfully completed.

Besides my advisor, for doing this thesis successfully, I would also like to express my appreciation to my instructor, Asst. Prof .Dr. Pichaya Supankoon for all his guidance and helps through all the years of my Doctoral Degree. He was one of the most responsible and caring persons to me during my Doctoral Degree study, as if it was not his responsible sense I don't know how my Doctoral Degree would turn. I greatly appreciate the contributions of my Doctoral Degree supervisory committee members, Assoc. Prof. Dr. Rangsan Wongsan, Assoc. Prof. Dr. Chuwong Phongcharoenpanich and Asst. Prof. Dr. Somkiat Lerkwaranyu.

I gratefully acknowledge the Japan International Cooperation Agency (JICA) under the AUN/SEED-Net (ASEAN University Network, Southeast Asia Engineering Education Development Network) project for the financial support and the selection committee in AUN/SEED-Net project in Myanmar for choosing me as one of the recipients of this scholarship. I would like to express my special thanks to Tokyo Institute of Technology (TIT) in Japan for accepting me as an affiliate visiting short-term study and my lab mates for their kindness and support at Takada lab during my short term study. Furthermore, I would like to thank of Faculty of Engineering, King Mongkut's Institute of Technology Ladkrabang, for financial support during my extension study in Thailand. Sincere appreciation is also extended to the Wireless Communication Laboratory at King Mongkut's Institute of Technology Ladkrabang for the support with regard to the anechoic chamber.

I am especially indebted to our Ministry of Science and Technology (MOST), Department of Information Technology (Yangon Technological University, YTU)

and Department of Information Technology (Mandalay Technological University, MTU), Myanmar, for the permission and consideration on my Doctoral Degree study in Thailand. I would like to thank Principal of Technological University (Toungoo) and Department of Information Technology (Toungoo) for supports and helps.

I am grateful to my fellow lab mates in Ultra Wideband Radio Systems (UWBRS) Laboratory at King Mongkut's Institute of Technology Ladkrabang for all their helps and more importantly the valuable and memorable times that we spent with each other. There have been numerous associates who have helped me over these few years, especially, Mr. Sanit Teawchim, Mr. Narongsak Manositthichai, Mr. Sarun Duanhsuwan, Mr. Jirapat Sangthong, Mr. Jiraphan Sahakit, Mr. W-boat Mooyai, Sirapop K. mingmanee and Ms. Wipassorn Vinicchayakul, Ammy Thongkam, Tity Phouthong, June C. Mahavana. I am also grateful to the international students who are also studying in KMITL for making my life in Thailand enjoyable and colorful.

Last but not the least, I would like to express my gratefulness and appreciation to my family: my parents, for giving birth to me in the first place and supporting me spiritually throughout my life and my two elder brothers who always give me love and encouragement.

Myo Myint Maw

TABLE OF CONTENTS

Page

Thai Abstract I

English Abstract II

Acknowledgement IV

Table of Contents VI

List of Tables X

List of Figures XI

List of Abbreviations XIII

Chapter 1 Introduction 1

1.1 Background 1

1.2 Literature Review 3

1.3 Objectives and Scope of This Thesis 4

1.4 Organization of the Thesis 5

Chapter 2 Principle of UWB Communication System and Application 7

2.1 Introduction of Ultra Wide Band 7

2.2 Ultra Wide Band Radar Technology 8

2.3 Regulator Bodies and Standards 10

2.3.1 UWB Regulation in the USA 10

2.3.2 Common Band Regulation 11

2.3.3 IEEE Working Groups 12

2.3.3.1 IEEE 802.15.3a Standard 13

2.3.3.2 IEEE 802.15.4a Standard 13

2.4 UWB Channel Model 13

2.4.1 Channel Measurement 13

2.4.1.1 Frequency Domain Channel Sounding 14

2.4.1.2 Time Domain Channel Sounding 15

2.4.2 UWB Transmitted Pulse Waveforms 15

2.4.2.1 Gaussian Pulse 16

2.4.2.2 Monocycle Pulse 17

2.5 Advantages and Disadvantages of UWB 19

TABLE OF CONTENTS (CONTINUE)

Page

2.6 Conclusion 19

Chapter 3 Modeling of Furniture Effect in an Indoor Propagation Channel..... 21

3.1 Introduction 21

3.2 Definition of RCS 21

3.2.1 Monostatic and Bistatic RCS 24

3.3 Scattering Region..... 26

3.3.1 Low Frequency Scattering Region or Rayleigh Region 26

3.3.2 Resonant Scattering Region..... 27

3.3.3 High Frequency Optics Scattering Region 27

3.3.3.1 Specular Reflection..... 27

3.3.3.2 Single Diffraction 27

3.3.3.3 Multiple Diffraction..... 28

3.4 Polarization 28

3.5 Near Field and Far Field 29

3.6 Radar Cross Section Prediction Methods..... 29

3.6.1 Method of Moments..... 30

3.6.2 Finite Difference Time Domain. 30

3.6.3 Ray Tracing..... 31

3.6.4 Physical Optics..... 32

3.6.5 Scattering Center Approach..... 32

3.7 Types of Measurement for RCS 33

3.7.1 Measurement of the Complex RCS..... 33

3.8 Factors of Measurement Inaccuracy 34

3.8.1 Reflection from Walls and Mounting Apparatus 34

3.8.2 Antenna Coupling 35

3.8.3 Object Alignment Error 35

3.8.4 Near field Effects 36

3.9 Types of RCS Measurement Ranges 36

3.10 Data Processing 37

TABLE OF CONTENTS (CONTINUE)

Page

3.10.1 Time Gating Method 39

3.11 Extension and Proposed of UWB Radar Equation 41

3.12 Conclusion 44

Chapter 4 Measurement Setup for Scattering from Furniture 46

4.1 Introduction 46

4.2 Description of Channel Measurement 46

4.2.1 HP-8510C VNA 46

4.2.2 Horn Antenna 48

4.2.3 Anechoic Chamber 49

4.2.4 Scattering Target 50

4.2.5 Modeling of Measurement Setup 51

4.3 Conclusion 53

Chapter 5 Experimental Results 54

5.1 Introduction 54

5.2 Measurement Results and Discussion 54

5.2.1 Channel Impulse Response 56

5.2.2 Magnitude of RCS 60

5.2.3 Magnitude and Phase of RCS with Time Gating 65

5.3 Statistical Analysis for RCS 70

5.3.1 Lognormal Distribution Model 70

5.4 RCS Characterization 71

5.5 Conclusion 79

Chapter 6 Conclusion and Future Works 80

6.1 Summary of Proceeding Chapters 80

6.2 Recommendation for Improvements 86

6.2.1 Measurement Errors 86

6.2.2 Equipments and Facilities 87

TABLE OF CONTENTS (CONTINUE)

Page

6.2.3 Near Field Measurement 87

6.3 Future Works 87

References 89

Appendix 94

Author Biography 108

LIST OF TABLES

Table	Page
2.1 Radiation limits specified by FCC for indoor and outdoor communication applications	10
2.2 Radiation limits of common frequency band for indoor application	12
4.1 The specifications of horn antenna	49

LIST OF FIGURES

Fig. Page

2.1 Generic system block diagram of UWB radar 9

2.2 Spectral masks specified by FCC for indoor and outdoor communication applications 11

2.3 Common frequency band spectral mask for indoor application 12

2.4 VNA-based frequency domain channel sounding system 15

2.5 Gaussian UWB waveform 17

2.6 Monocycle pulse UWB waveform 18

3.1 Monostatic and bistatic configurations 25

3.2 Scattering mechanisms 28

3.3 Illustration of orientation of each target model 36

3.4 Block diagram of data processing 38

3.5 Kasier-Bessel window 40

3.6 The proposed of UWB radar equation 41

4.1 Block diagram of experiment 47

4.2 VNA test set 48

4.3 The double-ridged waveguide horn antenna 49

4.4 The measurement setup in anechoic chamber 50

4.5 The illustration of the scattering targets 50

4.6 The model of side view 52

4.7 Bistatic measurement setups for an office chair and a steel desk 53

5.1 Gain and phase response of horn antennas 55

5.2 The impulse response of scattering from the office chair 58

5.3 The impulse response of scattering from the steel desk 60

5.4 Comparisons of RCS scattering from the office chair 62

5.5 Comparisons of RCS scattering from the steel desk 64

5.6 The RCS for the experimental office chair for VV polarization 66

5.7 The RCS for the experimental office chair for HH polarization 67

5.8 The RCS for the experimental steel desk for VV polarization 68

5.9 The RCS for the experimental steel desk for HH polarization 69

5.10 Mean of lognormal distribution of office chair 72

LIST OF FIGURES (CONTINUE)

Fig. Page

5.11 Mean of lognormal distribution of steel desk 74

5.12 Standard deviation of lognormal distribution of office chair 75

5.13 Standard deviation of lognormal distribution of steel desk 76

5.14 CDF of office chair 77

5.15 CDF of steel desk 78

6.1 Summary in scatter plots of RCS measured results without time gating at 3 GHz 81

6.2 Summary in scatter plots of RCS measured results without time gating at 4 GHz 82

6.3 Summary in scatter plots of RCS measured results without time gating at 5 GHz 82

6.4 Summary in scatter plots of RCS measured results without time gating at 6 GHz 83

6.5 Summary in scatter plots of RCS measured results without time gating at 7 GHz 83

6.6 Summary in scatter plots of RCS measured results with time gating at 3 GHz 84

6.7 Summary in scatter plots of RCS measured results with time gating at 4 GHz 84

6.8 Summary in scatter plots of RCS measured results with time gating at 5 GHz 85

6.9 Summary in scatter plots of RCS measured results with time gating at 6 GHz 85

6.10 Summary in scatter plots of RCS measured results with time gating at 7 GHz 86

LIST OF ABBREVATIONS

Radar Cross Section	RCS
RAdio Detection And Ranging	RADAR
Ultra Wide Band	UWB
King Mongkut's Institute of Technology Ladkrabang	KMITL
Vector Network Analyzer	VNA
Vertical to Vertical	VV
Horizontal to Horizontal	HH
Horizontal-Vertical	HV
Vertical-Horizontal	VH
Kolmogorov-Smirnov	KS
Cumulative Distribution Function	CDF
Probability Distribution Function	PDF
Signal-to-Noise Ratio	SNR
Intermediate Frequency Band Width	IFBW
Personal Area Network	PAN
Federal Communications Commission	FCC
European Telecommunications Standards Institute	ETSI
International Telecommunications Union	ITU
International Telecommunication Union Radio communication Sector	ITU-R
Ministry of Internal Affairs and Communications	MIC
Power Spectrum Density	PSD
Multi-Band Orthogonal Fequency Division Multiplexing	MB-OFDM
Direct Sequence Ultra Wideband	DS-UWB
Orthogonal Frequency-Division Multiplexing	OFDM
High Rate Wireless Personal Area Networks	HR-WPANs
Low Rate Personal Wireless Area Networks	LR-WPANs
Wireless Body Area Networks	WBANs
Wireless Local Area Networks	WLANs
Uniform Geometrical Theory of Diffraction	UTD
Geometrical Optics	GO
Physical Optics	PO

LIST OF ABBREVATIONS (CONTINUE)

Physical Theory of Diffraction	PTD
Finite Difference Time Domain	FDTD
Method of Moments	MOM
Geometrical Theory of Diffraction	GTD
Shooting and Bouncing Rays	SBR
Monostatic-to-Bistatic Equivalence Theorems	MBET
Frequency Modulation to Continuous Wave	FM-CW
Inverse Fast Fourier Transform	IFFT
Fast Fourier Transform	FFT
Transmit Antenna	Tx
Receive Antenna	Rx
Hewlett-Packard Interface Bus	HPIB
Continuous-Wave	CW
Radio Frequency	RF
Intermediate Frequency	IF
Line of Sight	LOS
Voltage Standing Wave Ratio	VSWR
Average	AVG
Extended Finite Difference Time Domain	XFDTD
Computer Simulation Technology	CST
High Frequency Structural Simulator	HFSS
Inverse Synthetic Aperture Radar	ISAR

CHAPTER 1
INTRODUCTION

1.1 Background

Deterministic propagation prediction by using ray tracing has been widely studied for the site planning. In particular, indoor environment has been extensively studied because of relatively small scale to be handled in personal computers (PCs). Ray tracing usually models reflection from and penetration through planar dielectric materials with finite thickness, and diffraction at edges of dielectric wedges [1].

However, ray tracing is a high frequency approximation and there are quite some limitations.

1. Scatterer surface should be smooth enough with respect to wavelength.
2. Scatterer surface should be flat.
3. Material of scatterer should be uniform, except for simple stratified structure.
4. Scatterer should be much bigger than the first Fresnel zone with respect to the specific ray path.

If these conditions are not satisfied, ray tracing prediction is erroneous [2]-[3]. In the indoor environment, non-square furniture such as table and chair, and human body are typical objects that cannot be accurately modeled in ray tracing simulation [4]. In this thesis, the influence of the existence of furniture in the channel response will be investigated.

In the planning and development of the wireless system, the indoor wireless communication system is the one of the most significant for channel propagation. The determination of radio channel characteristics in indoor applications is dominated by scattering considerations [5]-[7]. In indoor environments, the effect of all scattering targets such as obstacles, wall, and human body, etc. will contribute to the total received field. The propagation of radio wave depends on the environment. Different types of scattering targets or obstacles are main reasons to study and analyze of the radio wave propagation. Due to the complex and random geometry, their effects on the radio wave propagation are become to be difficult to investigate and model.

When an electromagnetic wave strikes a material discontinuity, electric currents are induced in the region of the discontinuity. These currents travel within the surface of the body and re-radiate an electromagnetic field. The radiation can, in general, be in any direction. This re-radiation is called scattering. The manner in which object scatter radiation is highly dependent on the geometry of an object and the direction of the incident radiation, and thus any given object has its own unique scattering signature. The scattered fields of the target are detected at far or near distances by transmitting radio waves and receiving waves. The scattered fields vary significantly with frequency, polarization and the target's shape, materials and orientation [8]. The scattering properties of the target are essential in designing, prediction and performance of the wireless systems.

Given knowledge of the incident filed, the electromagnetic properties of the target are completely described by the scattered field. The strength of the scattered field is indicated by the target's radar cross section (RCS) was used to describe the amount of scattered power from a target towards the receiver, when the target is illuminated by radio frequency (RF) energy. Radar operates by radiating electromagnetic waves and detecting echoes from an object. There are two purposes of radar, one is to determine the location of an object, and the second is to identify the object. Such identification is possible because every object has unique radar return called the RCS. The RCS is defined as the equivalent area of the object as if it were an isotropically scattering metal sphere. The RCS is primarily a function of the object's size, shape, composition, and orientation with respect to the radar. Since it can give insight into an object's identity, much research has been devoted to RCS characterization.

There are two major types of RCS: monostatic RCS and bistatic RCS. In this study, bistatic RCS of complex target in channel propagation are performed. The RCS of targets has become increasingly important in recent years with the emphasis the military has placed on the design of low observable or stealth technology platforms and wireless communication. There are many methods that can predict an object's RCS. An important factor in evaluating the accuracy of a RCS prediction understands the accuracy of the object model. If the object's size or shape is erroneous, the resulting RCS prediction is faulty, but these can typically be measured quite accurately. This is not true, however, when evaluating the accuracy of the object's material composition.

Although the RCS is a normalized scalar measure of the complex scattered filed, the term is often used to describe the scattering characteristics of a target [9]. Scattering responses of the target can be measured either in the time or frequency domain and the two responses are related by a Fourier transform. RCS measurements can be performed in outdoor, indoor or inside anechoic chamber. Using vector network analyzer (VNA) (HP 8510C), frequency-domain techniques are considered more stable, less susceptible to noise, and capable of spanning a wider measurement frequency range.

RCS is an important parameter to present the scattering properties of the target. The backscatter signal from complex target, such as furniture items, can vary rapidly with target aspect, polarization and frequency. A limited number of studies have been carried out to characterize the RCS of the complex objects such as furniture, aircraft, missiles, rockets, ships in indoor UWB radar application. It has been advantageous to treat the target RCS as a statistic items for the RCS with random fluctuation. Statistical distributions are used for RCS characterization. The RCS of such targets are usually characterized using statistical terms such as mean, variance and distributions [10]-[13]. Many distribution models are existed, such as Rayleigh, Rician, lognormal, chi-square and Weibull distribution models. These statistical RCS models are shown in the term of the cumulative distribution function (CDF) and their statistical parameters are reported. Our contribution is the statistical characterization of the measured RCS data of two furniture items. Frequency samples of RCS are used as random fading samples to model statistical behavior using Kolmogorov-Smirnov (KS) test [14]. Therefore, the statistical characteristics of two kinds of RCS values are investigated and the significant parameters are studied.

1.2 Literature Review

In the literature, the RCS measurements techniques and analysis for computing scattered electromagnetic waves due to various types of targets have been extensively studied. Depending on the target size and selected frequency range, RCS can be investigated in either an outdoor environment, indoor environment, or inside an anechoic chamber. [15] - [18] examined the RCS of scattering objects in an anechoic chamber. [19] and [20] analyzed the RCS of typical building walls, and [21]

investigated the scattering of trees. [22] studied the scattering from lampposts, traffic lights, and signboards. [23] researched the Bragg scattering from periodic surfaces in an ultra wide band (UWB) signal transmission. The full wave simulation technique is used to investigate the scattering from multi-shape or porous objects, e.g., bricks, tables, and chairs [24]. The scattering of buildings in a street microcell environment is studied in [25], and [26] simulated the effect of a moving human body on the statistical channel.

In indoor wireless communications, the channel fluctuation also depends largely on the types and shapes of the complex target, antenna position, and polarizations as well as the surrounding local environment. Due to the ground reflection and the irregularity of the complex object's shape related to the scattering characteristics, i.e. target strength variations due to aspect angle and grazing angle changes, there might be some multipath responses which may cause a fading. These types of fluctuation can hardly be separated from each other and, hence, are treated statistically. Therefore, the characteristics of fading should be investigated and efficiently modeled in order to appropriately design and develop the indoor wireless system. A simple statistical multipath model of the indoor radio channel [27] has presented. Multipath characteristics of non-specular scattering from building surfaces roughness have studied [28].

1.3 Objectives and Scope of This Thesis

Although the scattered electromagnetic fields and the RCS of objects were extensively investigated in [8-18, 29-33], the measurement and evaluation of RCS of complex target have not been established. The purpose of this research is to establish the capability to perform accurate bistatic radar cross section measurements in near field RCS range using vector network analyzer. The objective of this research is to investigate the RCS of complex target such as furniture and develop a capability for measuring frequency-domain scattering fields from 3 GHz to 7 GHz.

The extension of radar equation which includes the channel transfer function is proposed and the exact value of RCS is evaluated. From the extension of radar equation, the value of RCS for each scatterer is examined. Then, time gating method is utilized to remove the multipath effects from the environment. Kiaser-Bessel

window function is applied to time gating. The RCS results with time gating and without time gating are described. Due to the multipath effects, a statistical analysis was performed on measured RCS from complex scatterer. A commonly used lognormal distribution is used to analyze the characteristics of RCS from each target. To evaluate the goodness-of-fit of the lognormal distribution model, the KS test is adopted. The agreement of statistical characteristic between measurement and simulation is presented. The following five efforts were required to accomplish these objectives:

1. To study the indoor propagation channel
2. To study about the efficient of the complex furniture of the channel response
3. To extend the radar equation in order to find the scattering or RCS from the complex target in indoor environment from the VNA measurement
4. To reduce the multipath effect by using time gating method
5. To analyze the RCS values by using lognormal distribution

This effort developed the foundation required to perform accurate bistatic measurements in the near field RCS. The bistatic capability was to include both channel transfer function in free space measurements using anechoic chamber and frequency response measurements. The frequency response measurement provides the RCS in units of dBm^2 for a target versus frequency for a fixed target aspect angle. The system actually measures the complex return signal, and is thus capable of inverse Fourier transforming the data to generate the impulse response. The scattering characteristics of targets are important for the indoor wireless communication. If the building is mapped, what is inside the building is very interesting. Assume that the RCS of furniture at different incidence angles and different material types will be different. A novel study of RCS changes is helpful for target identification and wireless system design.

1.4 Organization of the Thesis

To fulfill the purpose of this thesis, numerous works must be carried out both theoretically and experimentally.

This thesis is organized into six chapters. The topic of Chapter 1 is Introduction. This chapter provides background, literature review and objectives and scope of research and thesis organization.

This chapter provides an overview of the knowledge required to understand the basics of this research. The topic of Chapter 2 presents the UWB communication system and application. Advantages and disadvantages of UWB system, regulation of UWB and UWB standards are explained. The application of UWB radar system is introduced.

The topic of Chapter 3 discusses the Theory, the concept of RCS and evaluation of RCS of complex target are presented. This chapter gives specific details of the RCS of target for the proposed theory. This chapter describes signal processing techniques. Inverse Fourier Transform (IFFT) techniques to convert from frequency domain data to time domain are discussed, in addition to important processing aspects of windows. Moreover, the factors of measurement inaccuracy and RCS prediction methods are described.

The topic of Chapter 4 illustrates the system for scattering from furniture in channel propagation. The Experimental Measurement Setup of bistatic RCS is explained. Detailed descriptions for the anechoic chamber, the HP-8510C network analyzer, and the antennas, objects are given.

The topic of Chapter 5 shows RCS results. This work describes the Results of RCS and the comparison of RCS with time gating and without time gating. The statistical analysis of RCS with lognormal distribution is studied. The comparison of CDF results of RCS for 0, 90, 180 degree are displayed.

Finally, the topic of Chapter 6 is Conclusion and Future Works. This chapter gives the conclusions and recommendations for improvements and future works.

CHAPTER 2
PRINCIPLE OF UWB COMMUNICATION SYSTEM AND APPLICATION

2.1 Introduction of Ultra Wide Band

Ultra wide band (UWB) communication technology increased in the field of wireless communication and ranging. UWB include short-pulse, nonsinusoidal, carrierless, and time domain. UWB is a technology for transmitting information spread over a large bandwidth (> 500 MHz) should be able to share spectrum with other users in theory and under the right circumstances. Regulatory settings of Federal Communications Commission (FCC) are intended to provide an efficient use of scarce radio bandwidth while enabling high data rate personal area network (PAN) wireless connectivity and longer-range, low data rate applications and radar and imaging systems [34]. UWB was traditionally accepted as pulse radio, but the FCC and International Telecommunication Union Radio communication Sector (ITU-R) now define UWB in terms of a transmission from an antenna for which the emitted signal bandwidth exceeds the minimum between 500 MHz and 20 % of the center frequency. Thus, pulse-based systems wherein each transmitted pulse instantaneously occupies the UWB bandwidth, or an aggregation of at least 500 MHz worth of narrow band carriers, for example, in orthogonal frequency-division multiplexing (OFDM) can gain access to the UWB spectrum. Pulse repetition rates may be either low or very high [35].

A significant difference between traditional radio transmissions and UWB radio transmissions is that traditional systems transmit information by varying the power level, frequency, and/or phase of a sinusoidal wave. UWB transmissions instead transmit information by generating radio energy at specific time instants and occupying large bandwidth, thus enabling both pulse-position and time-modulation. The information can also be modulated on UWB pulses by encoding the polarity of the pulse, the amplitude of the pulse, and/or by using orthogonal pulses. UWB pulses can be sent sporadically at relatively low pulse rates to support time/position

modulation, but can also be sent at rates up to the inverse of the UWB pulse bandwidth [35]. Assume that the current and future emphasis on low power, low interference and low regulation makes the use of UWB an attractive option for current and future wireless applications.

2.2 Ultra wideband Radar Technology

The information content of UWB radars increases because of the smaller pulse volume of the signal. UWB radar has better surveillance space and becomes more sensitive. Because the pulse waveforms have very high fractional bandwidth, the determination of a carrier frequency is generally impossible. Therefore, these techniques are also known as baseband or carrier-free transmission techniques. The fractional and relative bandwidths are defined as Equation 2.1 and Equation 2.2 [36].

$$\text{Fractional Bandwidth (FBW)} = \frac{2(f_H - f_L)}{(f_H + f_L)} = \frac{(f_H - f_L)}{f_0} \tag{2.1}$$

$$\text{Relative Bandwidth (RBW)} = \frac{(f_H - f_L)}{(f_H + f_L)} \tag{2.2}$$

where f_H and f_L are the upper and lower band edges of the signal, and f_0 is the average of f_H and f_L.

Ultra-wideband radar is defined as any radar whose fractional bandwidth is greater than 25%, regardless of the center frequency or the signal time-bandwidth product. Since the radar range resolution cell is sufficiently small, major scattering centers on the target can be well resolved. Since all radar signals have some target-related changes when reflected, the problem of detecting this change and uniquely relating it to the reflecting target is optimally solved using the UWB radar.

The ultra-wideband radar has many advantages. Using wider bandwidth by either using short duration impulses or nonsinusoidal waveforms can improve the performance of the radar. UWB radar generally has large absolute signal bandwidth, which it provides better range measurement accuracy and range resolution, as well as improving radar immunity to passive interference from rain, fog, aerosols, and

metalized strips. UWB radars have higher probability of target detection and good target tracking stability. The transmit power of UWB radar is much lower compared to narrowband radar. UWB radars also possess good spectrum efficiency because the UWB architecture enables high bandwidth transmission in an increasingly crowded spectrum. UWB radars in low operating frequencies enable the signals to propagate effectively through some materials, such as bricks and cement, and dense media such as foliage.

Despite a number of advantages, UWB systems have also some drawbacks. The shortness of the pulse, while gaining a high signal/symbol rate, makes the bandwidth become wider and reduces the signal to noise ratio (SNR). Wider bandwidth requires FCC approval and lower SNR requires signal averaging, which then lowers the signal/symbol rate [37]. The narrow band signal has better Doppler frequency estimation than wide band signal. The balance between time and frequency resolution needs to be considered in the system design.

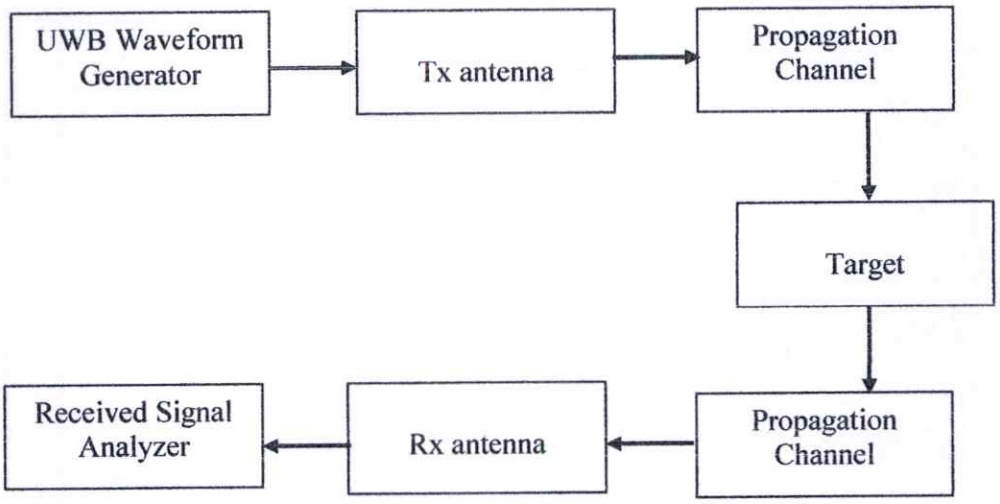

Figure 2.1 Generic system block diagram of UWB radar [37].

The current interest in UWB radar is based on the expectation that this type of radar will provide improvement in one or more of the following areas

1. Target detect ability through RCS enhancement and improved clutter suppression
2. Target identification through improved measurement resolution

3. Reduced cost through employment of high power switches as transmitter sources

To be able to recognize when a UWB waveform does offer unique performance advantage, it is important to understand how radar performance capabilities are related to the radar waveform characteristics. This section presents a discussion of those relationships. Figure 2.1 shows a generic system block diagram for radar, including the involvement of the target, antennas, and the propagation medium.

2.3 Regulator Bodies and Standards

In this section, the different regulations and standards of UWB are discussed. In this first set of UWB rules, the FCC determined that each proposed application area had unique attributes that required different levels of regulation.

2.3.1 UWB Regulation in the USA

Table 2.1 Radiation limits specified by FCC for indoor and outdoor communication applications [38].

Frequency (MHz)	PSD (dBm/MHz) Indoor communication	PSD (dBm/MHz) Outdoor communication
Below 960	-41.3	-41.3
960-1610	-75.3	-75.3
1610-1990	-53.3	-63.3
1990-3100	-51.3	-61.3
3100-10600	-41.3	-41.3
Above 10600	-51.3	-61.3

One of important topics in UWB communication is the frequency regulation. The FCC regulations for applications utilizing UWB technology are specified in USA. The FCC approved the deployment of UWB on an unlicensed basis in the 3.1 GHz–10.6 GHz band subject to a modified version of Part 15.209 rules. The spectral mask for indoor and outdoor applications specified by the FCC is shown in Figure 2.2. For

radiation limits, FCC specified the limits of power spectrum density (PSD) radiation for indoor and outdoor communication applications as shown in Table 2.1 [38].

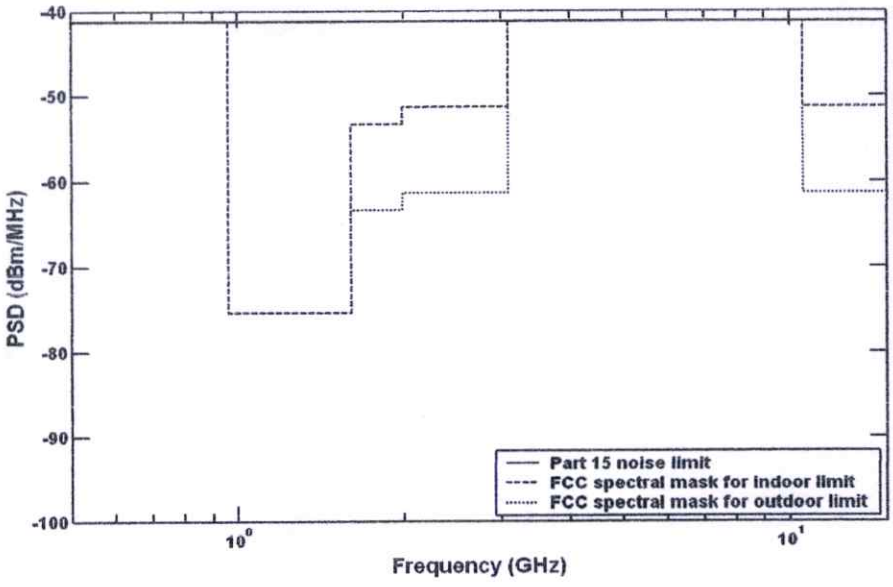

Figure 2.2 Spectral masks specified by FCC for indoor and outdoor communication applications [38].

2.3.2 Common Band Regulation

UWB signal regulation has been approved in other regions as well. Among FCC, ETSI and MIC, common frequency is available. The regulation of PSD radiation is satisfied all FCC, ETSI and MIC regulations and allows using only indoor application. The main frequency range is from 7.25 to 8.5 GHz, while the low frequency of 7.25 GHz is satisfied MIC regulation and highest frequency of 8.5 GHz is satisfied ETSI regulation as shown in Table 2.2. The common frequency band spectral mask for indoor application is shown in Figure 2.3 [39].

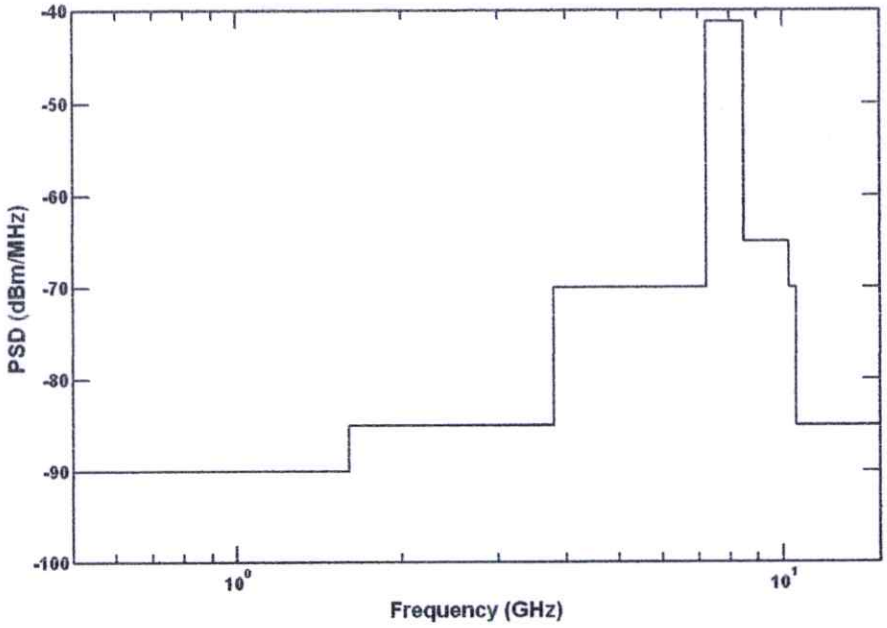

Figure 2.3 Common frequency band spectral mask for indoor application [39].

Table 2.2 Radiation limits of common frequency band for indoor application [39].

Frequency (GHz)	PSD (dBm/MHz)
Below 1.6	-90
1.6-3.8	-85
3.8-7.25	-70
7.25-8.5	-41.3
8.5-10.25	-65
10.25-10.6	-70

2.3.3 IEEE Working Groups

Two standards of UWB are IEEE 802.15.3a for high rate wireless personal area networks (HR-WPANs) such as pulse-based UWB radar and imaging systems [40], IEEE 802.15.4a for low rate personal wireless area networks (LR-WPAN) [41].

2.3.3.1 IEEE 802.15.3a Standard

IEEE 802.15.3a standard improved the data rate of IEEE 802.15.3 standard by using UWB technique for pulse-based UWB radar and imaging systems with short distance up to 10 m and high data rate up to 480 Mbps [40]. IEEE 802.15.3a standard was withdrawn in January 2006 because the members of task group were not able to decide between two technologies, multi-band orthogonal frequency division multiplexing (MB-OFDM) and direct sequence ultra wideband (DS-UWB).

2.3.3.2 IEEE 802.15.4a Standard

IEEE 802.15.4a standard utilizes UWB technique for LR-WPANs with long distance up to about 100 m and low data rate. This standard uses for new applications that require only moderate data throughput and low cost, but long battery life, such as wireless sensor networks and high accuracy localization systems. The transmitted signal is based on very short pulse and estimated to impulse, which causes the name of UWB [41].

2.4 UWB Channel Model

This section examines common UWB channel models, provides methods to measure UWB channel, and introduces the channel model adapted by IEEE802.15.3a study group, which be used as a reference model in UWB system performance studies.

2.4.1 Channel Measurement

In this thesis, the frequency and time domain measurement conception are presented. Theoretically, both techniques give the same result if there is a static measurement environment and an unlimited bandwidth.

2.4.1.1 Frequency Domain Channel Sounding

With frequency domain sounders, the RF signal is generated and received using a vector network analyzer (VNA) which makes the measurement setup quite simple. The sounding signal is a set of narrowband sinusoids that are swept across the band of interest. The UWB channel models can then be generated at the data post-processing stage. When the frequency domain sounder approach is used, the channel state during the sounding must be static to maintain the channel conditions during the sweep. The maximum sweep time is limited by the channel coherence time. If the sweep time is longer than the coherence time, the channel may change during the sweep. For fast changing channels, other sounding techniques are used [42].

The performance of the frequency domain sounder is also limited by the maximum channel delay. The upper bound for the detectable delay $\tau_{\max}$ can be defined by the number of frequency points used per sweep and the bandwidth B
This is given by

$$\tau_{\max} = (N_{\text{sam}} - 1)B \tag{2.3}$$

where N_{sam} is the number of frequency points.

In frequency-sweep mode, the sounding signal is rapidly swept across the whole ban of interest, For a transmitter and receiver that are in lock step sweeping across the frequency band of interest, very long propagation delays can cause the receive to take samples at a frequency that is higher than the receive frequency. This frequency shift Δf is a function of the propagation time t_{prop}, the frequency span and the sweep time t_{sw} as

$$\Delta f = t_{\text{prop}}\left(\frac{B}{t_{\text{sw}}}\right) \tag{2.4}$$

In general, Δf has to be smaller than the analyzer IF bandwidth to obtain reliable results. The concept used in frequency domain measurement is shown in Figure 2.4. After the channel frequency response has been measured, the time domain

representation or impulse response can be achieved by inverse Fourier transform (IFFT)

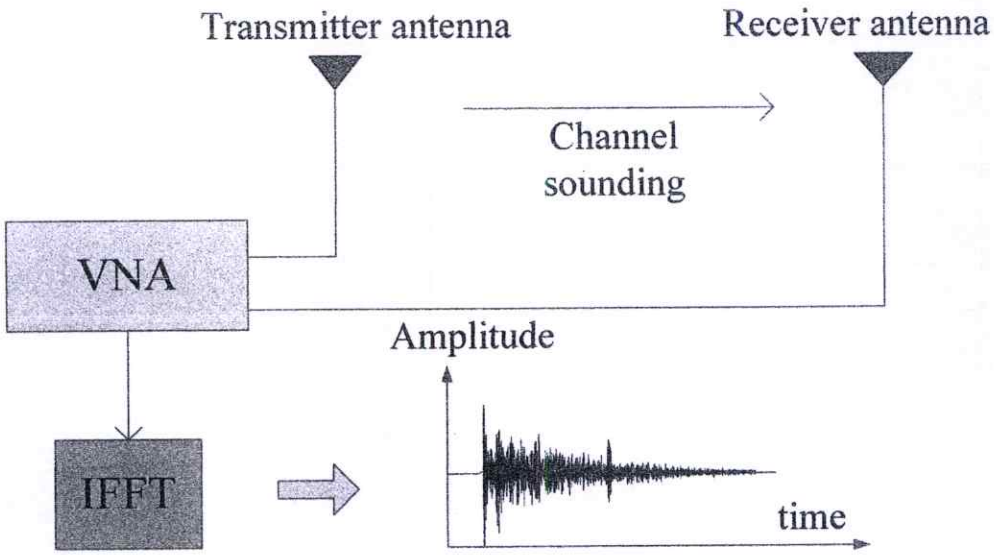

Figure 2.4 VNA-based frequency domain channel sounding system [34].

2.4.1.2 Time Domain Channel Sounding

One way to carry out time domain UWB radio channel soundings is to use of very short impulses. The receiver in this case is a digital sampling oscilloscope. The bandwidth of the sounder depends on the pulse shape and the pulse width used. By changing the pulse width, the spectral allocation can also be changed. However, the simpler the pulse shape, the easier it is to perform the deconvolution during the post-processing, where the channel impulse response is calculated by removing the transmitted pulse waveform from the results as a time gating method.

2.4.2 UWB Transmitted Pulse Waveforms

According to the UWB transmitted pulse waveform, the necessary of the appropriate UWB waveforms are discussed.

2.4.2.1 Gaussian Pulse

The Gaussian pulse is a simpler waveform described by the Gaussian distribution. In the time domain, the expression of Gaussian pulse is given by

$$g(t) = A\,exp[-(t/\tau_b)] \tag{2.5}$$

where A stands for the maximum amplitude and τ_b denotes the width of the Gaussian pulse. Figure 2.5 shows the time and frequency domain of Gaussian UWB waveform.

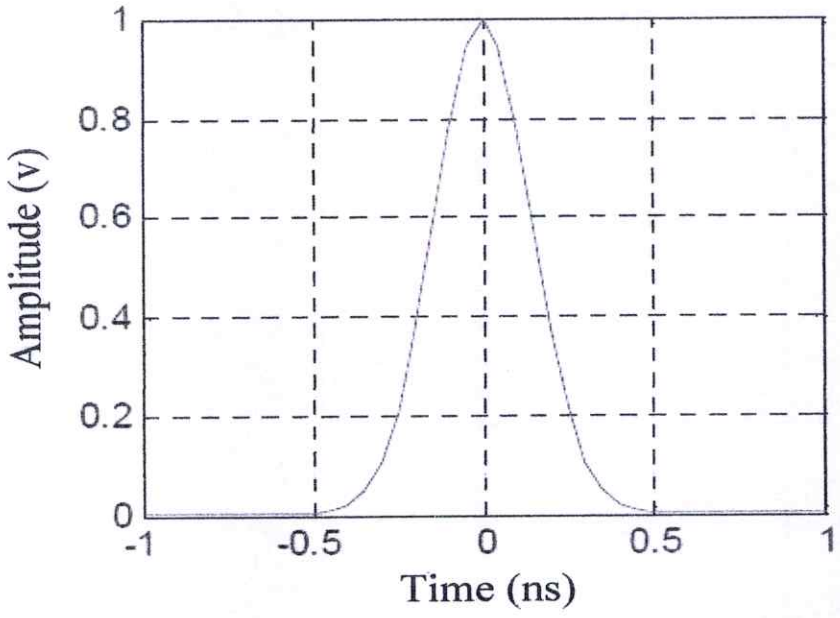

(a) Time Domain

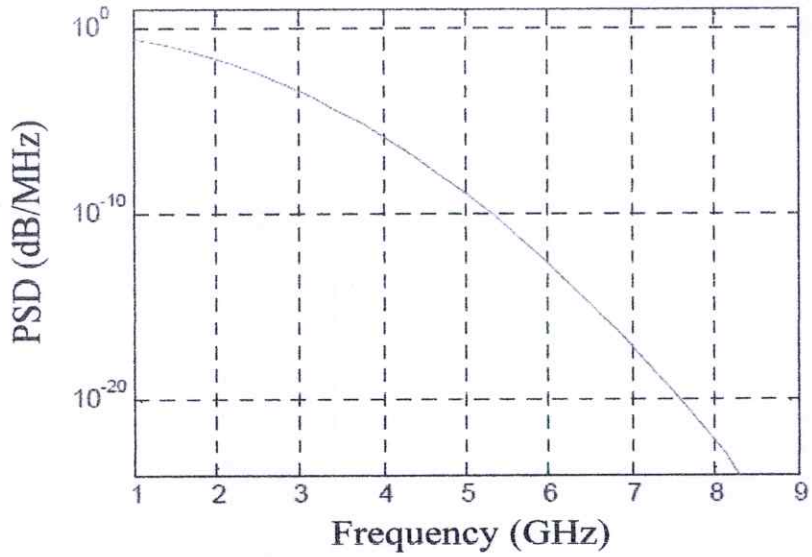

(b) Frequency domain

Figure 2.5 Gaussian UWB waveform [35].

2.4.2.2 Monocycle Pulse

The monocycle pulse is the first derivative of the Gaussian pulse. The expression for the monocycle pulse waveform is shown as

$$m(t) = \frac{t}{\tau_b}\exp[-(t/\tau_b)^2] \tag{2.6}$$

The n^{th} derivative of Gaussian pulse can be obtained from the following expression as

$$\mathrm{p}^n(t) = \frac{n-1}{\tau_b}\mathrm{g}^{(n-2)}(t) - \frac{t}{\tau_b^2}\mathrm{g}^{(n-1)}(t) \tag{2.7}$$

Figure 2.6 (a) and (b) show the time and frequency domain of monocycle pulse UWB waveform.

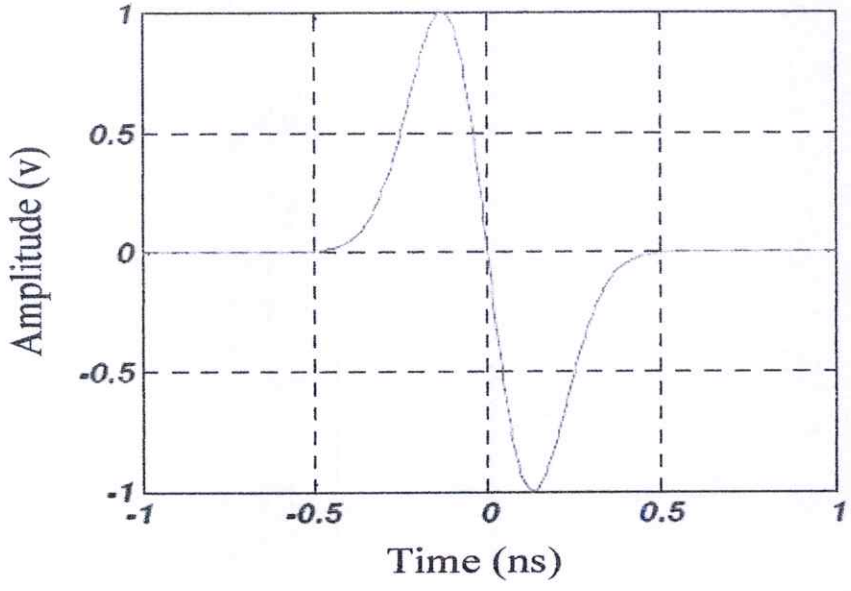

(a) Time domain

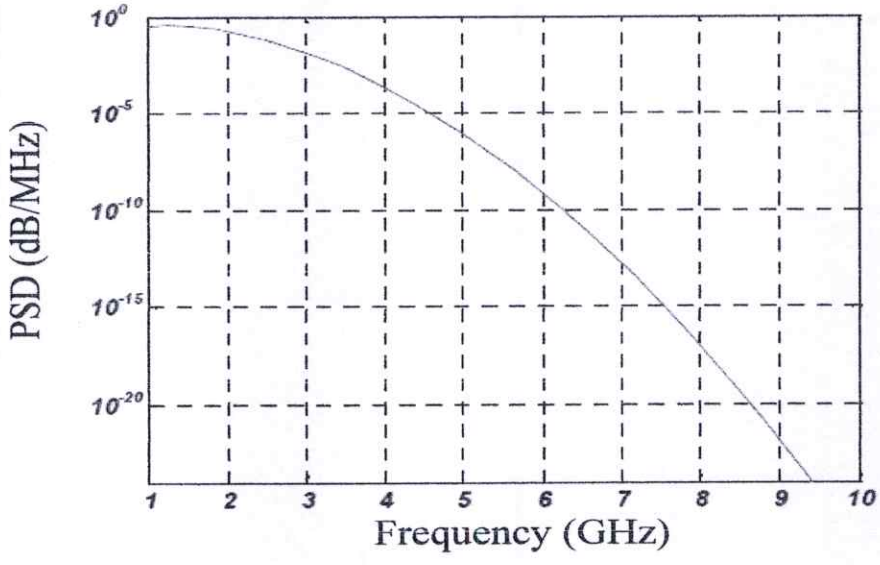

(b) Frequency domain

Figure 2.6 Monocycle pulse UWB waveform [35].

2.5 Advantages and Disadvantages of UWB

The ultra-short waveforms, in the nanoscale range, that UWB systems use offer several advantages. The enhanced ability to penetrate through obstacles, opening up possible uses such as radar imaging is offered. Fine precision ranging has at the centimeter level opening up possible uses such as positioning and tracking. The potential for high data rates are available in multi-user networks opening up possible uses such as high speed networking. Transmitting in short pulses decreases interference because the signals do not last long enough to interfere with other signals. Ultra-short UWB waves also require limited processing power. The use of low power waves allow UWB systems to working in tandem with existing systems and makes them difficult to intercept. UWB signals have a resistant to jamming because of the vast range of frequencies used by UWB. UWB systems are potentially low-cost because they use carrierless transmissions which mean they can be designed with simple hardware or nearly all digital. In addition, a single system can be adapted to multiple uses, from communications to radar and positioning.

UWB systems have considerable real and possible disadvantages that must be addressed in order to build real-world applications. UWB shares a wide swath of bandwidth with other RF technologies, which means there is potential interference, UWB receivers are subject to long synchronization times and must be complex enough to handle the multipath rich channels inherent to the short pulse signals used by UWB systems. UWB antennas also pose an engineering challenge due to the unique demands and challenges of UWB systems. Carrierless systems must rely on complex signal processing techniques to recover data from noisy environments. Channel characterization, an essential part of communications systems design, is difficult in UWB systems because of wide bandwidth and reduced signal energy [43].

2.6 Conclusion

The UWB is a leading technology for wireless applications including numerous indoor short range applications. The UWB technology can easily satisfy the target identification of radar and wireless communication. One of the important considerations for the success of UWB systems is the compatibility and coexistence

of such systems with other wireless local area networks (WLANs) or wireless personal area networks (WPANs). The ultra wide bandwidth cannot be assigned exclusively to UWB signals and overlapping with the bands of many other narrowband systems arise. In order to ensure a robust communication link, the issue of coexistence and interference of UWB systems with current indoor wireless systems must be considered. Due to the wideband nature of UWB emissions, it could potentially interfere with other licensed bands in the frequency domain if left unregulated.

UWB standard employs unlicensed 3.1 GHz – 10.6 GHz authorized by FCC. The assessment of mutual interference between UWB devices and existing narrowband systems during overlay is important to guarantee no conflicting coexistence and to gain worldwide acceptance of UWB technology. Hence, various technical challenges remain as open issues, which need to be confronted to ensure the successful deployment of this upcoming technology.

Moreover, FCC, ETSI and MIC strictly specify regulation of UWB signal to confirm that UWB signal would not interference with other narrowband systems. Three standards of UWB systems are IEEE 802.15.3a, IEEE 802.15.4a for HR-WPANs, LR-WPANs and WBANs, respectively. Therefore, our system used wide frequency range: 3 GHz to 7 GHz of UWB in order to analyze the multipath effect and study of RCS in an indoor environment.

CHAPTER 3

MODELING OF FURNITURE EFFECT IN AN INDOOR PROPAGATION CHANNEL

3.1 Introduction

This chapter is a brief introduction of radar cross section theory and evaluation techniques. In this chapter, the theory supporting the concept of both monostatic and bistatic RCS, and its role in radar equation and detailed description of scattering theory are discussed. Next, relevant equations will be provided and the extension of radar equation is described. The RCS is then formally defined, followed by a brief discussion regarding scattering regions. The significant scattering of RCS of simple and complex objects is decisively important to predict the received signal strength and identify targets such as aircraft, missiles, rockets, ships in radar application and other objects such as buildings in outdoor channel propagation and furniture items, human body, walls in indoor channel propagation of wireless with the purpose of improving or rendering difficult visibility in various frequency ranges [33]. The use of RCS measurements of targets has expanded to indoor wireless communication. Finally, a comparative discussion of some common methods for RCS prediction is described.

3.2 Definitions of RCS

The measurement of the RCS of targets, both simple and complex, is a difficult and challenging electromagnetic problem that has existed since radar was invented and analyzed. Although the principles of electromagnetic theory are well developed and employed, the application of those principles for predicting RCS often result in complex and extensive computations. Thus, there is always the need to test theory or verify predictions and these actions usually be accomplished by testing range measurements.

The spatial distribution of the energy depends on the size, shape and composition of the target, and on the frequency and nature of the incident wave. When an electromagnetic wave focuses on an object, the energy spreads in all

directions. This distribution of signal is called scattering and the target or object or obstacle itself is often called a scatterer [34]. The RCS of the scatterer is a parameter denoted by σ (called *Sigma*) which a ratio of the energy is scattered in a particular direction away from the scatterer to that which is incident on the scatterer. The RCS of the scatterer has become increasingly important in recent years with the emphasis outdoor and indoor application of the radar and wireless communication has placed on the design of low observable or stealth technology platforms.

In general, the RCS of a target depends on a function of the polarization of the incident wave, the angle of incidence, the angle of observation, the geometry of the target, the electrical properties of the target and the frequency of operation [13]. Normally, when an electromagnetic wave impinges on a target, some of the energy will be absorbed and some will be scattered. The absorption and scattering mechanisms are governed by Maxwell's equations under the relevant boundary conditions. σ has the dimensions of area. The RCS variables often consist of many orders of magnitude; transmitted powers may be in megawatts and received power may be in picowatts. Parameters are conveniently converted to logarithmic values, because of the wide range of variables involved. Typically, transmitted power, antenna gain, and RCS values are provided in dB. The RCS values are often expressed in dBsm – decibels relative to a square meter - where dBsm is a direct function of the logarithm to the base ten of the RCS of a target expressed in square meters. Wavelength and range are usually given in linear units and must be converted to dB.

The received power at the channel propagation is a function of several parameters [44], i.e. a function of the transmitter system, the propagation path from the transmitter system to the target, and the propagation path from the target to the receiving system. These dependents can be written as Equation 3.1:

$$P_r(f,\theta_i,\phi_i,\theta_s,\phi_s)=\frac{c^2}{64\pi^3 f^2 {d_t}^2 {d_r}^2}\sigma(f,\theta_i,\phi_i,\theta_s,\phi_s)G_t(f)G_r(f)P_t(f) \qquad (3.1)$$

where $P_t(f)$ is the transmitted power, $G_t(f)$ is the gain of the Tx, $G_r(f)$ is the gain of the Rx, d_t and d_r are the respective distances from the target to Tx and Rx, $\sigma(f,\theta_i,\phi_i,\theta_s,\phi_s)$ is the RCS of the target, c is the velocity of light, f is a carrier

frequency, θ_i and ϕ_i are the elevation and azimuth incident angles to the target, and θ_s and ϕ_s are the elevation and azimuth scattering angles from the target.

By rearranging Equation 3.1, the formula for RCS can be written as Equation 3.2:

$$\sigma(f,\theta_i,\phi_i,\theta_s,\phi_s)=\frac{64\pi^3 f^2 d_t^2 d_r^2 P_r}{c^2 G_t(f) G_r(f) P_t(f)} \tag{3.2}$$

Another definition of RCS is expressed as the portion of the scattering cross section corresponding to a specified polarization component of the scattered wave of a given scattering object. When expressed as a mathematical equation, then the RCS may be written as [31]-[32]

$$\sigma(\theta_i,\phi_i,\theta_s,\phi_s)=4\pi r^2 \frac{\Phi_{scat}(\theta_s,\phi_s)}{S_{inc}(\theta_i,\phi_i)} \tag{3.3}$$

$$\sigma(\theta_i,\phi_i,\theta_s,\phi_s)=4\pi R^2 \frac{|E_{scat}|^2}{|E_{inc}|^2}=4\pi R^2 \frac{|H_{scat}|^2}{|H_{inc}|^2} \tag{3.4}$$

where R is the far-field distance, σ is the radar cross section of the target (m^2), E_{scat} is a reflected or scattered electric field (V/m), H_{scat} is a reflected or scattered magnetic field (A/m), E_{inc} is an incident electric field (V/m) and H_{inc} is a incident magnetic field (A/m). RCS is a far-field quantity and the illuminating and scattered waves can be taken as plane waves with complex amplitudes E_{inc} and E_{scat}. It is dependent upon the incident wave (θ_i,ϕ_i) and the scattering wave (θ_s,ϕ_s). The direction of arrival of the incident wave is (θ_i,ϕ_i) and the direction of observation of the scattered wave is defined as (θ_s,ϕ_s).

It is important to note that the RCS is defined so that it is independent of the distance between the radar and the target. This has occurred since the scattered field decays as $\frac{1}{R}$. The limiting process in the definition ensures that the incident field is a plane wave. In what is called a far-field range, the transmit antenna directly illuminates the target. A large enough R is needed such that the illuminating field

satisfactorily approximates a plane wave. This is related to the far-field spoken of in antenna theory. This leads to [45]

$$R > \frac{2D^2}{\lambda} \tag{3.5}$$

where R is the range, D is a maximum target dimension, and λ is a wavelength. In the RCS problem, the target sees limited phase and amplitude variation in the incident field and that the receive antenna is effectively in the far zone of the target.

The RCS is a typical frequency domain quantity and is a function of frequency, object configuration, transmitter and receiver polarization and angular orientation of the object with respect to the incident field. The total field is the sum of the incident and the scattered fields in Equation 3.6. The scattered electric and magnetic fields are due to the presence of a target, so,

$$E_{\text{total}} = E_{\text{scat}} + E_{\text{inc}} \tag{3.6}$$

3.2.1 Monostatic and Bistatic RCS

When transmit antenna (Tx) and received antenna (Rx) are co-located, it is known as the monostatic cross section as shown in Figure 3.1(a). As shown in Figure 3.1(b), the Tx and Rx antennas are separated by some bistatic angle, it is called a bistatic cross section. In bistatic scattering, the electromagnetic wave arrives at the target from the Tx and scatters in all directions, one of which is detected by the Rx. It follows that bistatic RCS measurements are performed to determine the scattering from a target at particular bistatic geometry.

The use of bistatic radar has its advantages over the monostatic case. The electromagnetic scattering signature (most often referred to as radar cross-section (RCS) can be determined in a much more complete way as opposed to monostatic radar. Monostatic radar can only observe the backscatter of an object, or the radiation that returns from the object directly back in the direction of the source. From an electromagnetic scattering theory that objects, in general, radiate in all directions, not just the backscatter direction. A bistatic measurement can observe how the object scatters in every direction in a plane that intersects the object, for a given look angle.

A complete bistatic measurement can require hundreds of times the amount of data as a monostatic measurement for a given look angle. Analysis of the data becomes computationally expensive and much less intuitive than in the monostatic case.

The disadvantage of bistatic is that the theoretical RCS of the reference objects for a bistatic calibration, which are necessary to compare with the measurement in order to calibrate, are often more rigorous than in a monostatic calibration. In a complete, full polarimetric calibration for instance, usually three objects are used and each must have precisely known scattering characteristics, which often means several days of moment method calculations on a fast computer.

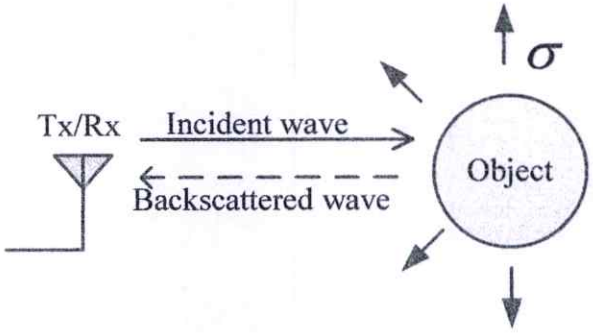

(a) Monostatic geometry

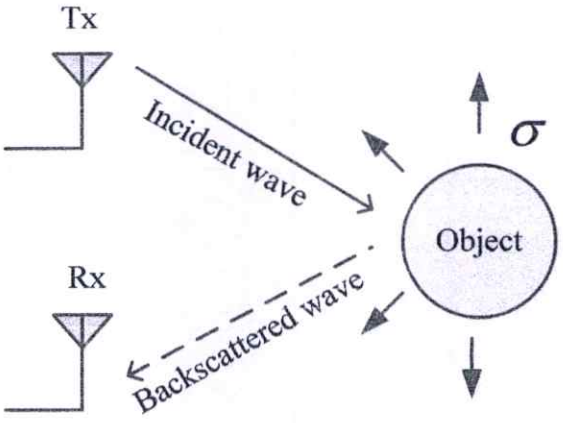

(b) Bistatic geometry

Figure 3.1 Monostatic and bistatic configurations [33].

This thesis focuses on the bistatic nature of complex objects. To fully exploit bistatic advantages requires a better understanding of bistatic scattering mechanisms. Without such a proper understanding, exploitation of bistatic key benefits may not be fully realized. The scattering mechanisms which interact to form an object's far field signature pertain to both monostatic and bistatic situations. However, whereas the monostatic pattern is usually dominated by specular returns, the bistatic can be dominated by non-specular ones.

3.3 Scattering Regions

In general, scattering obstacles are described into three different regions based on their body size in wavelengths (λ). Three regimes are distinguished: Low frequency scattering, resonant scattering and high frequency optics scattering [31]-[33].

3.3.1 Low Frequency Scattering Region or Rayleigh Region

If the wavelength of the incident field is much larger than the largest object dimension, the object is like as a point scatterer. Assume that only little amplitude and phase variations of the incident field can be occurred over the complete area of the object.

The field is defined as a quasi-static field is related to the size, the type of material and the dimension with respect to polarization of the object.

Rayleigh region scattering occurs when the object's physical dimensions are much less than a wavelength, and arises from the fact that the phase front of the impinging field remains relatively constant over the object's surface. Signature analysis in this region can be accomplished through static field methods, and, in general RCS amplitudes are inversely proportional to fourth power of the wavelength. However, because most objects of practical importance are much larger than the incident field wavelength, resonant and optical scattering are of greater concern.

3.3.2 Resonant Scattering Region

When the wavelength is on the order of the object size, the signal variations across the body of the target are much stronger. Every part of the target affects received signal strength. The scattered field at any point on the body of the target is determined by the sum of the incident field and the scattered field from every other point on the body.

3.3.3 High Frequency Optics Scattering Region

The high frequency scattering mechanism is an important factor in reference object selection. In the high frequency regime, three scattering mechanisms are distinguished.

3.3.3.1 Specular Reflection

It is limited to a small angular area, but the amplitude of the backscattered field in this area is very large. It occurs when a wave strikes a smooth surface and reflects back at the same angle from the normal vector to the surface (Snell's Law). The method of Geometrical Optics (GO) predicts this mechanism by the use of ray tracing [44].

3.3.3.2 Single Diffraction

Signal diffraction is the scattering of electromagnetic fields at the edges, tips or other discontinuities of surfaces. For a large set of geometries, diffraction can be modeled as a local phenomenon and solved for numerically by the Uniform Geometrical Theory of Diffraction (UTD) [46]. This technique predicts diffraction from features that create an instantaneous change of the radius of curvature of an object. It models an arbitrary object as an assembly of canonical objects that the code can calculate precisely.

3.3.3.3 Multiple Diffraction

Edges do not only diffract the electromagnetic field back to the observer, but can also diffract the field in the direction of another edge. The amount of energy scattered by the second edge in the direction of the observer is the double diffraction contribution. Similar to double diffraction, triply diffracted waves are generated. An object with a large number of diffraction-producing features can be calculated using asymptotic high-frequency codes. Codes utilizing Geometrical Optics (GO), Physical Optics (PO), UTD, or the Physical Theory of Diffraction (PTD), are often used, but it is sometimes not well known whether the solution that is output will be completely accurate, especially in the case of bistatic predictions. For complex bodies, it is usually desirable to use a prediction code based on the Method of Moments (MoM) [47], which can produce an exact solution at the cost of computational time.

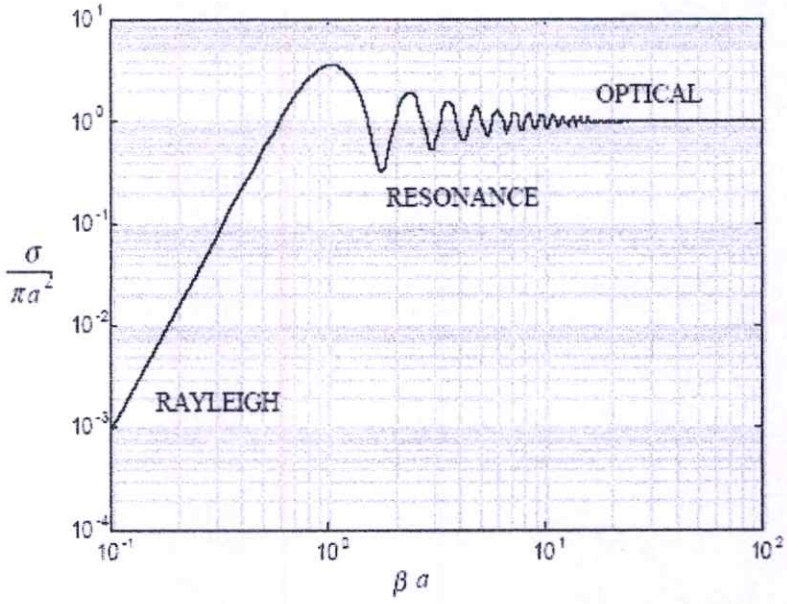

Figure 3.2 Scattering mechanisms [33].

3.4 Polarization

Polarization is an important property of an electromagnetic wave. The term polarization can be defined as the orientation and regularity of the electric and

magnetic field component, in a plane orthogonal to the direction of propagation of the wave.

The commonly used polarization is horizontal (H-polarization) and vertical (V-polarization). The H-polarized wave is transmitted with the E-field vector aligned parallel to the horizontal axis (in the x-y plane), and a V-polarized wave is transmitted with the E-field vector aligned perpendicular to the horizontal axis (parallel to the z-axis). In studies of scattering, the transmitter and the receiver work with either horizontal or vertical polarizations. Thus, there is a total of four modes available when studying scattering vertical-vertical (VV), horizontal-horizontal (HH), horizontal-vertical (HV), and vertical-horizontal (VH) [48]. Studying different scattering modes is very useful due to the diversity of ways in which waves and surfaces can interact. In this research, the type of measurement of polarization is co-polarization.

3.5 Near Field and Far Field

In RCS measurements, the incident wave is assumed to be a plane wave. The power emitted from the Tx antenna travels a short distance before merging into a coherent beam. This distance is known as the near zone (or near field) and marks the beginning of the Fresnel zone.

The object is located at a long range of the antenna. The wave front of this antenna is roughly spherical, so the radius of curvature of the wave front is the range from the antenna to the object. The region in which a spherical wave front can be assumed to be planar is called the far-field.

For obvious practical reasons an acceptable approximation must be used so that at some real range the wave front may be taken to be sensibly planar. This range is usually chosen to be as D/λ, and D denotes the maximum dimension of the antenna. The region beyond this range is known as the Fraunhofer zone [49].

3.6 Radar Cross Section Prediction Methods

Two types of RCS prediction methods are exact and approximate methods. The exact methods are based on integral or differential form of Maxell's equation.

Even when exact solutions are achievable, they are often difficult to interpret and to program using digital computers [33].

Due to the difficulties associated with the exact RCS prediction, approximate methods become attractive to predict the RCS. The majority of the approximate methods for computing scattered fields is available in both the Rayleigh and the optical regions, and each has its own strengths and limitations. These methods are usually the main source for predicting RCS of complex and extended targets such as aircrafts, ships, and missiles. When experimental results are available, they can be used to validate and verify the approximations.

The most common numerical RCS prediction methods for any arbitrary three–dimensional target are the method of moments (MOM), the finite difference time domain method (FDTD), and ray tracing methods. For each method, its advantages and limitations will be discussed.

3.6.1. Method of Moments

The most common technique used to solve an integral equation is the MOM. In the RCS prediction case, integral equations are derived from Maxwell's equations and the boundary conditions, with the unknown quantity being an electric or magnetic current (either volume or surface).

Another advantage of the MOM is that it provides a rigorous solution to the RCS prediction problem, yielding very accurate results. However, this method tends to produce large matrices, resulting in high computational requirements and increased run time. This method is therefore a numerical experimental tool.

3.6.2. Finite Difference Time Domain

The FDTD is today one of the most popular technique for the solution of electromagnetic problems. The FDTD method is a time domain solution of the Maxwell's equations described in differential form and is widely used in circuit analysis because of its simplicity. The method divides the space investigated into finite grid elements and on the grid the time and space approximation of the electrical and magnetic field strength is performed [50].

There exist many various forms of the FDTD in one, two or three dimensions and for many coordinate systems or grids and material types. For the indoor wireless channel simulation the three dimensional rectangular coordinate system was chosen with linear lossy dielectric materials in volumes.

In particular, the FDTD method has been explored by some researchers in the field of indoor radio propagation modeling. FDTD method has been employed in a wide range of electromagnetic propagation modeling studies. It has been successfully applied to an extremely wide variety of problems, such as scattering from metal objects and dielectrics, antennas, micro strip circuits, and electromagnetic absorption in the human body exposed to radiation. By directly solving Maxwell's equations in the time domain, the method fully accounts for the effects of reflection, diffraction and radiation. The medium constitutive relation is automatically incorporated into the solution of Maxwell's equations by using the FDTD method. Therefore, it is well suited to study wave interactions in complex media. The advantages of the FDTD method are its accuracy and that it simultaneously provides a complete solution for all points on the map, which can provide signal coverage information throughout a given area.

However, as a numerical analysis method, FDTD model requires large amounts of memory to keep track of the solution at all locations and for extensive calculations to update the solution at successive instants of time. With today's computational capabilities, it is generally unwieldy to do three-dimensional FDTD simulations for typical indoor areas which have dimensions on the order of meters.

This method also provides a rigorous solution to the RCS prediction problem. However, since it calculates the fields in a computational grid around the target, the calculation of the RCS of a target with a characteristic dimension of several orders of magnitude of the wavelength would entail a considerable amount of time to execute [51].

3.6.3. Ray Tracing

Ray tracing methods that can be used to analyze electrically large targets of arbitrary shape are referred to as microwave optics. This term actually refers to a collection of ray tracing techniques that can be used individually or in concert. The

most used methods are the geometrical optics (GO) method and the geometrical theory of diffraction (GTD) method, shooting and bouncing rays (SBR), physical optics, scattering center approach. The rules for ray tracing in a simple medium (i.e., linear, homogeneous and isotropic) are similar to reflection and refraction in optics. In addition, this method takes into account diffracted rays, which originate from the scattering of the incident wave at edges, corners and vertices. The major disadvantage of this method is the bookkeeping required when tracking a large number of reflections and diffractions for complex targets.

3.6.4. Physical Optics

The physical optics (PO) method estimates the surface current induced on an arbitrary body by the incident radiation. On the portions of the body that are directly illuminated by the incident field, the induced current is simply proportional to the incident magnetic field intensity. On the shadowed portion of the target, the current is set to zero. The current is then used in the radiation integrals to compute the scattered field far from the target.

This method is a high frequency approximation that provides the best results for electrically large targets as well as in the specular direction. However, the simplicity of the approach ensures low demands on computing resources and convenient run–times.

3.6.5. Scattering Center Approach

A much more intuitive approach to scattered field prediction is through analysis of radiation from scattering centers. Scattered field energy will constructively and destructively interfere as it is reflected from a target surface depends on the target geometry, transmitter/receiver orientation, frequency, and polarization. The nature of the contractive/destructive field zones can be described through a statistical relationship of the relative amplitude and phase between any two of a collection of simple scattering components of which the object appears to be comprised. From the receiver's perspective, the simple scattering component zones in which significant

constructive interference occurs appears to be the source locations from where the fields arise, and are thus called scattering centers.

Fields may or may not actually arise from these points, and in fact may be spatially separated from the target surface altogether. Yet they provide a basis from which target identification characteristics can be extrapolated quickly and efficiently. And, unlike the PO method, they capture the totality of the scattering contribution from all the scattering sources, including specular, diffraction, traveling waves, etc. This method is highly dependent on the target geometry in relation to transmitter and receiver, and in general, scattering centers exist only over a small angular extent. This implies that, although the approach may be valid for both monostatic and bistatic scattering, any monostatic scattering center model may not accurately represent a bistatic signature. However, several monostatic-to-bistatic equivalence theorems (MBET) have been proposed to establish just such a relationship, allowing one to convert monostatic information to an approximate bistatic data set.

3.7. Types of Measurement for RCS

For RCS measurement techniques, it is possible to distinguish between the following principles procedures:

1. Scalar RCS measurements $\Rightarrow \sigma, S$
2. Complex RCS measurements $\Rightarrow \overline{\sigma}, \overline{S}$
3. Polarimetric RCS measurements $\Rightarrow [\overline{\sigma}], [\overline{S}]$

The following types of modulation have a considerable influence on the measurement system: Pulse modulation, frequency modulation to continuous wave (FM-CW) modulation, Stepped frequency.

Measurements can be carried out in closed, low-reflective rooms, so-called anechoic chambers, and in open-air. This work considers the complex RCS measurement system.

3.7.1 Measurement of the Complex RCS

The Radar signature of scattering objects, expressed by the complex RCS, $\overline{\sigma}$, is a function of various parameters:

$$\bar{\sigma} = f(\text{frequency}, \text{polarization}, \text{angle}) \tag{3.7}$$

The requirements of the measuring system for a possible description of the scattering object result accordingly: broadband, coherent, for measuring a complex Radar cross-section $\bar{\sigma}$, measurement of the complex polar metric RCS Matrix, variable aspect angle $(\theta_i, \phi_i, \theta_s, \phi_s)$.

There has been a new generation of modern VNA for the measurement of microwave components. The VNA can be employed as the critical of a new type of RCS measurement system, especially for use in laboratories.

In principle the RCS measuring system is continuous wave (CW) Radar, however with substantially extended abilities. Equipment of this kind is called instrumentation Radar. The Fourier transform of the signals, received in the frequency range, into the time domain corresponds to a pulse response with a resolution corresponding to the measurement bandwidth. This procedure is related to pulse compression [9].

3.8 Factors of Measurement Inaccuracy

The calibration is applied to minimize the effect of systemic errors in the measurement. When a non-calibrated data are taken, it includes undesirable information and noise. Therefore, it must be filtered out before the data can have any value. There are several factors of the measurement inaccuracy such as: ground plane effect, antenna considerations and multipath.

3.8.1 Reflections from Walls and Mounting Apparatus

An indoor environment is surrounded with wall and ceiling and type of concrete ground. To minimize reflections from the ground and other effects, and the transmitting antenna that would interfere with the scattered field from the object, thus time gating method is applied. It is often desirable to reduce it further by means of background subtraction and range gating, but these methods introduce errors of their own.

3.8.2 Antenna Coupling

At large bistatic angles, as the receiving antenna moves into the main beam of the transmitter, the incident field of the transmitter becomes much larger than the scattered field from the object. Therefore, the antenna coupling is caused in the measurement.

3.8.3 Object Alignment Error

For measurement or calibration, it can sometimes be very difficult to precisely align an object. A misalignment of an object will always produce a deviation from the theoretical behavior of the object, but some objects may be more sensitive to alignment error, and produce deviations that are much worse than another object. In this work, Figure 3.3 for each target is modeled.

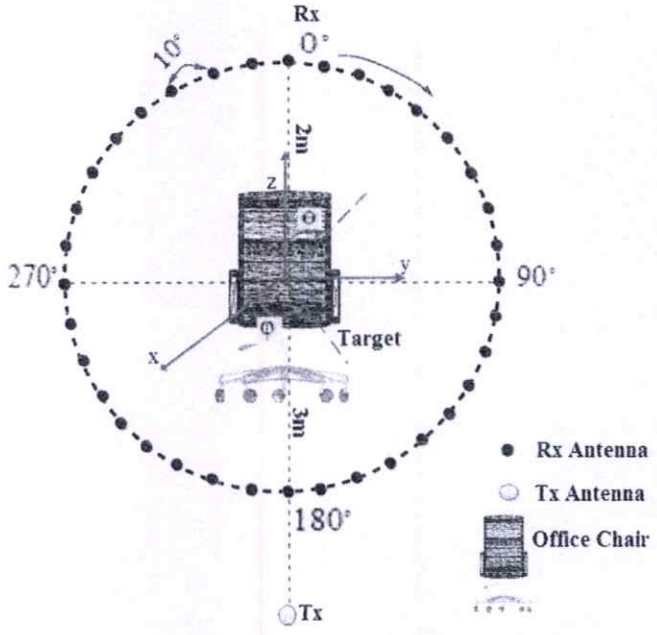

(a) Office chair model

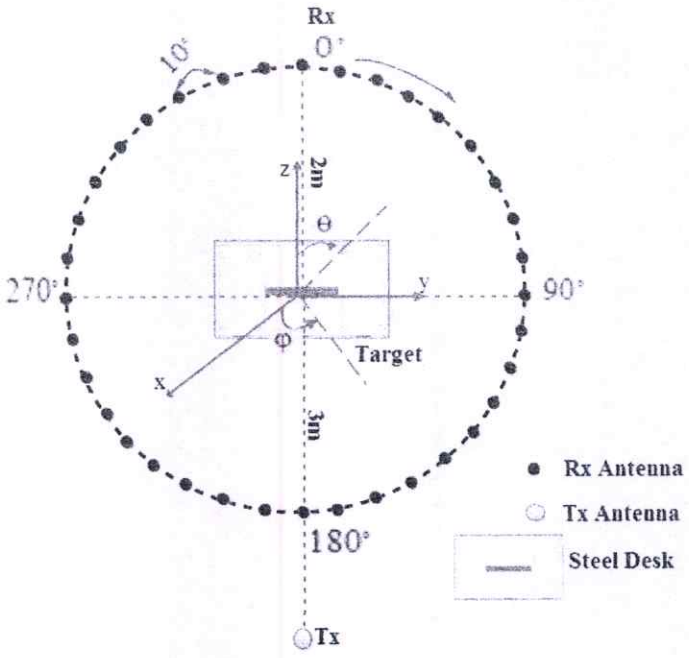

(b) Steel desk model

Figure 3.3 Illustration of orientation of each target model.

3.8.4 Near Field Effects

The scattering behavior of an object is not the same in the near-field as it is in the far field. A spherical wave front does not illuminate a distributed object with a single phase. Scattering points along the object are illuminated at a phase dictated by their location relative to the axis defined by the direction of propagation. The object will scatter these various phases, and they will interfere, as in the far-field case; but this interference will obviously produce different patterns because the relative phase of each scattering point from a near-field excitation are different than that of a far-field excitation.

3.9 Types of RCS Measurement Ranges

The RCS measurement facilities are indoor anechoic chambers, a large number of both indoor and outdoor ranges are in operation and testing of many applications.

To reduce the multipath effect from wall and ceiling, and ground reflection, anechoic chamber is used a test environment where the reflected electromagnetic energy from the chamber walls is attenuated and controlled to a specified low value. Indoor ranges suffer limitations in the size of the targets that can be measured, whereas outdoor ranges suffer downtime problems due to weather conditions. Although the indoor ranges offer protection against the weather and intruders, outdoor ranges can often measure full-scale targets under far-field conditions. Hence, it becomes necessary to have a suitable RCS measurement facility depending on the target size and measurement specifications. In this research, indoor ranges were applied to test all practical phenomena into consideration.

3.10 Data Processing

In this section, the procedure for processing the measured data and evaluation of RCS are presented. However, the irregularity of the shape larger than the wavelength can make it impossible to use the reflection model. In such a case multiple scattering centers may be identified, and each of them is modeled as a small scatter. When the scatterer size is smaller than the first Fresnel zone of the path under investigation, as well as when the scattering centers are modeled, radar equation is applicable.

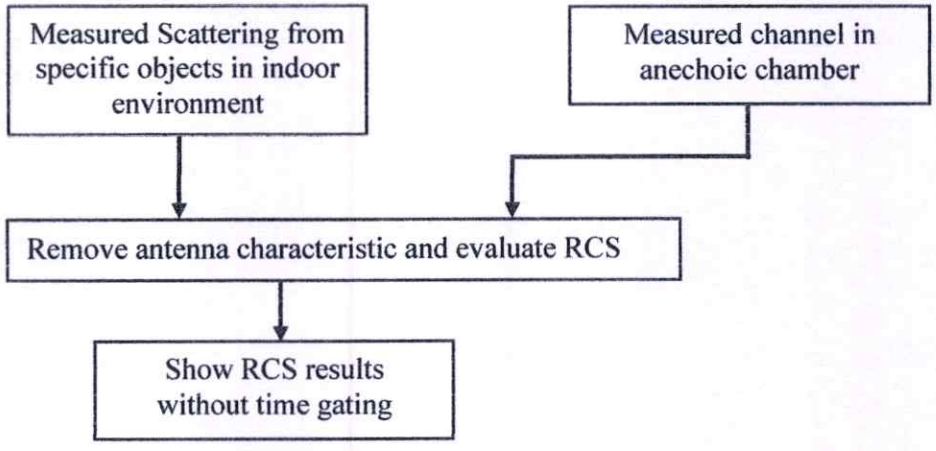

(a) Evaluation of RCS without time gating

The procedure is summarized in the block diagram shown in Figure 3.4. As mentioned earlier, two measurements are performed; the first is the free-space in the absence of the material at anechoic chamber, while the second is the measurement that is performed with the target in place. Measurements are carried out in the frequency domain. Then, the characteristic of antenna is removed and the RCS of the complex target in propagation is evaluated. Time gating approach is used to reduce the multi-path effects caused by the surrounding environment.

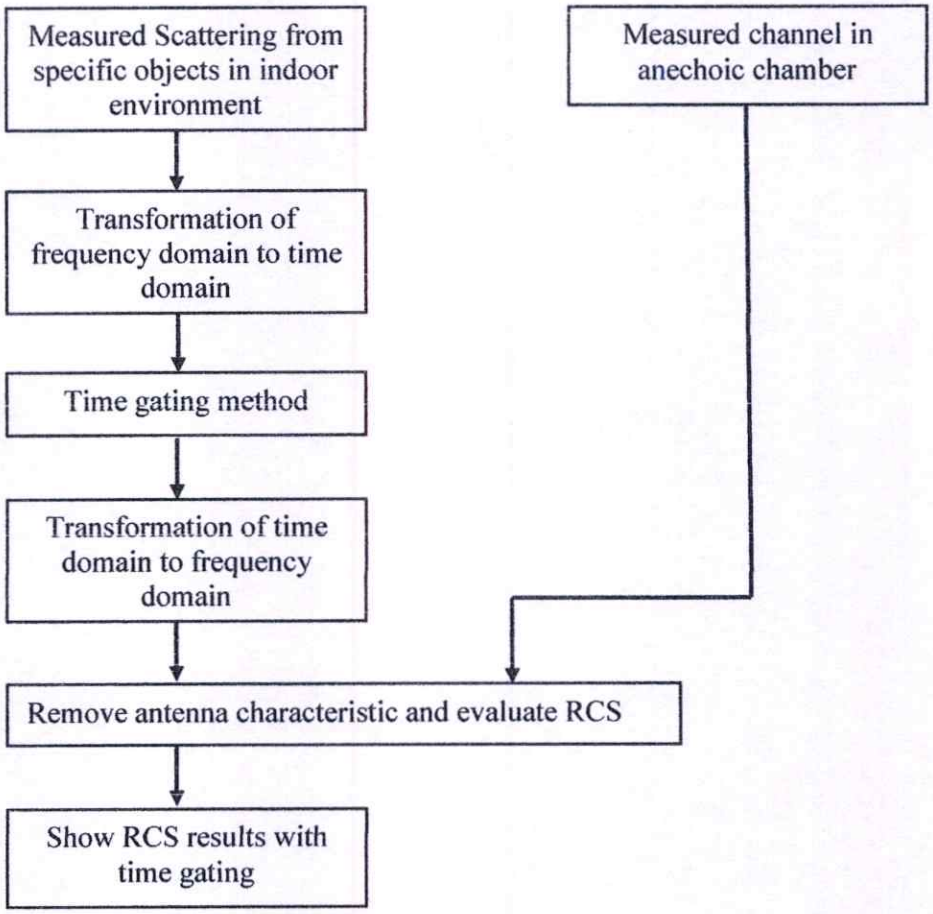

(b) Evaluation of RCS with time gating

Figure 3.4 Block diagram of data processing.

The RCS of a target is a function of frequency, polarization, and target orientation and should be independent of measurement instrumentation and surrounding environment such as walls. However, the raw data obtained from RCS

measurements contain unwanted effects such as noise, antenna coupling, ground reflection, multi- path effects, antenna gain, and distance to target. The unwanted effects fall into two groups; the first is caused by extraneous signals such as noise, antenna coupling and multi-path effect, ground reflection, and the second is caused by the dependence of the measurement system on transmitting power level, cable loss, antenna gain, distance to target, and receiver mixer performance. In an ideal case, the receiver output in the absence of the target should be zero. However, an undesirable background signal exists in all measured data due to residual scattering of the surrounding environment and significant coupling between the transmitting and receiving antennas. This undesirable signal can be removed by measuring the background data and performing a complex subtraction of the target data or by using time gating approach. This research proposed the time gating method to remove the unwanted signal for RCS measurement data.

3.10.1 Time Gating Method

Time gating is required to remove the multi-path components in receiving signals. The original frequency domain data (magnitude and phase) are transformed using an Inverse Fourier Transform to give a time domain impulse response and filter out the late time pulses, which are caused by the multi-path interferences, by imposing a modified gating window. The extracted time domain response is then transformed back to provide more accurate frequency domain responses.

To avoid abrupt changes on the signal level, the gating window should have a smooth transition from zero to the flat level. The frequency-domain data are weighted by a window function prior to inverse Fast Fourier Transform (IFFT) in order to reduce sidelobes in the time domain. Among well-known as window shapes are very useful in many signal processing, such as the Kaiser window [52]. The actual equation of the Kaiser window in the library is given in Equation 3.8.

$$w(n) = \frac{I_0\left(\pi\alpha\sqrt{1-(\frac{2n}{N-1}-1)^2}\right)}{I_0(\pi\alpha)}, 0 \le n \le N-1 \qquad (3.8)$$

where N is the length of the sequence. I_0 is the zeroth order Modified Bessel function of the first kind.

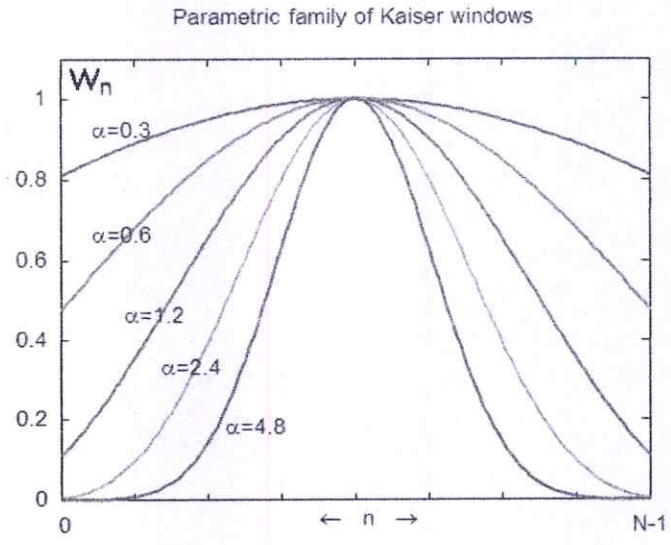

Figure 3.5 Kasier-Bessel window [52].

Also, α is an arbitrary, non-negative real number that determines the shape of the window. In the frequency domain, it determines the trade-off between main-lobe width and slide lobe level, which is a central decision in window design. The Kaiser-Bessel window is illustrated in Figure 3.5 for some different beta values. The performance of the Kaiser-Bessel window has the ability to keep the maximum energy in the main lobe (i.e. narrow main lobe width) and can reduce side-lobe level.

The time domain impulse response is then gated using a modified Kaiser-Bessel window. This allows the high frequency portion of the impulse response to be maintained, while smoothing the late-time effects of the gate truncation. The overall length of the gating window can be adjusted to remove unwanted multi-path reflections. Once the gated impulse response is complete, the data are transformed back to the frequency domain. The length of the gating window determines the lowest valid frequency in the gated frequency domain data, and a low frequency correction using the original low frequency data, is required as the final step. The gate is centered on the target, and the gate width corresponds to approximately 17 nanoseconds. The gated data are transformed back to the frequency domain with FFT routine in the MATLAB library.

3.11 Extension and Proposed of UWB Radar Equation

The acronym RADAR stands for RAdio Detection And Ranging. The radar range equation provides a very useful mathematical relationship for assessing and for the effectiveness of efforts to alter radar target cross section. Knowing radiation power of an antenna and some variables that can be measured, the power measured at a receiving antenna can be computed. The derivation follows closely the ones that can be found in Kingsley and Quegan [53], Sullivan [54], Woodhouse [55], and Skolnik [31]. The process used by the bistatic type, for the transmission by an antenna, to the reception by the antenna is theoretically explained by the radar equation as described in Figure 3.6.

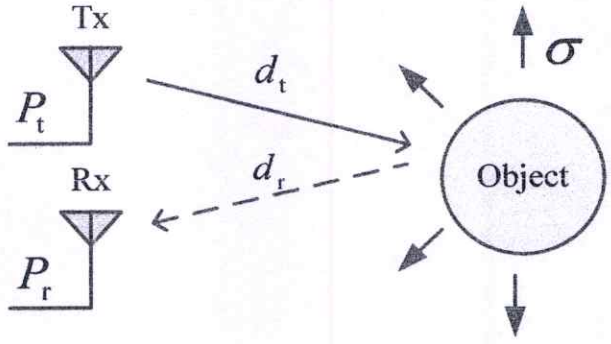

Figure 3.6 The proposed of UWB radar equation [9].

The radar equation accounts for radar system parameters, target parameters, background effects (clutter, noise, interference, and jamming), propagation effects (reflection, refraction, and diffraction) and propagation medium (absorption and scatter). The equation shows that the received power is a direct function of the transmitted power, the gains of the transmitting and receiving transmitters, the frequency (wavelength), and the RCS, and is indirectly proportional to the fourth power of the distance from the target to the receiving antenna.

The UWB radar equation [9] is commonly used to describe the relationship between the received power and a target. For the radar link from a Tx to a receiver antenna Rx and with the polarizations of both antennas pointing to a scattering target, the received power $P_r(f,\theta_i,\phi_i,\theta_s,\phi_s)$ can be calculated from:

$$P_r(f,\theta_i,\phi_i,\theta_s,\phi_s)=\frac{c^2}{64\pi^3 f^2 d_t^{\,2} d_r^{\,2}}\sigma(f,\theta_i,\phi_i,\theta_s,\phi_s)G_t(f)G_r(f)P_t(f) \tag{3.9}$$

where $P_t(f)$ is the transmitted power, $G_t(f)$ is the gain of the Tx, $G_r(f)$ is the gain of the Rx, d_t and d_r are the respective distances from the target to Tx and Rx, $\sigma(f,\theta_i,\phi_i,\theta_s,\phi_s)$ is the RCS of the target, c is the velocity of light, f is a carrier frequency, θ_i and ϕ_i are the elevation and azimuth incident angles to the target, and θ_s and ϕ_s are the elevation and azimuth scattering angles from the target.

This thesis has adopted the extended version of the radar equation which incorporates the channel transfer function of scattering to evaluate RCS. The experimental targets are singly placed between Tx and Rx under a bistatic condition. The channel transfer function of scattering in frequency domain, $H_{sc}(f,\theta_i,\phi_i,\theta_s,\phi_s)$, can be written as

$$H_{sc}(f,\theta_i,\phi_i,\theta_s,\phi_s) = \left[\frac{c}{8(\pi)^{3/2} f d_t d_r}H_\sigma(f,\theta_i,\phi_i,\theta_s,\phi_s)e^{-j2\pi f(d_t+d_r)/c}+H_c(f,\theta_i,\phi_i,\theta_s,\phi_s)\right]H_t(f)H_r(f) \tag{3.10}$$

where $H_c(f,\theta_i,\phi_i,\theta_s,\phi_s)$ is the transfer function in the indoor environment without scattering targets, such as floors, walls, ceiling, and the mutual coupling between Tx and Rx, $H_t(f)$ is the transfer function of Tx, $H_r(f)$ is the transfer function of Rx, and $H_\sigma(f,\theta_i,\phi_i,\theta_s,\phi_s)$ is the channel transfer function of scattering, where σ can be determined from

$$\sigma(f,\theta_i,\phi_i,\theta_s,\phi_s)=\left|H_\sigma(f,\theta_i,\phi_i,\theta_s,\phi_s)\right|^2 \tag{3.11}$$

The experiments attempt to evaluate the indoor RCS of the furniture items, $H_\sigma(f,\phi_s)$. However, the channel transfer function in an indoor environment without scattering, $H_c(f,\phi_s)$, is inevitable in such measurement. The time gating method is applied to remove $H_c(f,\phi_s)$ using the Kaiser-Bessel window in time

domain, $w(t,\theta_i,\phi_i,\theta_s,\phi_s)$ in Equation 3.12, and the impulse response of scattering component, $h_{sc}(t,\theta_i,\phi_i,\theta_s,\phi_s)$ in Equation 3.14. Then, channel transfer function after time gating, $H_{ti}(f,\phi_s)$ in Equation 3.15, is scaled by the channel transfer function in free space, $H_{fr}(f)$ in Equation 3.16, to remove $H_t(f)$ and $H_r(f)$. The final result is $H_\sigma(f,\phi_s)$ in Equation 3.17.

The Kaiser-Bessel window is used in time domain to extract scattering from the target at a delay time of $(d_t+d_r)/c$. The Kaiser-Bessel window $w(t,\theta_i,\phi_i,\theta_s,\phi_s)$ is defined as

$$w(t,\theta_i,\phi_i,\theta_s,\phi_s)=\begin{cases}\dfrac{I_0\left(\pi\alpha\sqrt{1-\left\{\dfrac{2\left[t-t_p(\theta_i,\phi_i,\theta_s,\phi_s)\right]}{T}\right\}^2}\right)}{I_0(\pi\alpha)} & t_p-\dfrac{T}{2}\le t\le t_p+\dfrac{T}{2}\\ 0 & \text{otherwise}\end{cases} \tag{3.12}$$

where T is the window width, α is a window shape parameter whose value is 4.8, $t_p(\theta_i,\phi_i,\theta_s,\phi_s)$ is set at the time around $(d_t+d_r)/c$ to capture the impulse response corresponding to the scattering component, and $I_0(x)$ is the zero-th order modified Bessel function of the first kind which can be expressed as

$$I_0(x)=\frac{1}{\pi}\int_0^{\pi}e^{x\cos(\theta)}\,d\theta \tag{3.13}$$

The impulse response of scattering component $h_{sc}(t,\theta_i,\phi_i,\theta_s,\phi_s)$ can be calculated from

$$h_{sc}(t,\theta_i,\phi_i,\theta_s,\phi_s)=\int_{-\infty}^{\infty}H_{sc}(f,\theta_i,\phi_i,\theta_s,\phi_s)e^{j2\pi ft}df \tag{3.14}$$

The frequency transfer function after time gating $H_{ti}(f,\phi_s)$ can be estimated from

$$H_{ti}(f,\theta_i,\phi_i,\theta_s,\phi_s)=\int_{-\infty}^{\infty}h_{sc}(t,\theta_i,\phi_i,\theta_s,\phi_s)w(t,\theta_i,\phi_i,\theta_s,\phi_s)e^{-j2\pi ft}dt$$

$$\approx\frac{c}{8(\pi)^{3/2}fd_td_r}H_\sigma(f,\phi_s)e^{-j2\pi f(d_t+d_r)/c}H_t(f)H_r(f) \qquad (3.15)$$

The measurement of the channel transfer function of free space, $H_{fr}(f)$, was carried out in an anechoic chamber prior to substituting in (3.14) to remove $H_t(f)$ and $H_r(f)$. The Tx and Rx antennas were aligned such that they pointed at each other to obtain a direct link. The channel transfer function of free space, $H_{fr}(f)$, can be written as, where d_f is the distance from Tx to Rx.

$$H_{fr}(f)=\frac{c}{4\pi fd_f}e^{-j2\pi fd_f/c}H_t(f)H_r(f) \qquad (3.16)$$

The channel transfer function of scattering, or RCS, is finally derived and can be expressed as

$$H_\sigma(f,\phi_s)=\frac{\sqrt{4\pi}\,d_td_r}{d_f}e^{j2\pi f(d_t+d_r-d_f)/c}\frac{H_{ti}(f,\theta_i,\phi_i,\theta_s,\phi_s)}{H_{fr}(f)} \qquad (3.17)$$

Therefore, time gating is a more simple and natural way to evaluate and eliminate the noise which is occurred in channel propagation.

3.12 Conclusion

This chapter discussed the importance of RCS, its role in the radar equation, and its significance in the outcome of indoor channel model. It provides the formal definition of RCS, its behavior in the scattering regions and the most common methods for RCS prediction are explained. The block diagram of data processing for

improvement and evaluation of RCS is shown. The approach of time gating method and evaluation of RCS of complex target is described. Finally, the extension and evaluation radar equation for RCS in indoor channel propagation is described.

CHAPTER 4

MEASUREMENT SETUP FOR SCATTERING FROM FURNITURE

4.1 Introduction

The measurement setup system in this thesis is shown in Figure 4.1. The exact solution needed for frequency response RCS measurements using the HP 8510C network analyzer consists of the real and imaginary parts of the scattered field at the desired bistatic angle. The HP based system requires the real and imaginary field for the desired bandwidth divided into 800 equal intervals or 801 data pairs. A vector signal analyzer (VNA) captures the phase and magnitude response of the frequency. Vector signal analyzers (VSA) are typically very flexible and can display results at the time, frequency and modulation domains. In this measurement system, the double waveguide horns antennas are used for transmit and receive antennas; two furniture items such as an office chair and a steel desk are used as test equipments. Frequency domain measurement systems are used in this research. The measurement frequency range is from 3 GHz to 7 GHz for UWB range. Different polarizations: Vertical to Vertical (VV) and Horizontal to Horizontal (HH) polarizations test for RCS measurement.

4.2 Description of Channel Measurement

In this section, equipments and tools which are necessary to test the experimental result in practice are discussed.

4.2.1. HP-8510C VNA

The frequency-domain scattered field measurement system, depicted in Figure 4.2, is implemented on an HP-8510C network analyzer [56] using its stepped frequency mode. The system consists of an Synthesized Sweepers (HP 83620A) as a

radio frequency (RF) source, an 8514B S-Parameter test set, 45 MHz to 20 GHz, an HP-8510C network analyzer as an intermediate frequency (IF) receiver, horns antennas as transmitting and receiving antennas, and an IBM PC-compatible computer with MATLAB as a data acquisition workstation.

System components are selected for scattered field measurements of 3 GHz to 7 GHz. The system operates by spanning the frequency bandwidth 801 steps. The maximum number of frequency steps allowed by the analyzer is used to maximize the unambiguous time extent. The magnitude and phase data for 3 GHz to 7 GHz frequencies are transferred from the HP-8510C to the computer over the Hewlett-Packard interface bus (HPIB) bus, stored on the internal hard disk, and subsequently processed by a digital signal processing algorithm written in MATLAB.

For each frequency step, the system is continuous-wave (CW) signals are transmitted through the transmitting antenna in an indoor environment. The RF energy reflected by the target is collected by the receiving antenna.

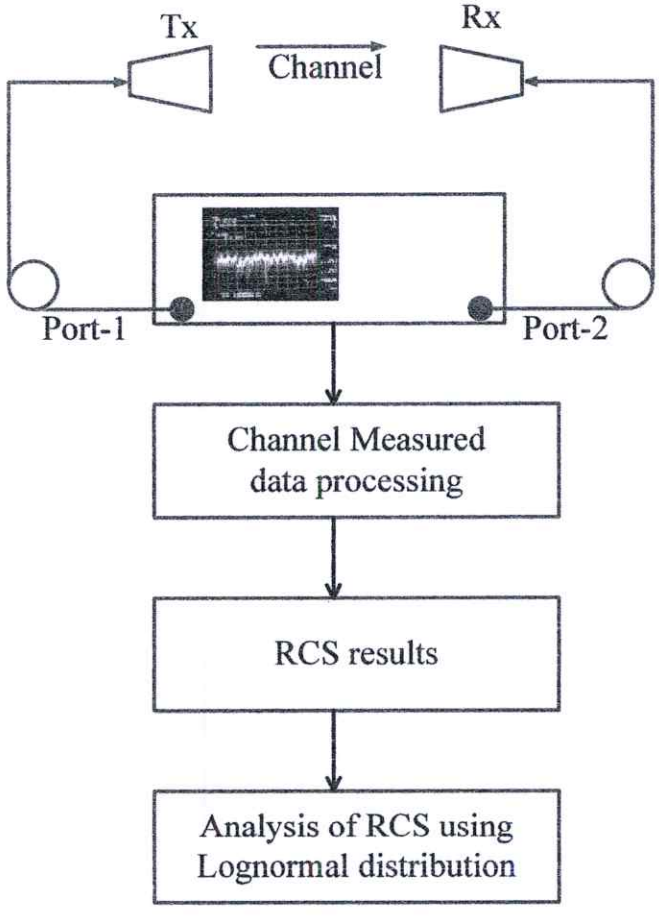

Figure 4.1 Block diagram of experiment [56].

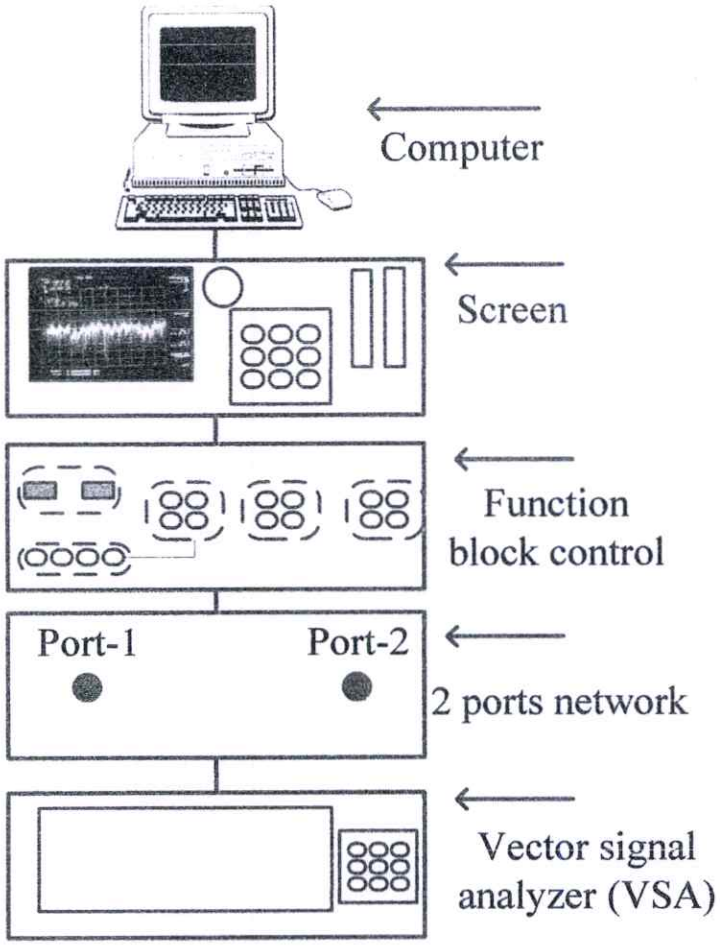

Figure 4.2 VNA test set [56].

4.2.2 Horn Antenna

Double waveguide horns (Model 3115) [57] are used for transmitting and receiving antennas to meet wideband requirements. This coaxially-fed, it covers wide frequency range between 1 GHz to 18 GHz. The 1 GHz to 18 GHz frequency range of horn antenna is shown in Figure 4.3. The channel variation can be affected by the movement of the antenna, the change of the alignment and distance between the antennas as well as the shadowing effect that line of sight (LOS) path can be excluded by introducing obstacles between them. Table 4.1 shows the specifications of horn antenna.

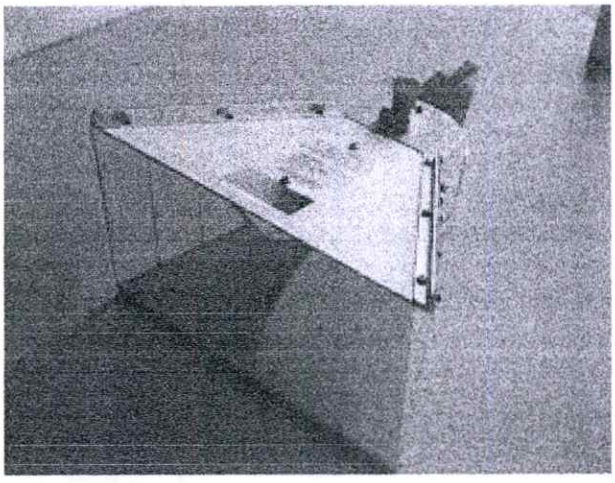

Figure 4.3 The double-ridged waveguide horn antenna [57].

Table 4.1 The specifications of horn antenna [57]

Frequency range	1 GHz – 18 GHz
VSWR	1.5
Impedance	50 Ohms
Connector type	N Type
Width	24.4 cm (9.6 in)
Depth	27.9 cm (11.0 in)

4.2.3. Anechoic Chamber

To measure the channel transfer of the antennas, the anechoic chamber is employed. The anechoic chamber, shown in Figure 4.4, is located in the wireless communication laboratory, King Mongkut's Institute of Ladkrabang (KMITL), measures 3.5 m × 6 m × 2.95 m meter in length, width, and height and is shielded using Styrofoam. Double waveguide horns [57] are used for Tx and Rx antennas are utilized to measure the transfer function in an anechoic chamber free space. Both of antenna heights are 1.4 m and the distance from the Tx antenna to the Rx antenna is 2 m and aligned pointing at each other in Figure 4.4.

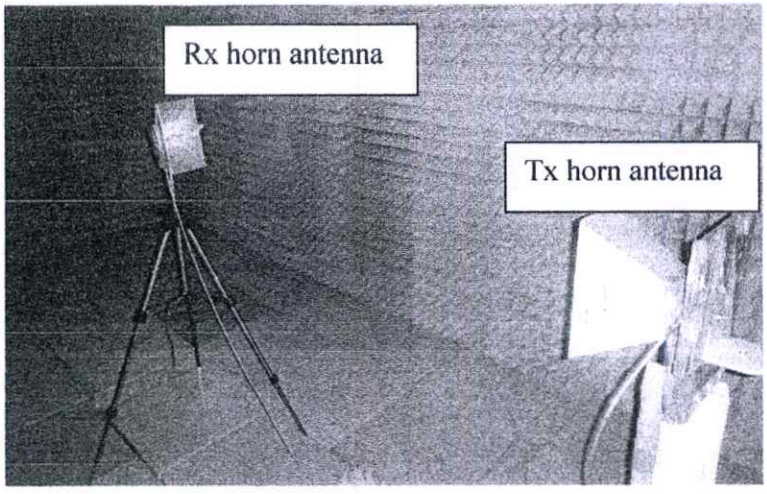

Figure 4.4 The measurement setup in anechoic chamber.

(a) Office chair (b) Steel desk

Figure 4.5 The illustration of the scattering targets.

4.2.4 Scattering Target

Measurements were performed on two furniture items at the frequencies 3 GHz to 7 GHz. The object under test is an office chair is made from copper and a steel desk which is made from aluminum. The office chair is 1 m × 0.62 m × 0.44 m (H × W × L). The size of the desk is 0.76 m × 1.37 m × 0.66 m (H × W × L). Figure 4.5 shows the photograph of objects. Figure 4.5 (a) shows a chair and (b) as desk respectively.

4.2.5 Modeling of Measurement Setup

In this section, the details about the measurement procedure are presented. Locations where the measurements were conducted are also described to allow for understanding some of the site-specific trends.

The VNA (HP-8510C) is used to define measurement parameters and control the measurement process; it can be operated manually with front panel keys or remotely through an HPIB bus. In remote operation, measurement parameters such as frequency range, number of frequency points, and averaging factor, can be set from a computer by sending proper commands on the HPIB bus. Setting the appropriate parameters is essential to step-frequency RCS measurement system.

A sequence of measurements was completely undertaken prior to analysis of the RCS of the experimental furniture items. The measurement setup and procedure are detailed next.

The VNA was utilized to measure the magnitude and phase of the transmission coefficients. The VNA was operated in the response measurement mode, where port-1 and port-2 where the transmitter and receiver ports, respectively. The full 2-port method was utilized to calibrate the analyzer to suppress the noise level and to improve the sensitivity and accuracy measurement. Two double-ridged waveguide horn antennas were used, one as Tx and the other as Rx, with an operating frequency range of 1 GHz to 18 GHz for both vertical and horizontal polarizations. Two experimental scattering targets were an office chair of 1 m × 0.62 m × 0.44 m (H × W × L) and a steel desk of 0.76 m × 1.37 m × 0.66 m (H × W × L).

In general, an accurate RCS is achievable only in an anechoic chamber in which the effects of walls, floor, ceiling, and other background clutters are removed. Nevertheless, since the available anechoic chamber is too small to fit the two horn antennas and either of the scattering targets with sufficient space remaining for running the experiments, the experiments were thus carried out in two steps: (1) the evaluation of RCS with the existence of either target in the indoor open area of floor 6 of Engineering-Building; and (2) the antenna calibration in the anechoic chamber.

For the setup, the frequency range is from 3 GHz to 7 GHz with a total of 801 frequency points. The averaging factor was set at 4096 to reduce the noise level and improve the signal-to-noise ratio (SNR). The sweep time was 200 ms and the

intermediate frequency bandwidth (IFBW) of the vector network analyzer was 10 kHz. The measurement at each angle required approximately 15 minutes. The maximum transmitted power of 10 dBm was selected to obtain the maximum system dynamic range, and the received impulse response of each receiver position was recorded. For the RCS in the presence of either of the scattering targets, the distance from Tx to the center of the target was 3 m, and the distance between the center of the target and the Rx antenna was 2 m. The experiments were conducted in the near field (Fresnel) region due to space and power limitations. Both Tx and Rx were placed at a height of 1.5 m from the ground. The receiving antenna was rotated with a 10-degree increment around the scattering target for a total of 36 positions. The measurements were thus repeated with varying the angle of Rx while that of Tx remained stationary to achieve the directional pattern of bistatic RCS between Tx and Rx, assuming that $\theta_i = \theta_s = 90°$, $\phi_i = 180°$ and $\sigma(f, \theta_i, \phi_i, \theta_s, \phi_s)$ is simplified to $\sigma(f, \phi_s)$. Figure 4.6 illustrates the top and side views of the bistatic RCS, while Figure 4.7 (a)-(d) are photographs of the measurement setups for the chair and desk for vertical-vertical (VV) and horizontal-horizontal (HH) polarizations.

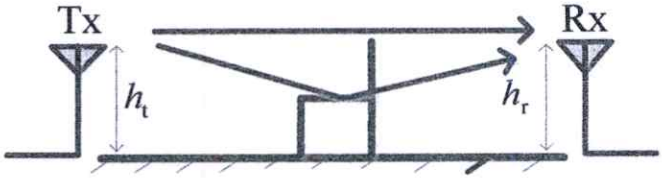

(a) Office chair

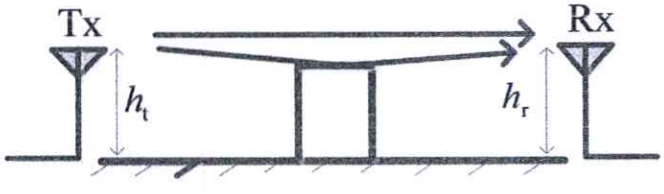

(b) Steel desk

Figure 4.6 The model of side view.

In the calibration, the antenna measurement in the anechoic chamber was carried out to determine the channel transfer function of free space as shown in Figure 4.4.

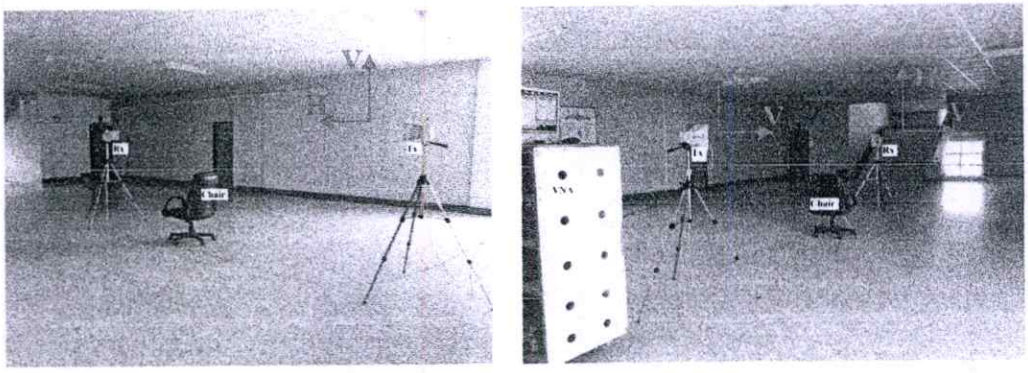

(a) VV polarization with chair (b) HH polarization with chair

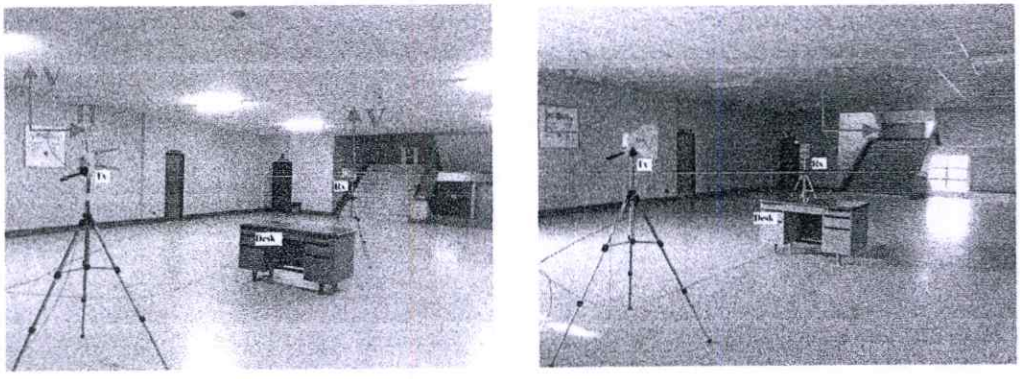

(c) VV polarization with desk (d) HH polarization with desk

Figure 4.7 Bistatic measurement setups for an office chair and a steel desk.

4.3 Conclusion

In this chapter, the measurement configuration of office chair and steel desk are discussed. Measurements for RCS of furniture are done by using VNA channel sounding in frequency domain and two double wave guide horn antennas are used. In this measurement system, vertical-vertical and horizontal to horizontal polarizations are considered. After the experimental setup is completed, the result discussion will be shown in the chapter 5.

CHAPTER 5
EXPERIMENTAL RESULTS

5.1 Introduction

When a frequency response RCS measurement is performed, an exact target data file is acquired. As the bistatic angle between the antennas change, the exact target's data solution changes as well. In this chapter, the results of RCS and the comparison of RCS with time gating and without time gating are described.

The backscatter signal from complex target in an indoor environment varies statistically with aspect angles and frequencies. The characterization of the fluctuation statistics of RCS of complex target using the lognormal distribution model is proposed in this work. A significant multipath can occur due to the ground reflections and the irregularity of the complex target shape. Thus, frequency samples are used as random fading samples to model the statistical behavior of the RCS. Two samples such as an office chair and a steel desk are applied.

In order to determine an acceptable fit between the RCS data and the lognormal distribution model, Kolmogorov-Smirnov non-parametric goodness of fit test procedures are applied to the data. A number of significant statistical parameters: mean, standard deviation and cumulative distribution function are displayed. It is not only important to understand the RCS characteristics of a target but also to look into the diagnostic mode of study where factors contributing to a particular RCS values are studied.These results can be used to predict the backscatter from the complex target.

5.2 Measurement Results and Discussion

Figure 5.1 (a) and (b) show the broadside-broadside (0°) gains and phases of the horn antennas relative to the frequency. Moreover, this section is described the results of RCS for each object and different volarization.

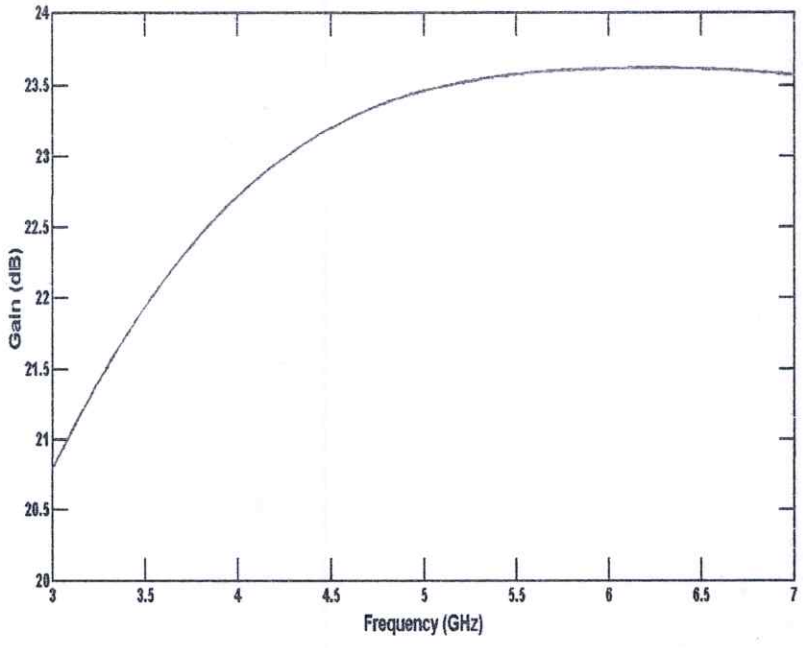

(a) Gain

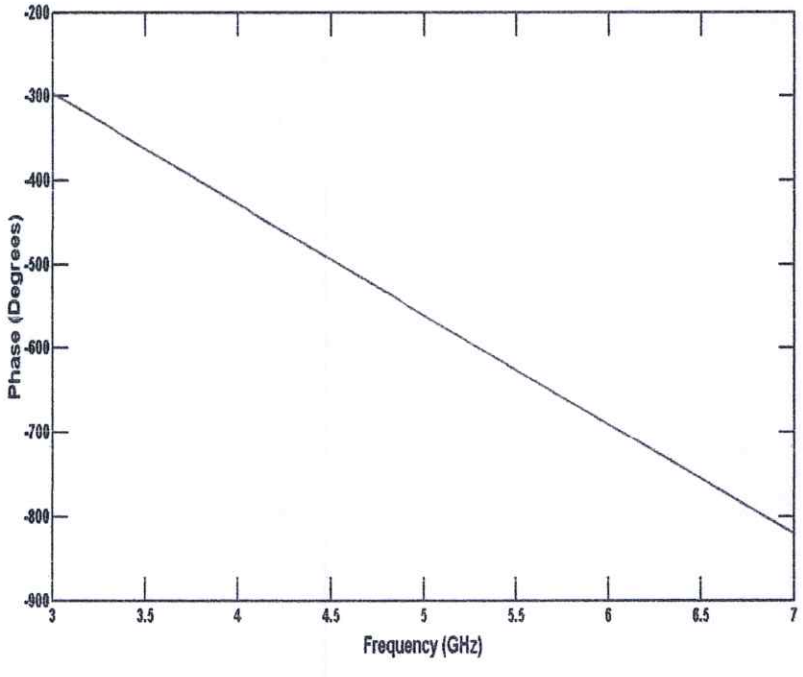

(b) Phase response

Figure 5.1 Gain and phase response of horn antennas.

5.2.1 Channel Impulse response

This section presents how the accuracy of conventional ray tracing simulation technique can be improved upon with the proposed extended radar equation. The indoor RCS of the two scattering targets, i.e., office chair and steel desk, were evaluated in the frequency range of 3 GHz to 7 GHz in VV polarization and HH polarization. It is found that the VV- and HH-polarizations yielded different RCS.

This thesis utilized time gating to remove the multipath effect in the received signals. The time gating method transforms the frequency domain response into a time domain response and also filters out the late time pulses, which are attributable to the multipath effect as shown in Figure 5.2 and Figure 5.3 of each target. It is observed from Figure 5.2 (a), (c) and Figure 5.3 (a), (c) that the multipath effects are very small and some undesired but significant signals are difficult to remove from the main signals. As can be seen that unwanted signal is removed by using time gating. Therefore, smooth signals of RCS have been obtained. For all targets, the large response after 17 ns is the backscatter of the object. The signal between 17.5 ns and 18 ns is caused by reflections probably at the antenna input and the pulse shaper output. This reflection is also transmitted and scattered by the object.

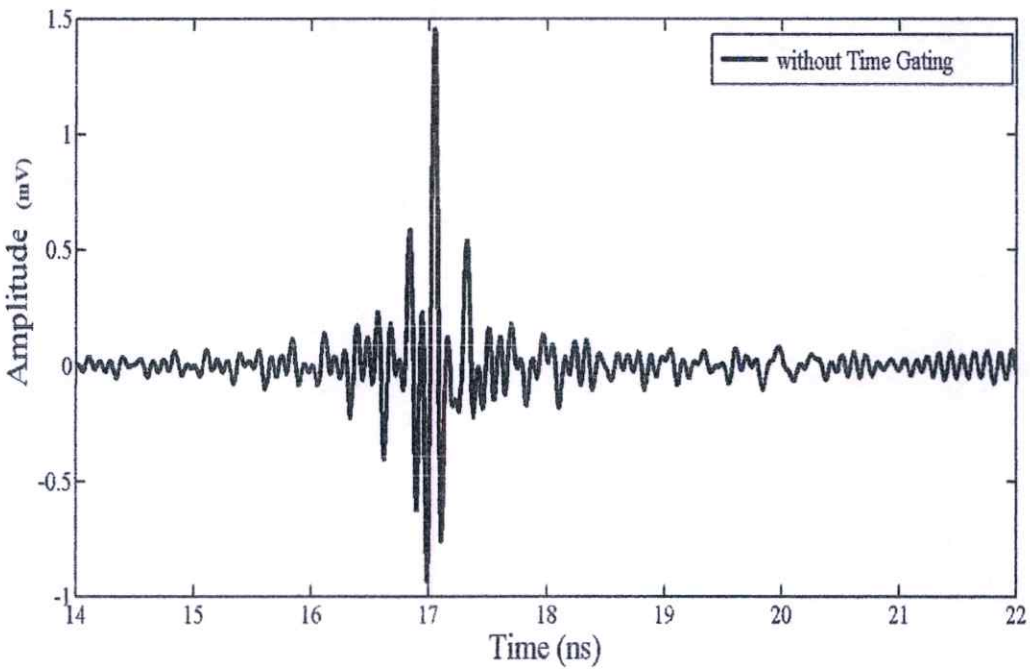

(a) Without time gating in VV polarization

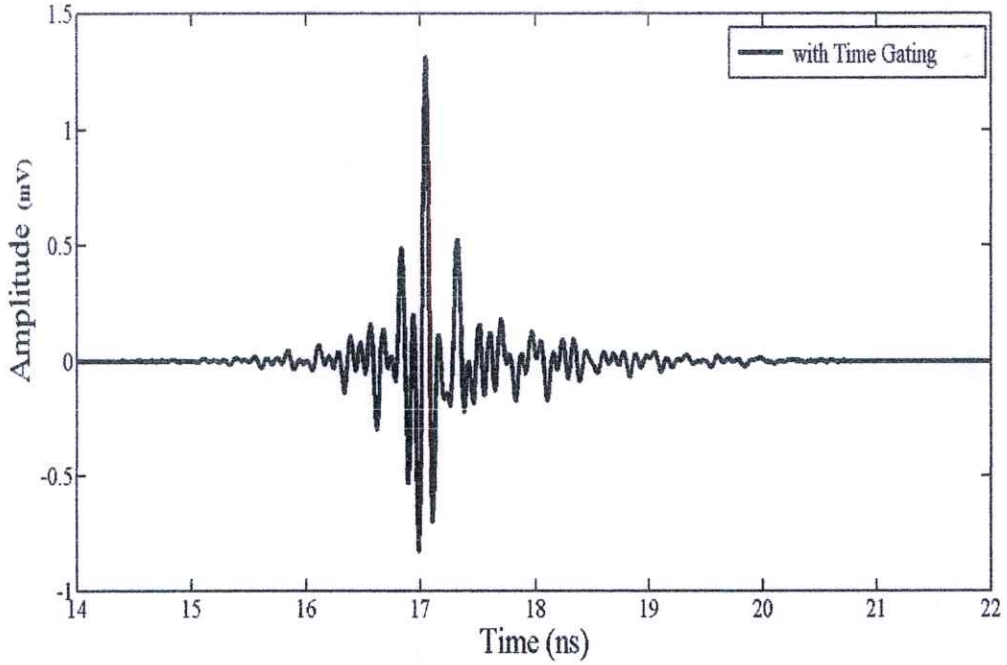

(b) With time gating in VV polarization

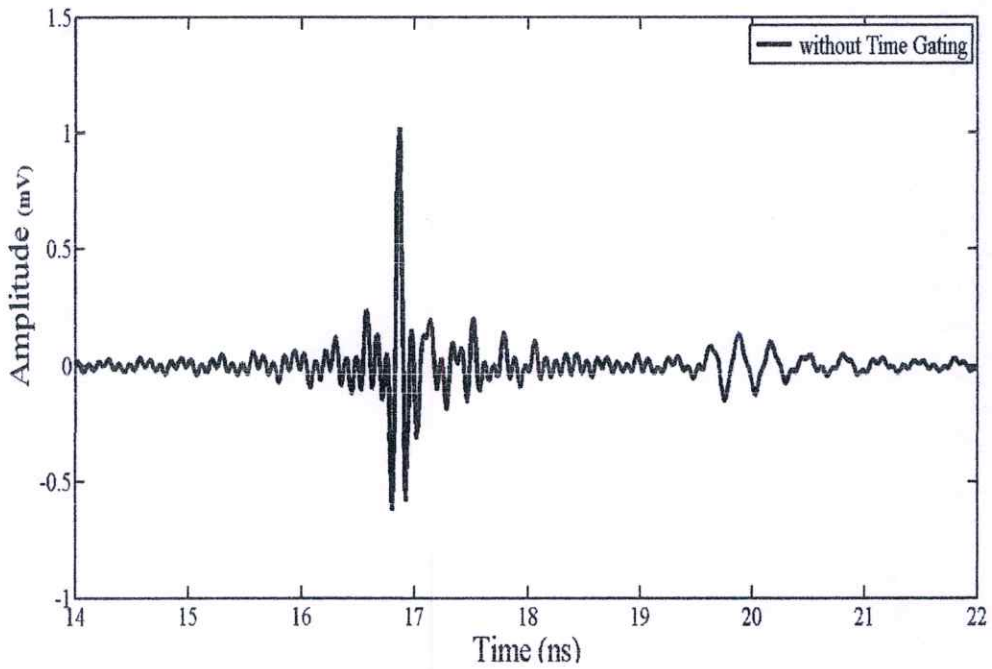

(c) Without time gating in HH polarization

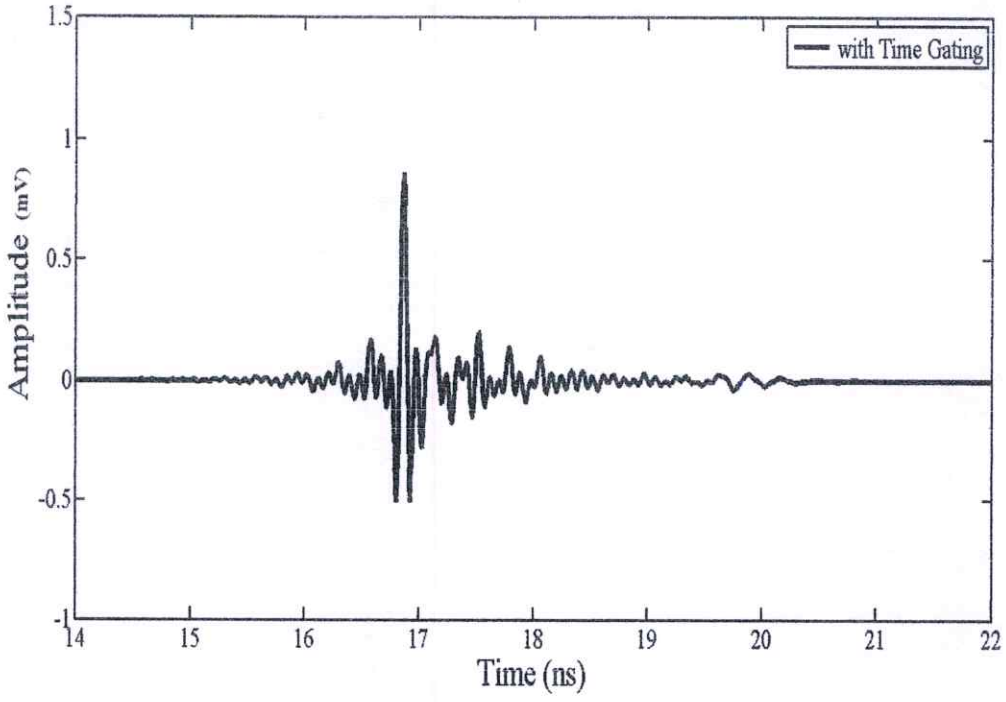

(d) With time gating in HH polarization

Figure 5.2 The impulse response of scattering from the office chair.

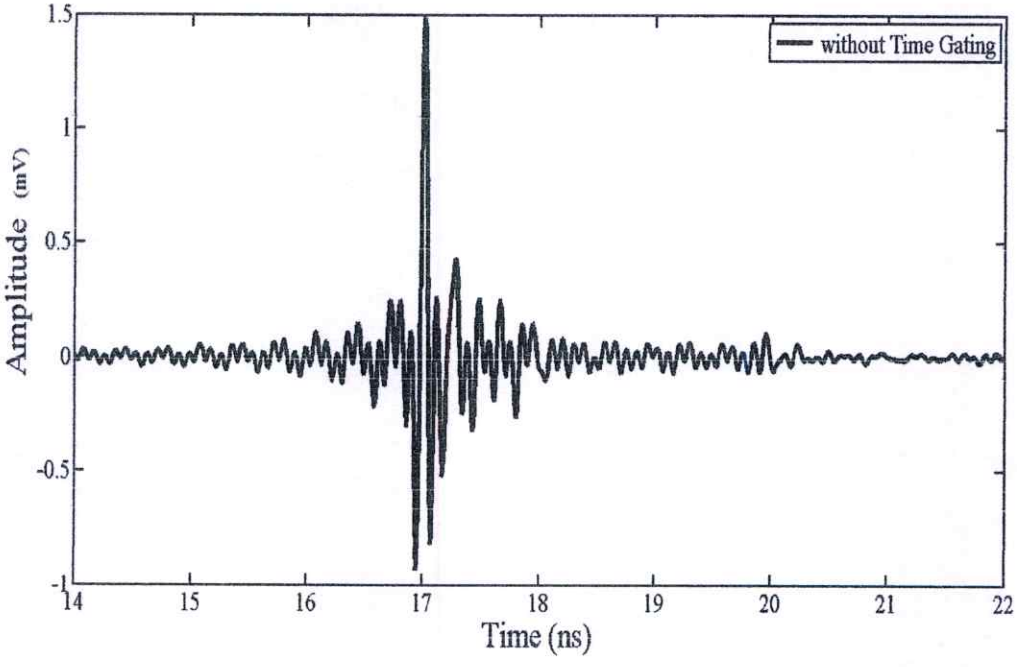

(a) Without time gating in VV polarization

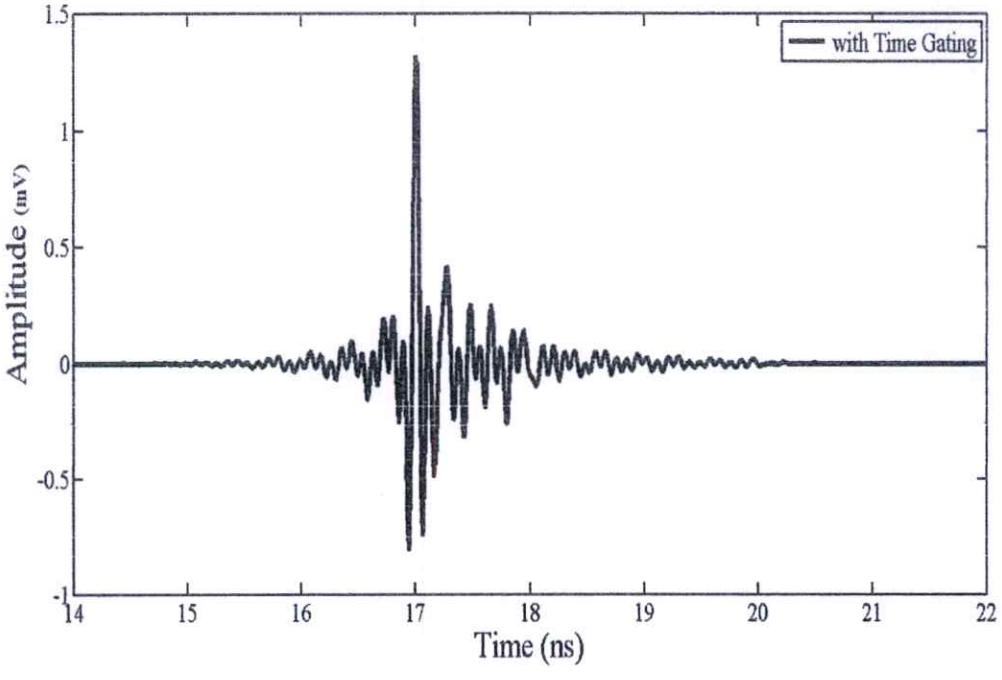

(b) With time gating in VV polarization

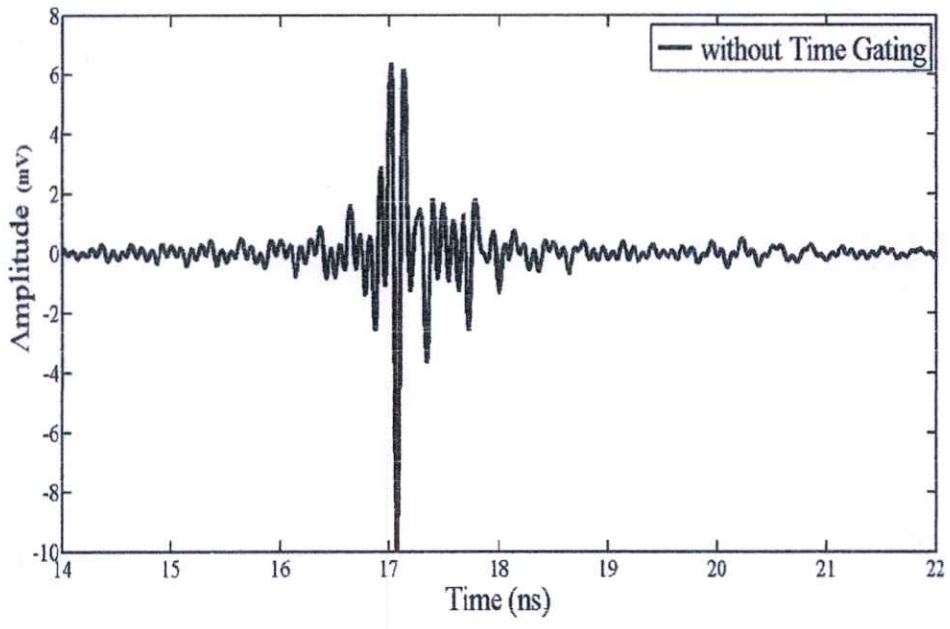

(c) Without time gating in HH polarization

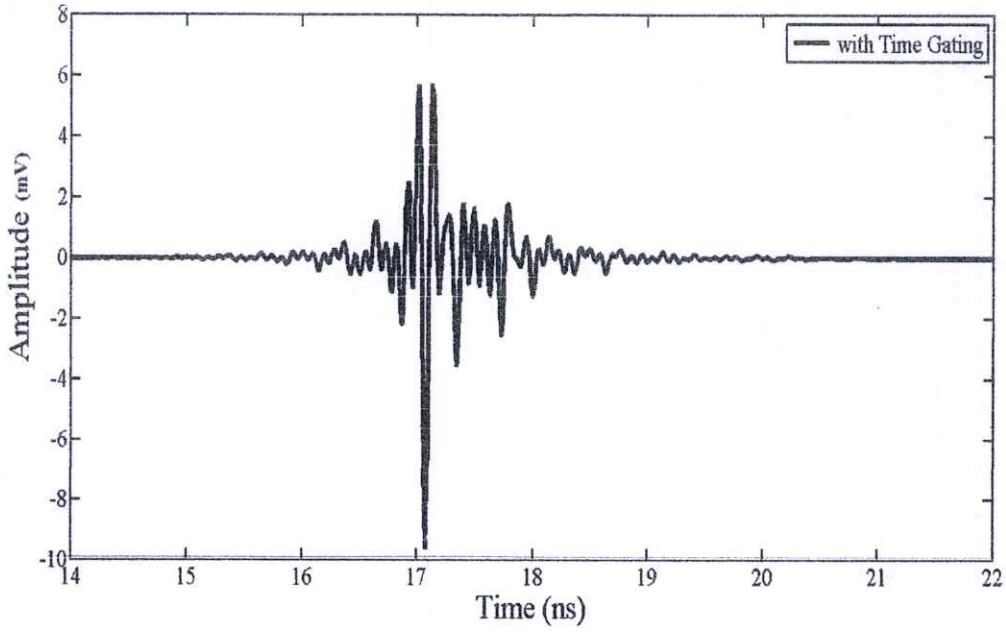

(d) With time gating in HH polarization

Figure 5.3 The impulse response of scattering from the steel desk.

5.2.2 Magnitude of RCS

To demonstrate the effectiveness of time gating in removing the multipath effect, the comparison between the RCS of the chair without and with time gating is provided as shown in Figure 5.4 and Figure 5.5, respectively.

Figure 5.4 shows the comparison of the RCS without and with time gating along the frequency range of 3 GHz to 7 GHz and different incident angles for each object. Figure 5.4 (a) and (b) are chair for VV polarization and Figure (c) and (d) are RCS results of HH polarization of chair. In Figure 5.4 (a) and (c), without time gating the scattering from the chair induces the interferences and ripples in RCS, while in Figure 5.4 (b) and (d), the time gating reduces the ripples in the main beam.

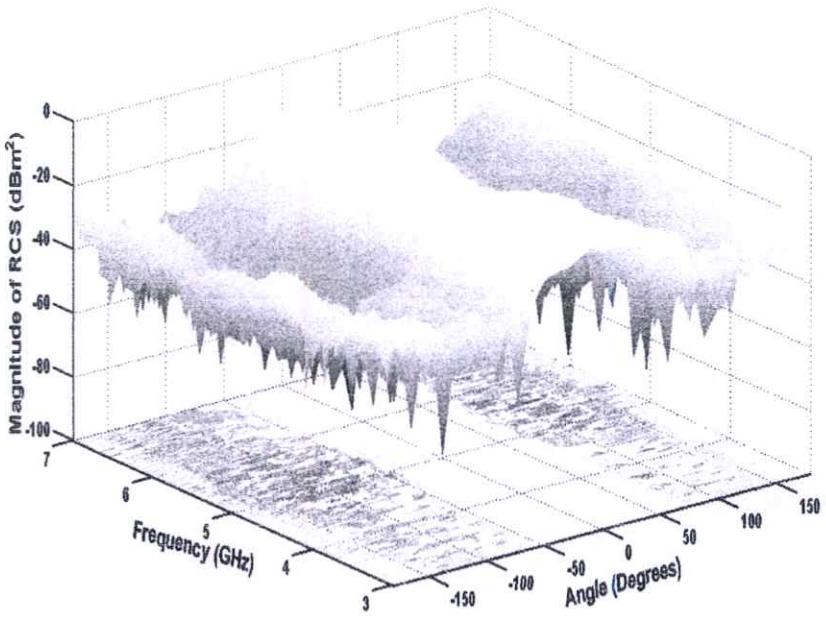

(a) Without time gating in VV polarization

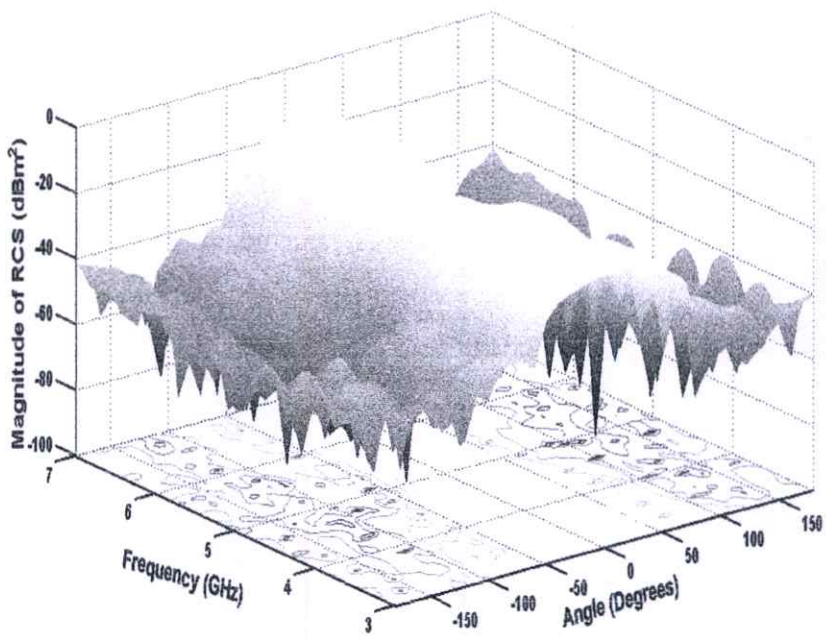

(b) With time gating in VV polarization

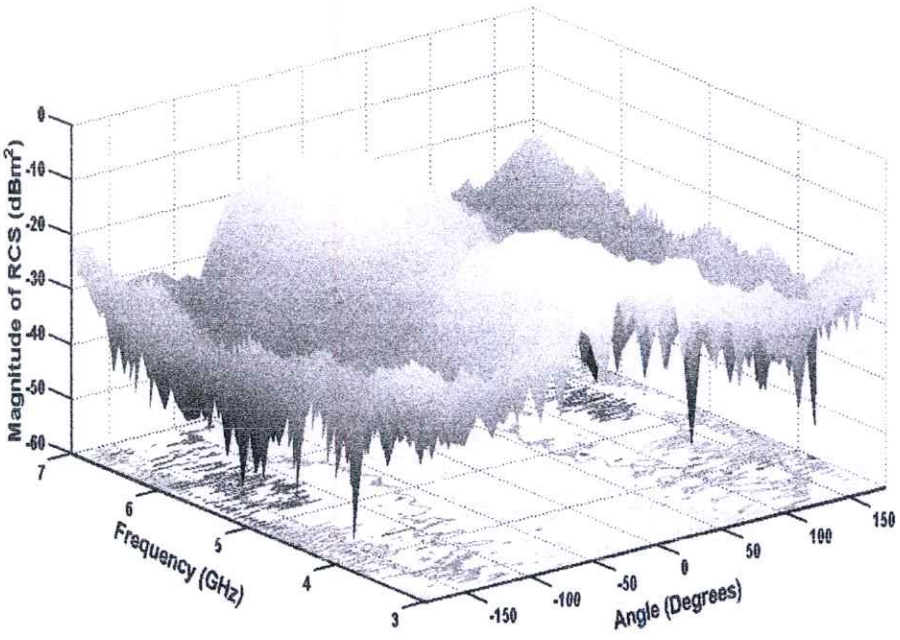

(c) Without time gating in HH polarization

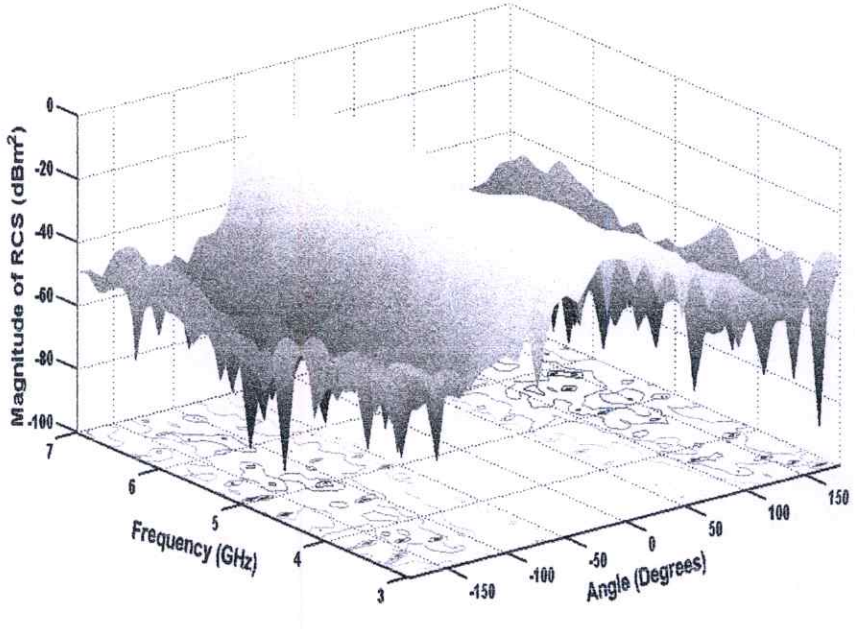

(d) With time gating in HH polarization

Figure 5.4 Comparisons of RCS scattering from the office chair.

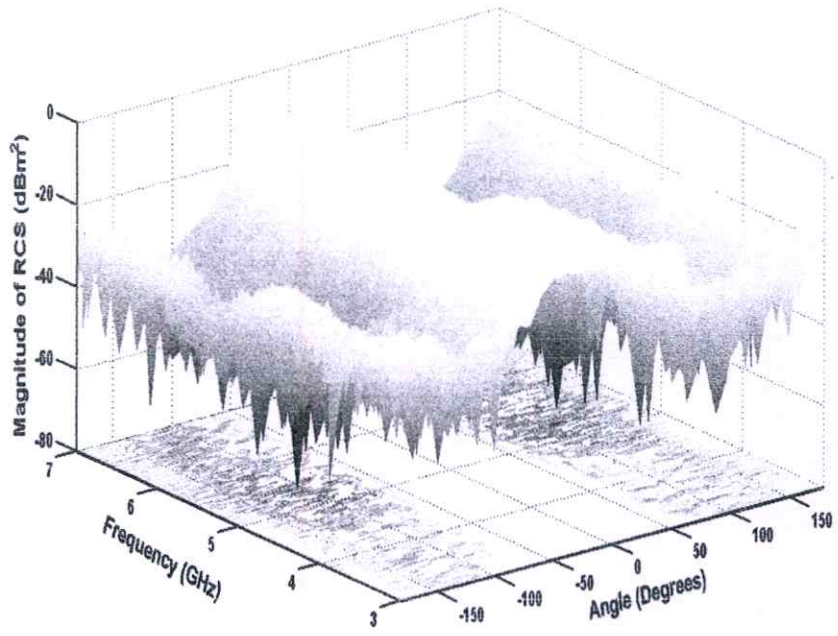

(a) Without time gating in VV polarization

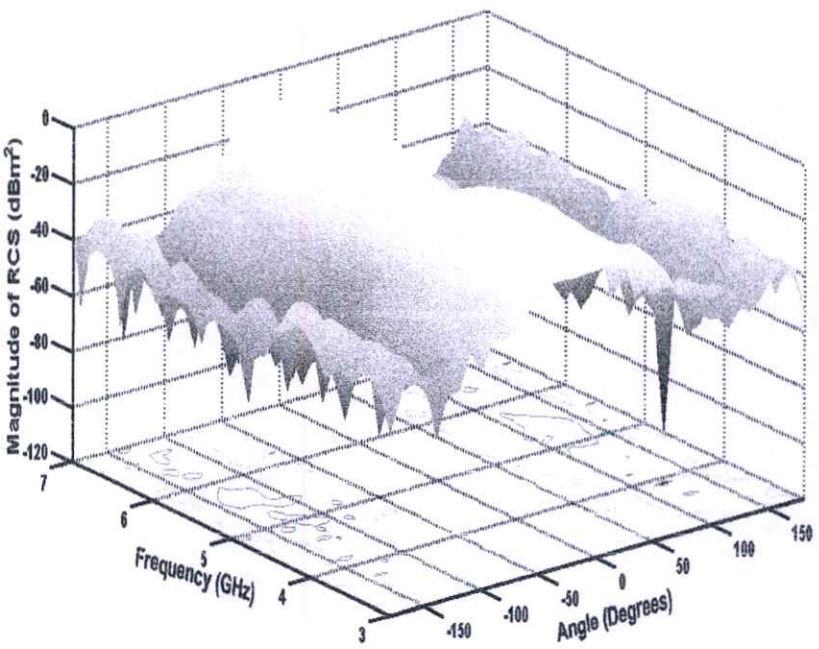

(b) With time gating in VV polarization

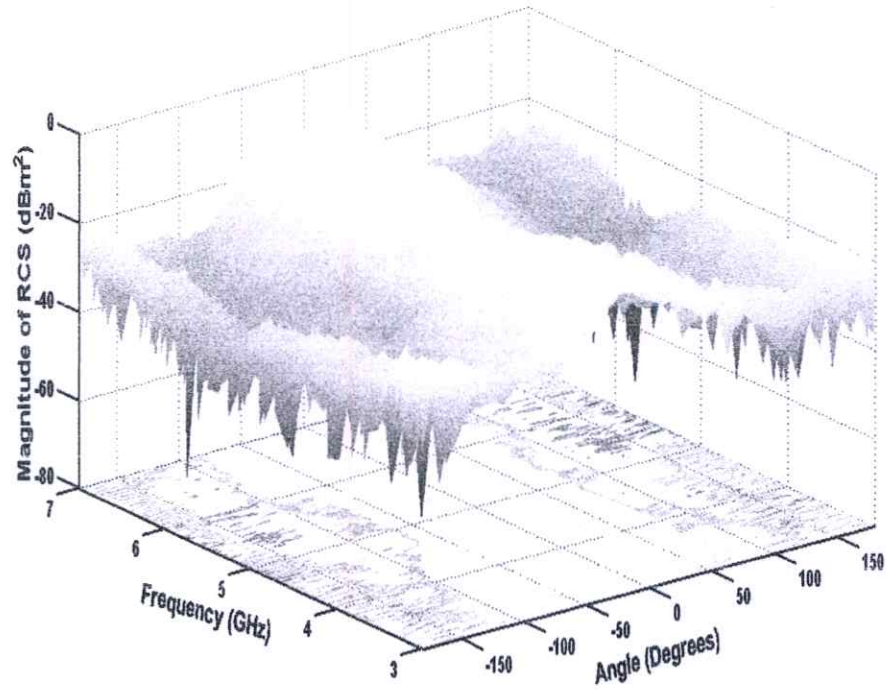

(c) Without time gating in HH polarization

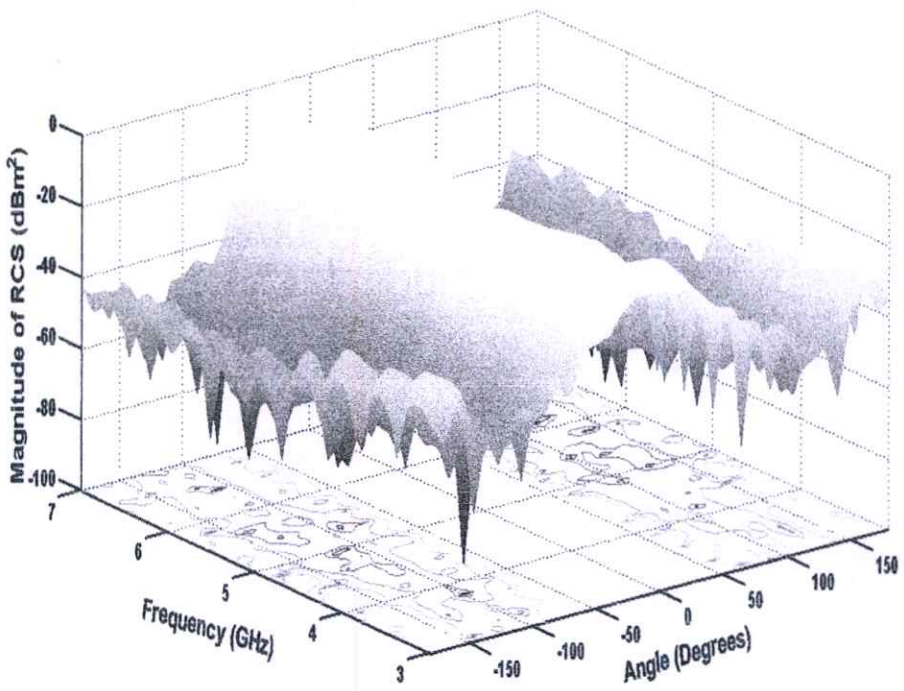

(d) With time gating in HH polarization

Figure 5.5 Comparisons of RCS scattering from the steel desk.

For desk for each polarization, as shown in Figure 5.5 (a) and (c) are without time gating of RCS and Figure 5.5 (b) and (d) are with time gating of RCS. In Figure 5.5 (a) and (c), without time gating the scattering from the chair also induces the interferences and ripples in RCS, while in Figure 5.5 (b) and (d), the time gating also reduces the ripples in the main beam. Besides, the scattering lobes beyond 90° are reduced to below 20 dBm^2, resulting in a significant reduction in the edge diffraction effect, which in turn makes the scattering effect easier to extract for each scatterer. As shown in Figure 5.4 (b) and (d) and Figure 5.5 (b) and (d), the multipath effects from 90° to 180° and -90° to -180° along the frequency range of 3 GHz to 7 GHz is considerably removed. Finally, the more accurate RCS with time gating can be achieved.

5.2.3 Magnitude and Phase of RCS with Time Gating

For frequency response RCS measurements using the HP 8510C network analyzer, the real and imaginary parts of the scattered field are at the desired bistatic angle. As the bistatic angle between the antennas increase, the magnitude of the difference between the measured main lobes peaks increases as well. The side lobes from the measurements match in quantity, placement, and width.

The 3D graphics of RCS with time gating of the experimental chair for VV and HH polarizations are illustrated in Figure 5.6 and Figure 5.7, respectively, while those of the desk for VV and HH polarizations are depicted in Figure 5.8 and Figure 5.9. It was observed that the RCS for HH polarization is larger than that of VV polarization for most observation angles. In addition, RCS varies with changes in incident angle and frequency.

For instance, RCS at 0° of the chair for VV polarization at the frequencies of 3 GHz and 5 GHz are -40 dBm^2 and -62 dBm^2, respectively; and for HH polarization are -36 dBm^2 and -53 dBm^2 at the same frequencies. In the case of the desk at 0°, the RCS for VV polarization at 3 GHz and 5 GHz are respectively -55 dBm^2 and -47 dBm^2; and -36 dBm^2 and -46 dBm^2 at the same frequencies for HH polarization. The findings indicate that RCS is subject to types of scattering objects, angle, frequency and polarization.

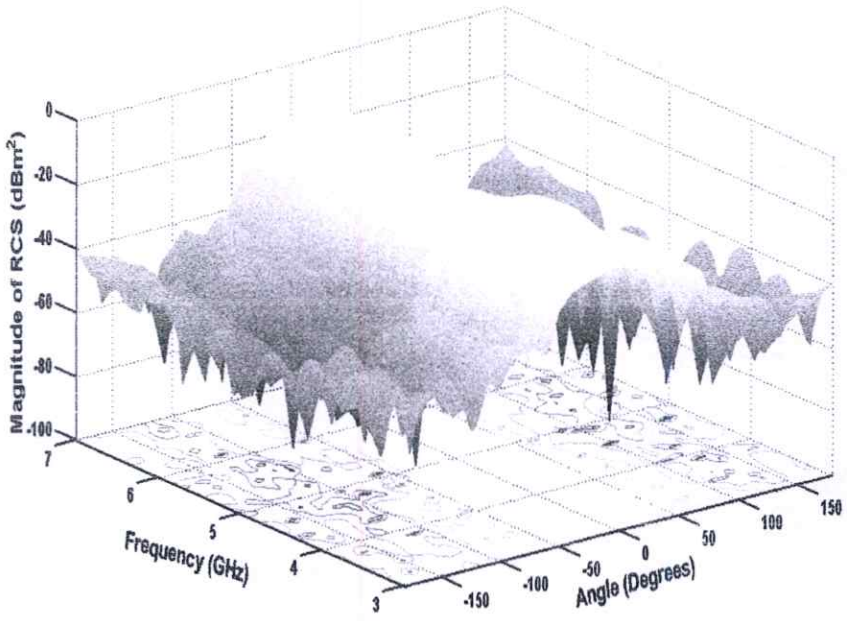

(a) Magnitude

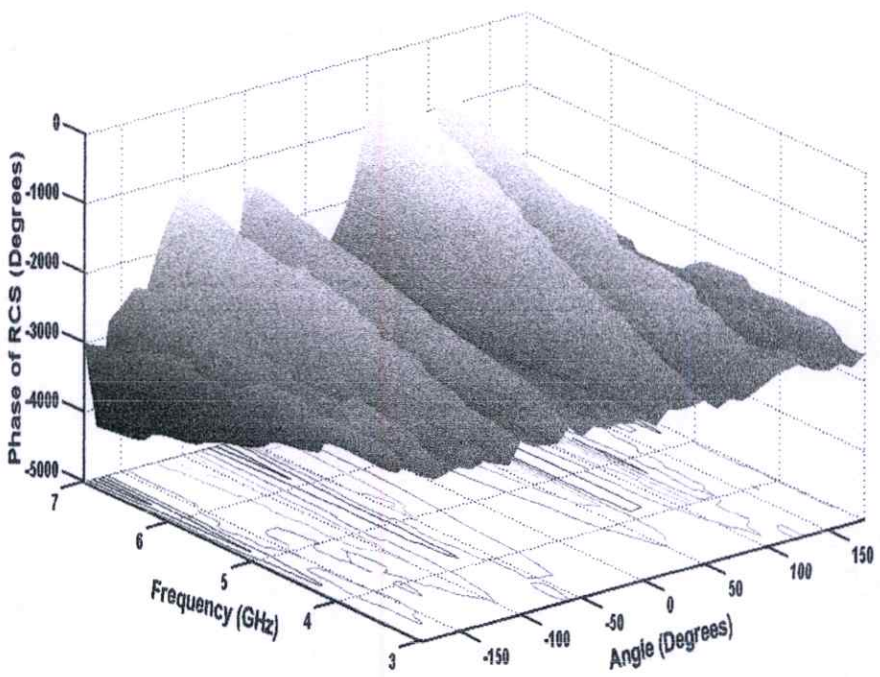

(b) Phase

Figure 5.6 The RCS for the experimental office chair in VV polarization.

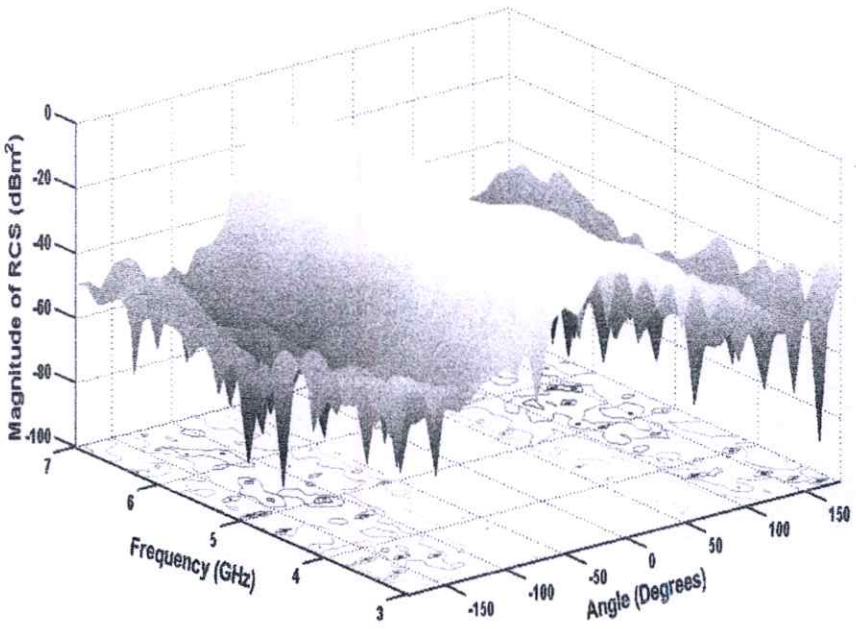

(a) Magnitude

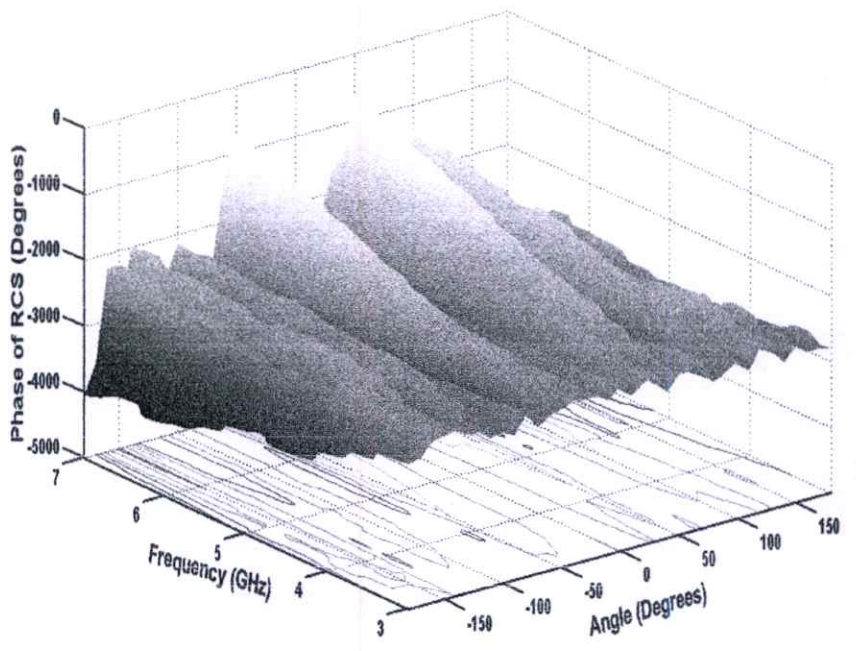

(b) Phase

Figure 5.7 The RCS for the experimental office chair in HH polarization.

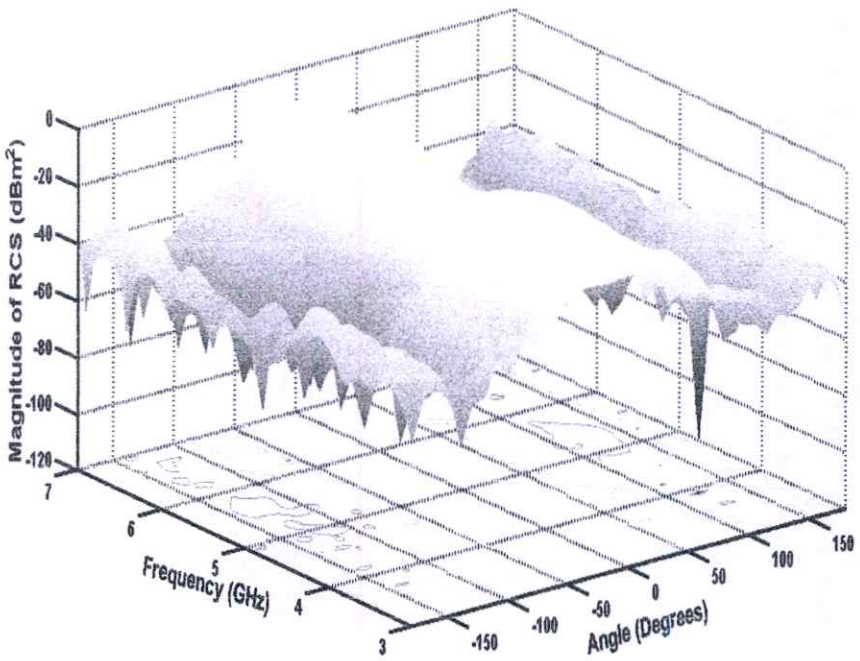

(a) Magnitude

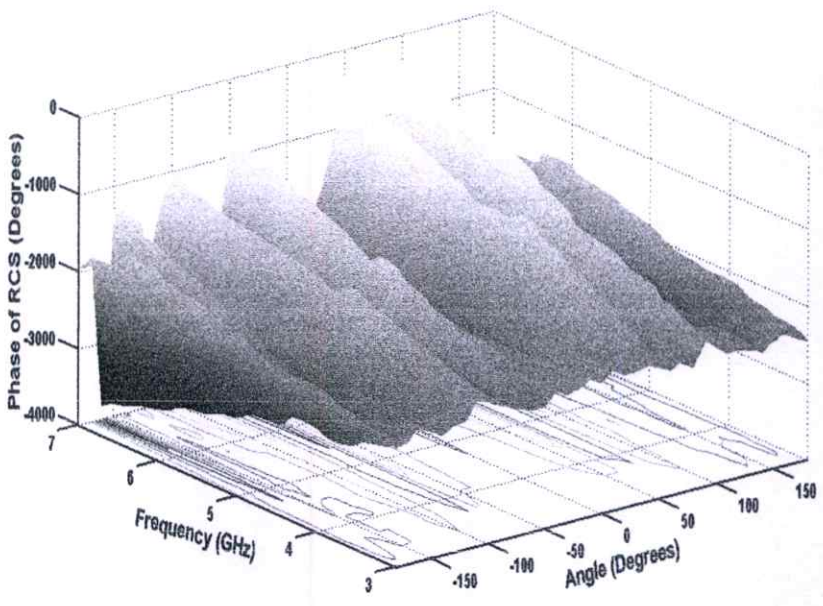

(b) Phase

Figure 5.8 The RCS for the experimental steel desk in VV polarization.

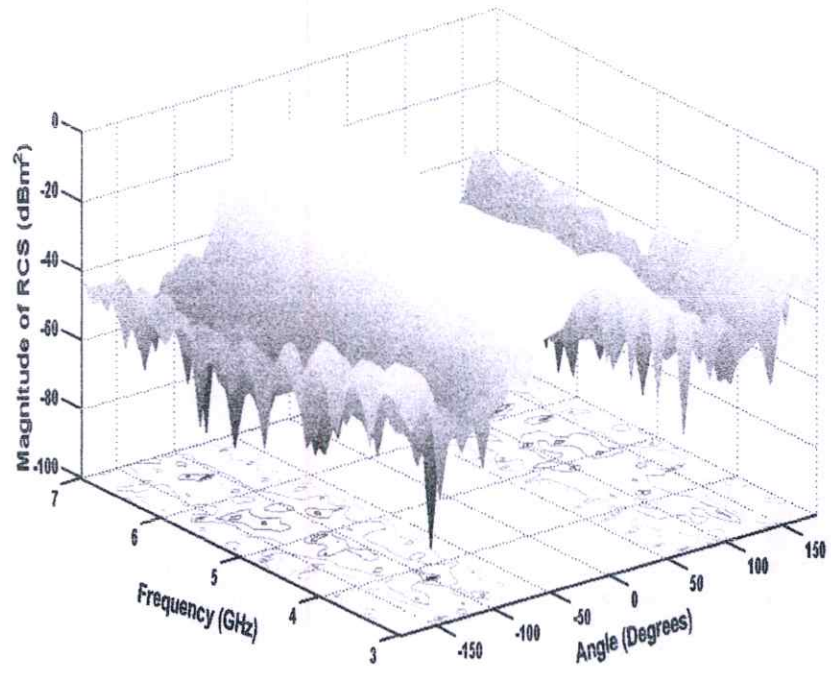

(a) Magnitude

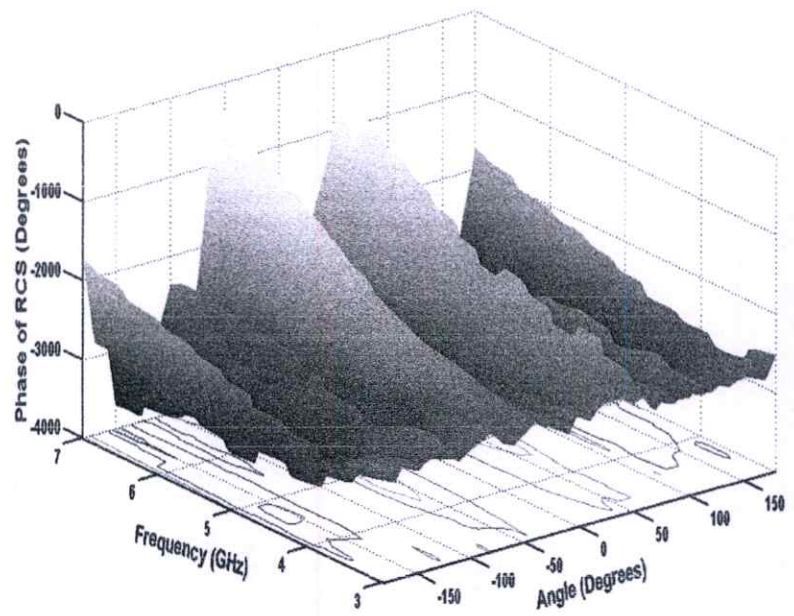

(b) Phase

Figure 5.9 The RCS for the experimental steel desk in HH polarization.

5.3 Statistical Analysis for RCS

The RCS data from all measurements are collected to represent and analyze in terms of first order. In this section, the significance of the distribution parameters is studied. How the distribution changes with its parameters is shown with its probability curve plotted. Based on the analysis, the RCS characterization for different targets are shown. The graph includes all aspects from 0 degree to 360 degree.

The following conventional statistical parameters are used to characterize the statistical RCS of target modeling. For a measured target RCS data in dBm^2 at k frequency point, σ_k, [58]

Mean value:

$$\bar{\sigma} = \frac{1}{N} \sum_{k=1}^{N} \sigma_k \tag{5.1}$$

Standard deviation:

$$\sigma_{SD} = \sqrt{\frac{1}{N} \sum_{k=1}^{N} (\sigma_k - \bar{\sigma})^2} \tag{5.2}$$

where N is the total number of frequency points, $\bar{\sigma}$ is a mean of RCS and σ_{SD} is a standard deviation of RCS.

Several commonly used in theoretical target fluctuation models are: normal, lognormal, rice and chi-square models. Of these models, the lognormal distribution is chosen to fit the measured target RCS data.

5.3.1 Lognormal Distribution Model

The most popular treatment for general distribution is lognormal distribution. This is a probability distribution for the amplitude of received signal, due to multipath

interference from scatterers. A probability density function for amplitude based on a given variance σ (the average energy is σ^2) A statistical distribution of measured target RCS data is characterized by using the lognormal distribution model. The probability distribution function (PDF) of the lognormal distribution model is

$$f(\sigma;\bar{\sigma},\sigma_{SD}) = \frac{1}{\sigma_{SD}\sqrt{2\pi}} e^{-\left[\frac{1}{2\sigma_{SD}^2}(\sigma-\bar{\sigma})^2\right]} \tag{5.3}$$

Kolmogorov-Simrnov test (KS test) is applied to the data to perform and verify the probability model [59]. The KS test is based on the empirical cumulative distribution function of the observed data. Mathematically, the test function is given by Equation 5.4, in which $F(x)$ is the empirical cumulative distribution of the RCS data and $\hat{F}(x)$ is the fitting function.

$$D = \left|F(x) - \hat{F}(x)\right| \tag{5.4}$$

5.4 RCS Characterization

This section examines the statistical RCS characterization of the complex targets. A statistically significant and independent sample data are required for the probability modeling and testing procedures. To fulfill this requirement, enough frequency samples are used as random fading samples to describe the distribution characteristics of such targets. Therefore, 401 independent frequency samples ranging within 3 GHz to 7 GHz is used to model the statistical distribution under the assumption of stationary.

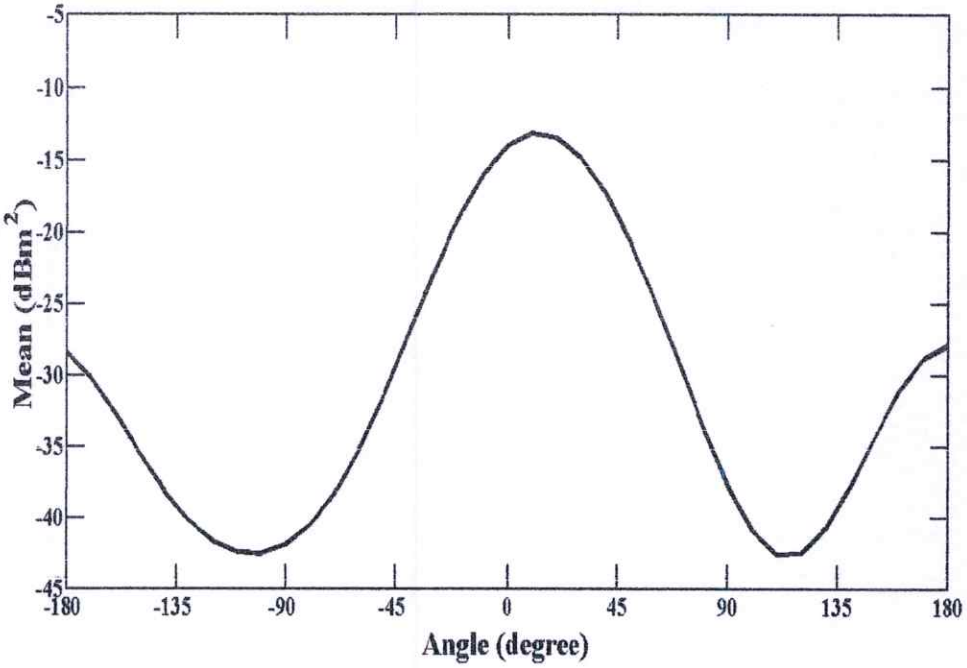

(a) VV polarization

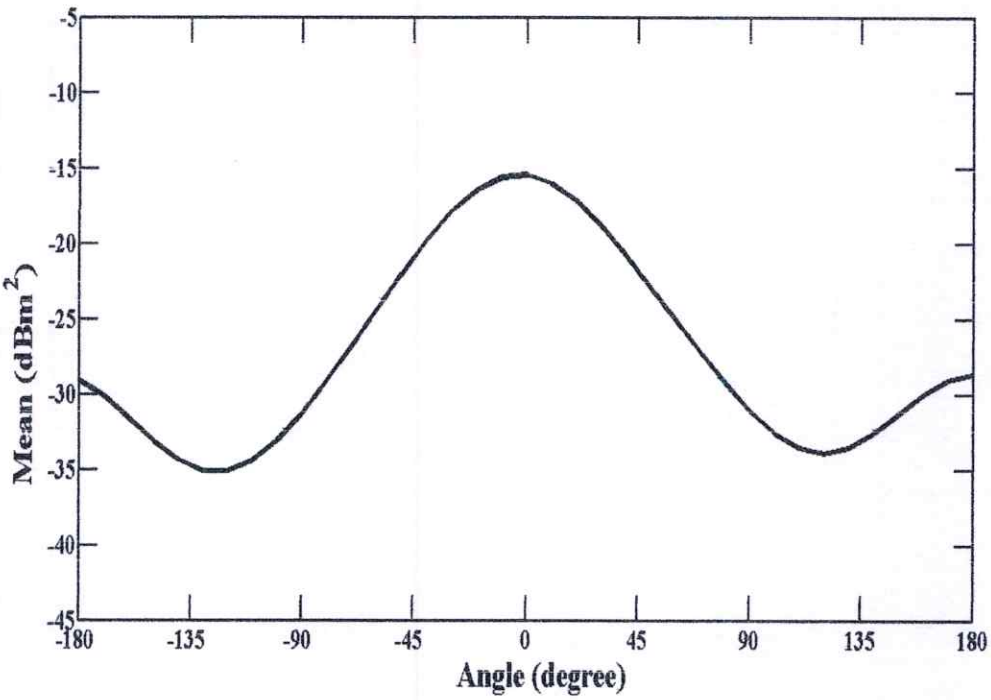

(b) HH polarization

Figure 5.10 Mean of lognormal distribution of office chair.

The sample mean and standard deviation are derived from RCS data. Plots of mean and standard deviation for two furniture items are shown in Figures 5.10 to Figure 5.13. Figures 5.10 to Figure 5.13 are plots of RCS versus angle. As can be seen, the degree to which RCS varies as a function angle depends upon the separation of the targets relative to the operating frequency. The mean RCS of chair for horizontal polarization demonstrates consistent higher result than the vertical polarization, showing average of 3 dBm^2. In case of desk, the mean RCS for horizontal polarization demonstrates consistent higher result than the vertical polarization, showing average of 4 dBm^2.

Mean RCS value as a function of scattered angle tend to vary significantly. As will be noted, the maximum mean value of RCS is approximately –13 dBm^2 and minimum value of RCS is approximately – 43 dBm^2 for two targets for VV polarization. For HH polarization of two targets, the maximum mean value is about – 15 dBm^2 and that of minimum is approximately – 37 dBm^2.

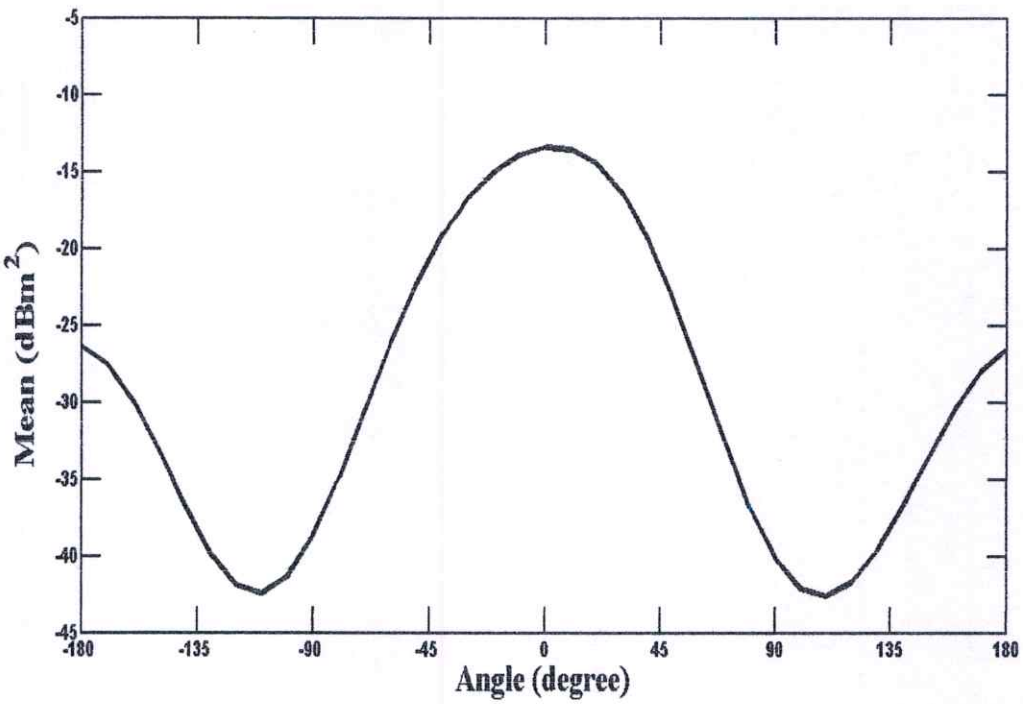

(a) VV polarization

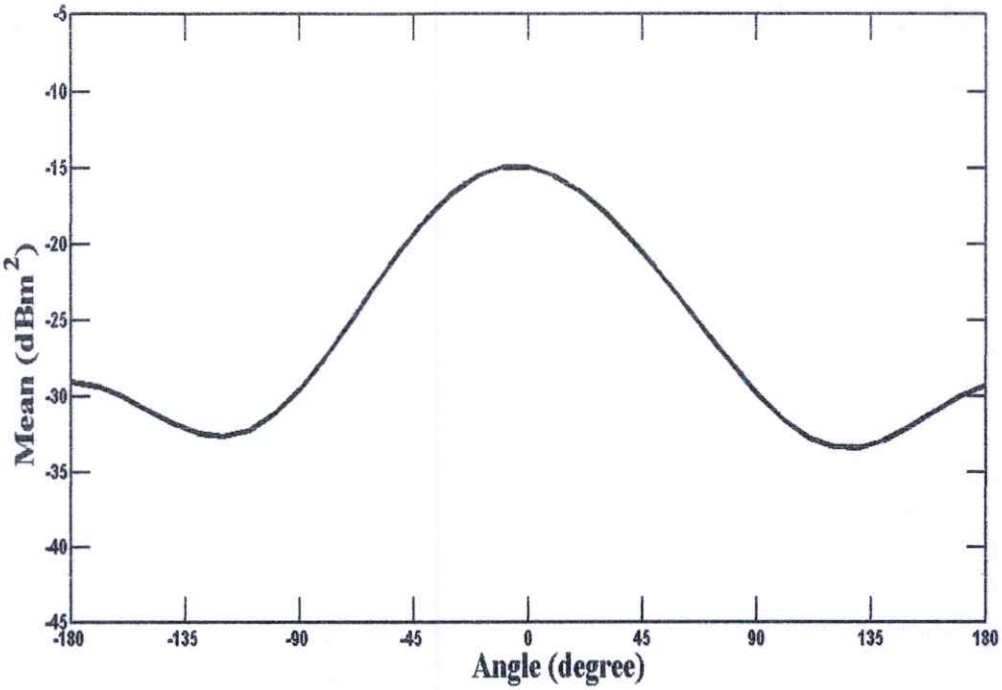

(b) HH polarization

Figure 5.11 Mean of lognormal distribution of steel desk.

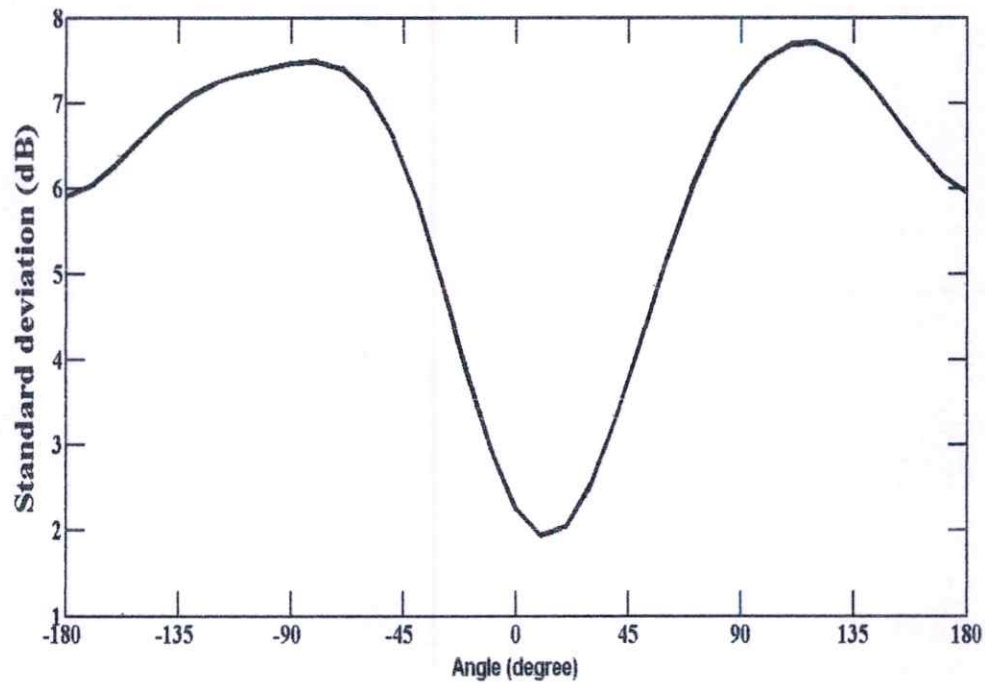

(a) VV polarization

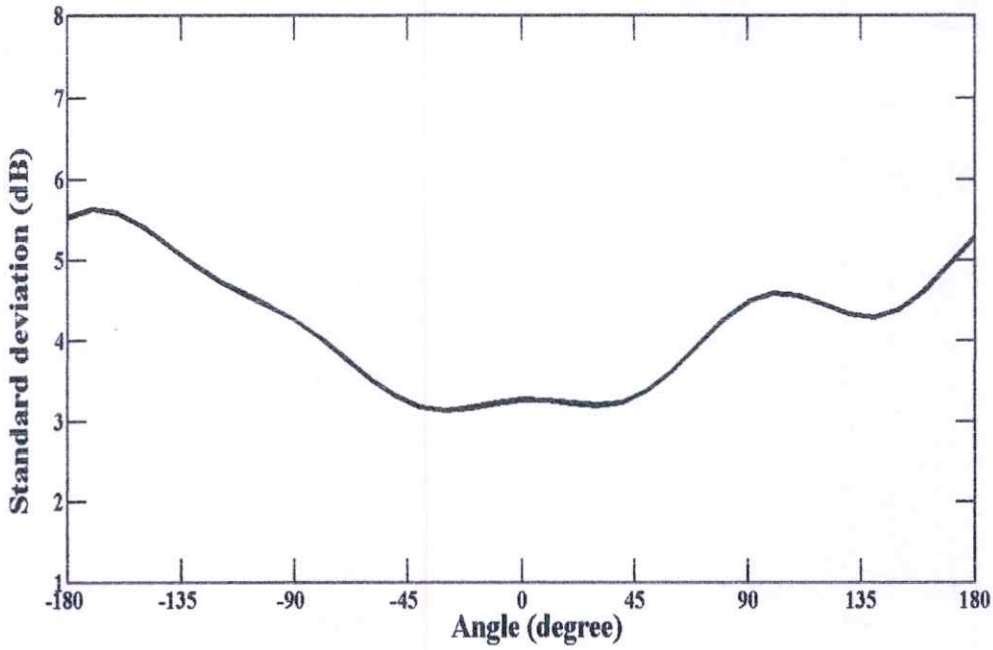

(b) HH polarization

Figure 5.12 Standard deviation of lognormal distribution of office chair.

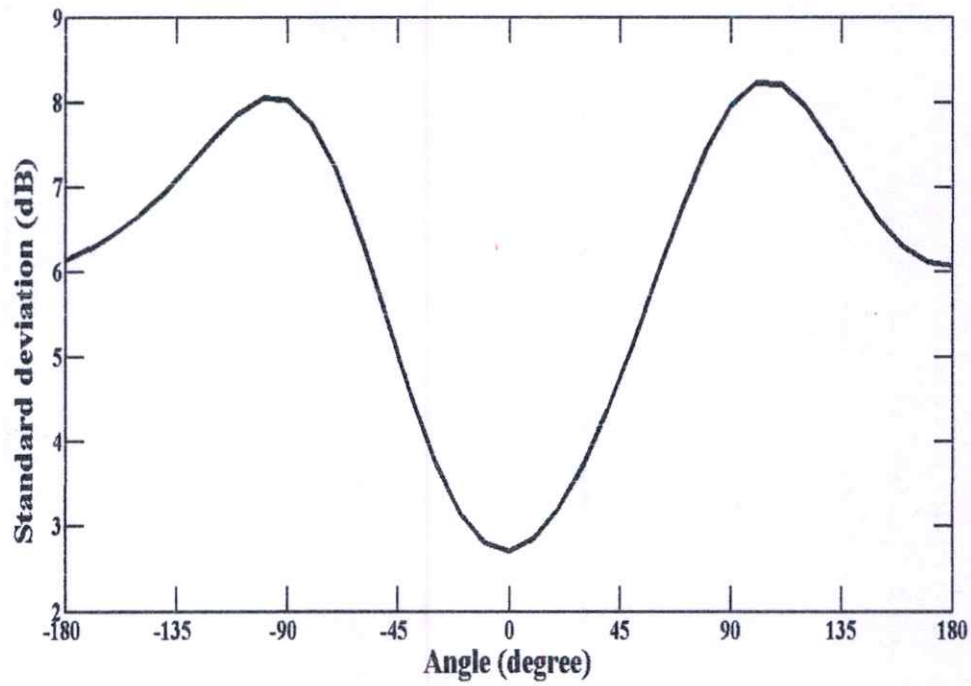

(a) VV polarization

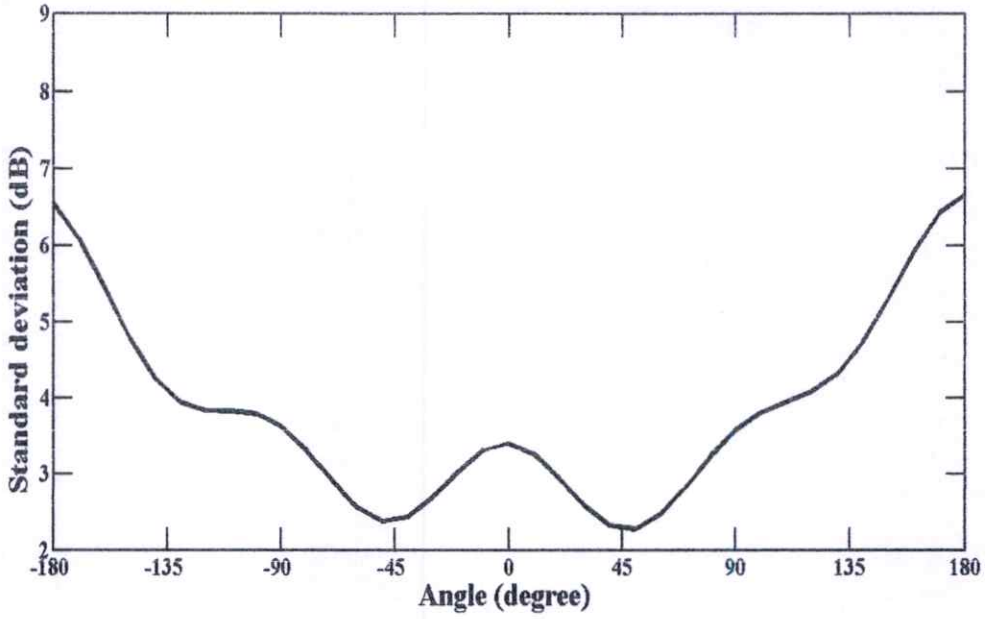

(b) HH polarization

Figure 5.13 Standard deviation of lognormal distribution of steel desk.

Standard deviation is closely related as a measurement variability to show the characteristics of how much variation the RCS from the mean. In all of the measurements, horizontal polarization showed less variation of RCS than the vertical polarization. This means that multipath components are found to contribute more fluctuation in RCS when using horizontal polarization. The standard deviation of the two targets is from 2 dB to 8 dB for VV polarization. For HH polarization, the maximum standard deviation is 7 dB and the minimum value is 2 dB.

In order to verify the probability model, the K-S test procedures is applied to the data. Log-normal distribution was tested to fit the measured RCS data at each angles. Measured CDF and its fitting by log-normal distribution are compared for 0 degree, 90 degree and 180 degree, just to present as examples. The statistical properties of lognormal variations are the same and governed by the density function and the test was accepted for more than 95% of the data with 5% significance level. The CDF of measured RCS data is compared with the theoretical lognormal distribution model. Figure 5.14 shows the CDF of RCS along with the angles for both VV and HH polarizations for chair, respectively. In Figure 5.15, the comparison CDF of measured RCS and lognormal distribution model for both VV and HH

polarizations for steel desk is illustrated. Assuming that the lognormal distribution model gives a good fitting model with the experimental RCS data of both office chair and steel desk.

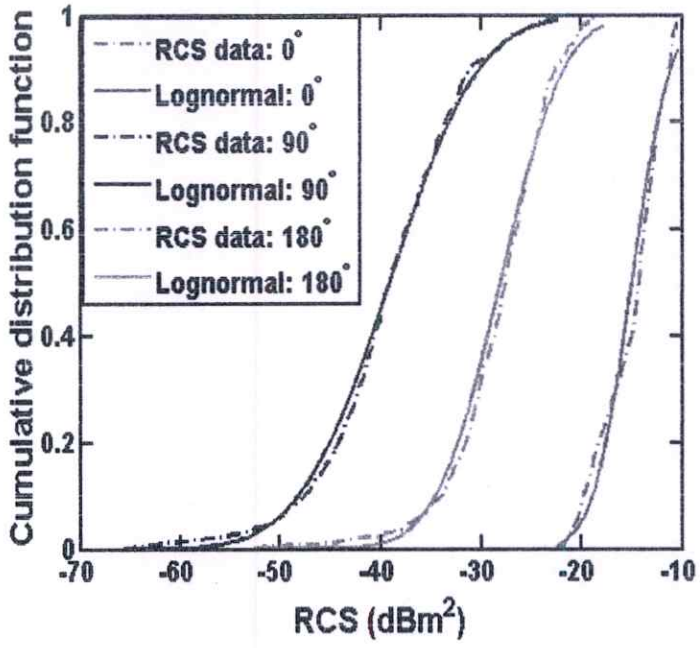

(a) VV polarization

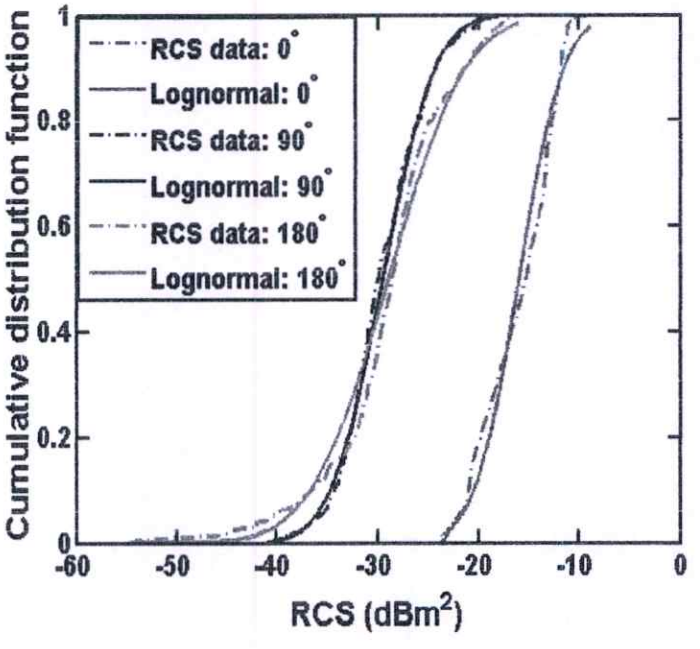

(b) HH polarization

Figure 5.14 CDF of office chair.

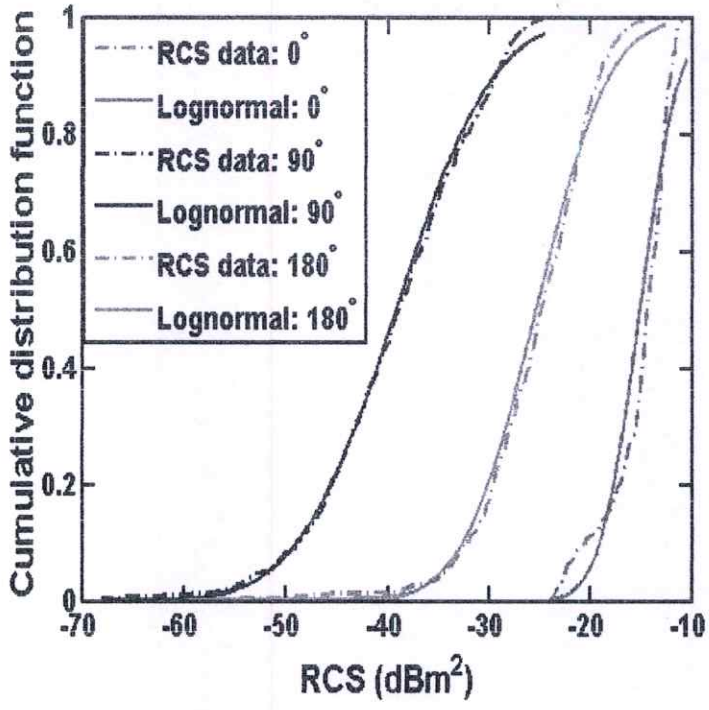

(a) VV polarization

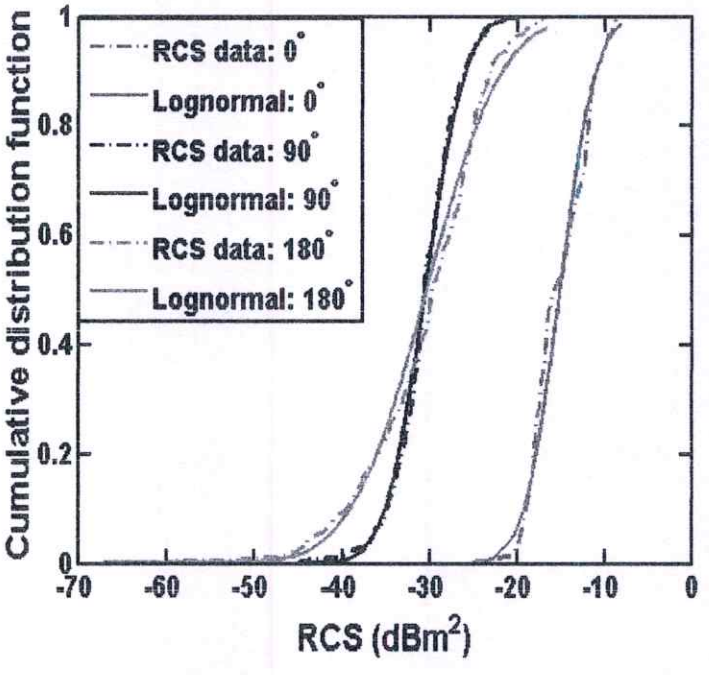

(b) HH polarization

Figure 5.15 CDF of steel desk.

5.5 Conclusion

In this chapter, the measurement system and procedures and the experimental RCS results of office chair and steel desk at 3 GHz to 7 GHz are shown and characterized in the term of the statistical model for VV and HH polarizations. It can be seen that time gating approach has proven by comparing the RCS results. These results with time gating are less significant multi-path than the RCS results without time gating. Statistics of the measured RCS data are fit to the lognormal distribution model. Then, the important parameters of mean and standard deviation are extracted along the angles for co-polarization. The CDF of lognormal distribution closely agrees with that of measured RCS data. The RCS distribution model for a complex target in indoor propagation may utilize classical detection statistics to calculate the probability of detecting the target and can be used to predict the backscatter from complex target.

CHAPTER 6
CONCLUSION AND FUTURE WORKS

6.1 Summary of Proceeding Chapters

This thesis presents theoretical and experimental aspects of complex target for indoor application. The developments of this evaluation of RCS work are based on the concept of radar. It is clearly established from theoretical formulation and corresponding experiments that the behavior of the RCS can be completely and accurately analyzed. In this chapter a summary of this thesis is presented, together with a discussion of the main contributions to the field of bistatic RCS of each scatterer. Possible further developments to measurement model, proposed an evaluation of RCS and statistical analysis of the target RCS data are also discussed.

This thesis presents a bistatic RCS measurement model for furniture items such as chair and desk and evaluation of RCS for those items. The time gating method is applied to reduce the multipath effects and noise from measurement.

Moreover, this thesis presented overview of the UWB communication system. The necessary theoretical background to understand the work presented in this thesis. It describes the significant of RCS theory. It started with a concise review of the bistatic geometry of the complex target. The definition and the fundamental radar equation are presented and the proposed extension of that equation is examined. Moreover, the details of scattering regions and prediction methods are displayed.

This thesis proposes the RCS in radar equation. The extension and evaluation method of RCS derivation is described. The antenna transfer function of horn antenna is measured in anechoic chamber and the experimental data are plotted. It was shown that there is limited theoretical and experimental information available on bistatic RCS and particularly in geometry. Assume that the measurement model is suitable for scattering from the target and proposed equation gives the guarantee for RCS of complex scatterer in indoor channel propagation.

In the RSC measured results, the summary of without time gating and with time gating are shown in Figure 6.1 to Figure 6.10 respectively. The measurements performed relied on many variables. One problem encountered in the bistatic measurement approach was the positioning the transmit antenna properly. While the

bistatic angles in the indoor were accurately marked using a transit, aligning the antenna sitting on top of the high tripod proved difficult. As the bistatic angle increased, the differences between the measured and predicted RCS values increased as well, with the largest differences appearing at 135 degree. As shown in Figure 6.1 to Figure 6.10, the bistatic RCS is very dependent on the correct bistatic angle. Since the measured RCS depends on the antenna position must be correct.

While this does not mean that this is the contributor for the larger differences in RCS magnitude obtained as the bistatic angle increased, it is simply meant to show that something as simple as correctly placing the antenna can really have an adverse effect on the data.

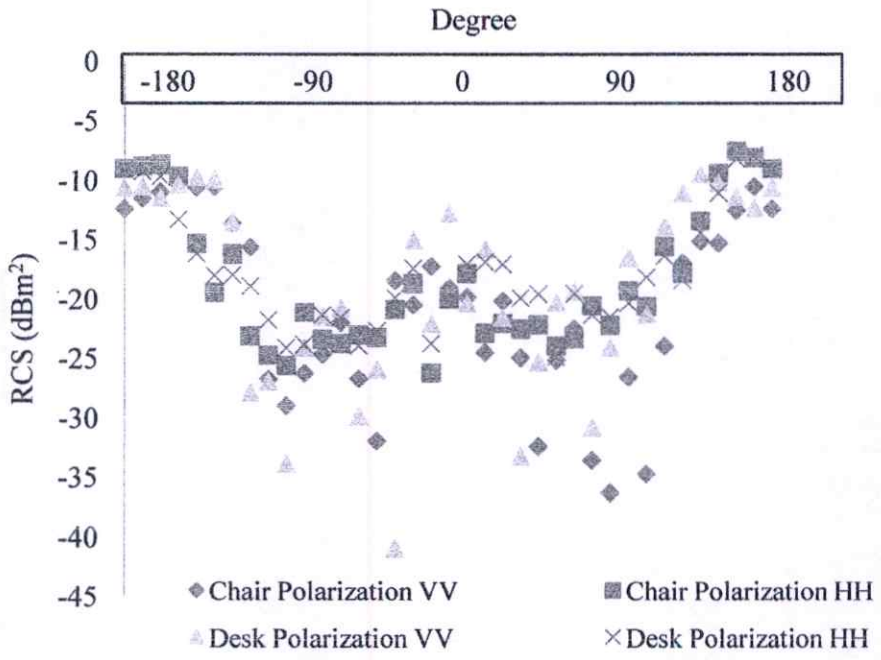

Figure 6.1 Summary in scatter plots of RCS measured results without time gating at 3 GHz.

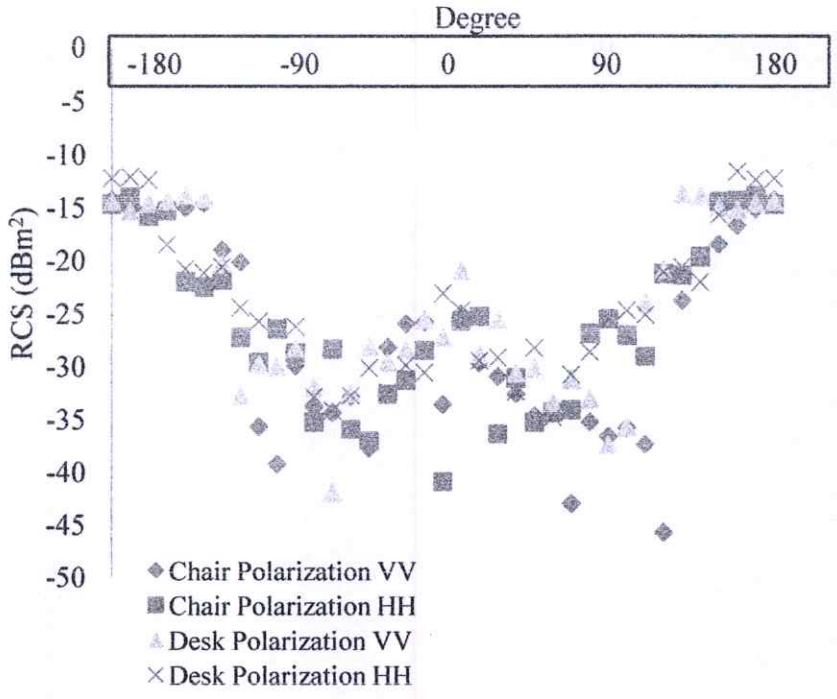

Figure 6.2 Summary in scatter plots of RCS measured results without time gating at 4 GHz.

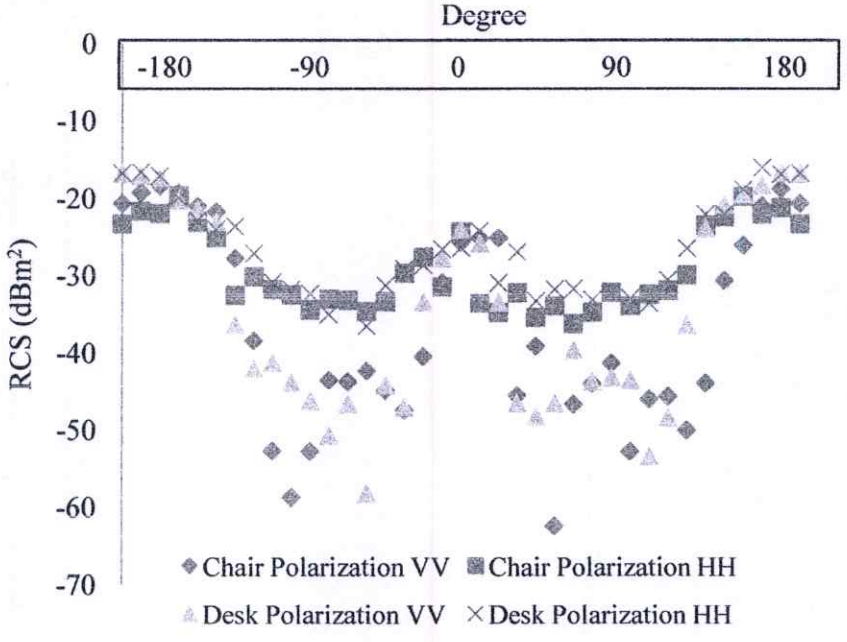

Figure 6.3 Summary in scatter plots of RCS measured results without time gating at 5 GHz.

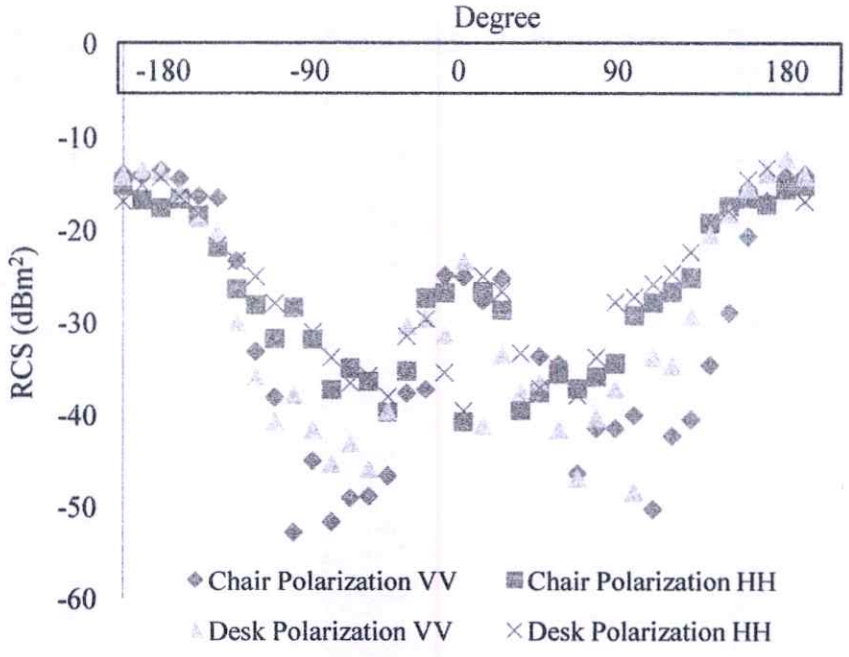

Figure 6.4 Summary in scatter plots of RCS measured results without time gating at 6 GHz.

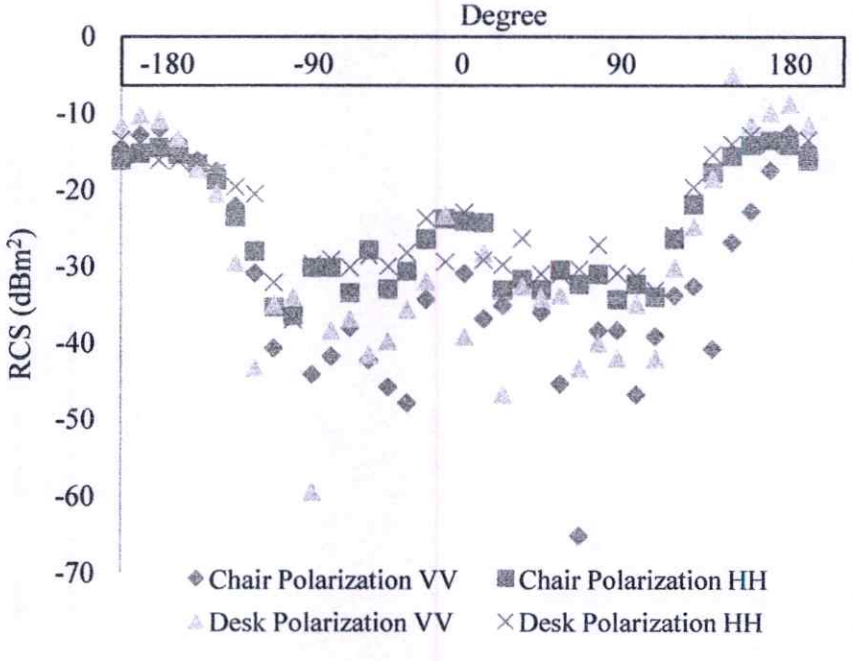

Figure 6.5 Summary in scatter plots of RCS measured results without time gating at 7 GHz.

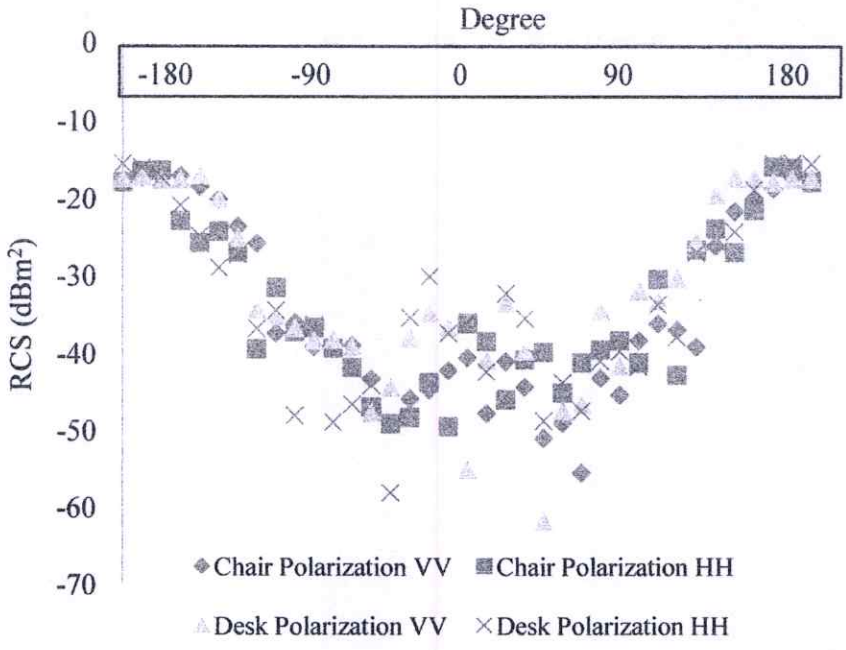

Figure 6.6 Summary in scatter plots of RCS measured results with time gating at 3 GHz.

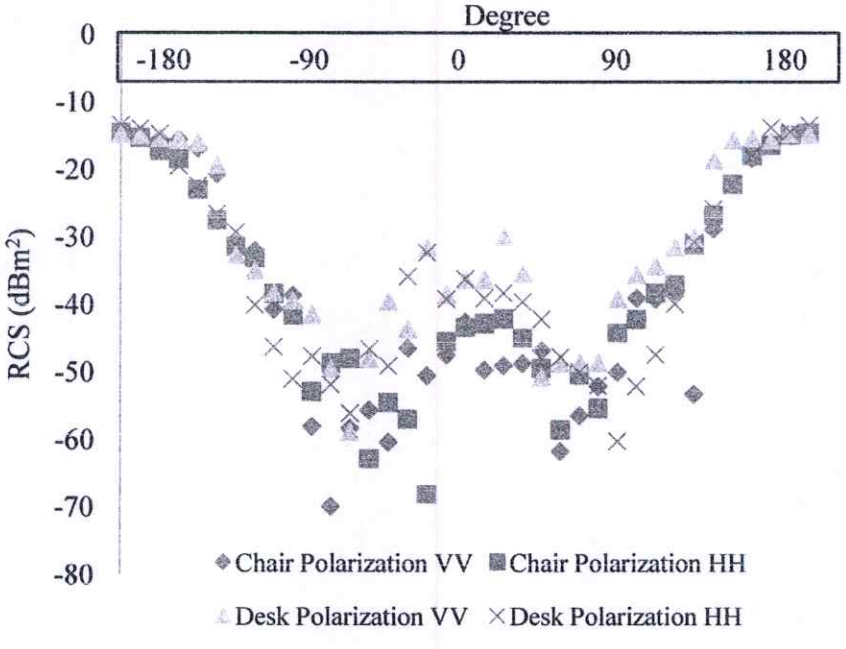

Figure 6.7 Summary in scatter plots of RCS measured results with time gating at 4 GHz.

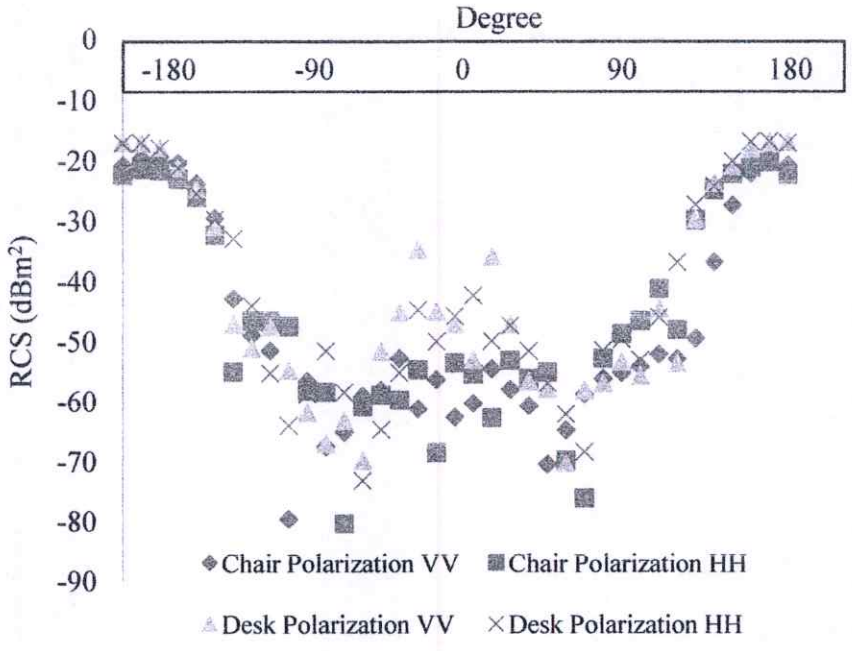

Figure 6.8 Summary in scatter plots of RCS measured results with time gating at 5 GHz.

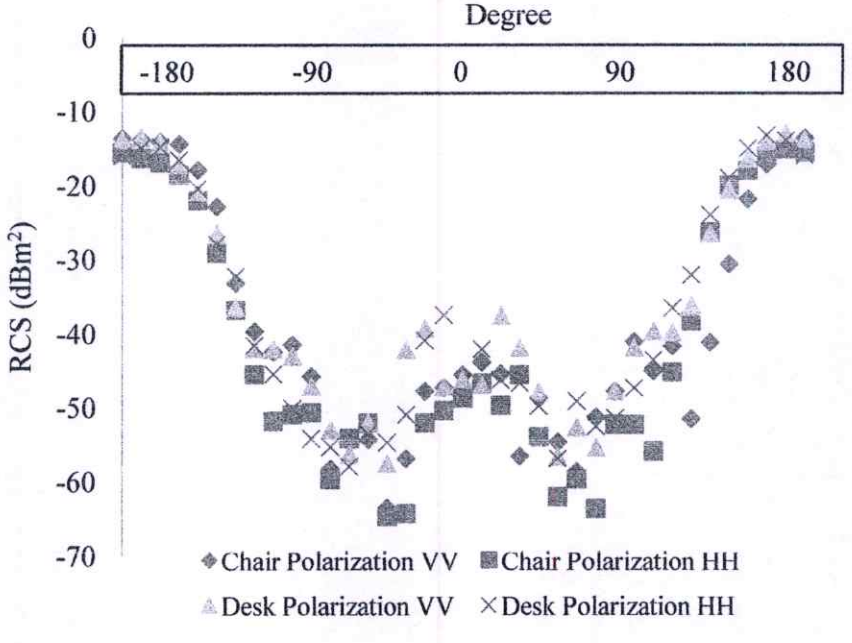

Figure 6.9 Summary in scatter plots of RCS measured results with time gating at 6 GHz.

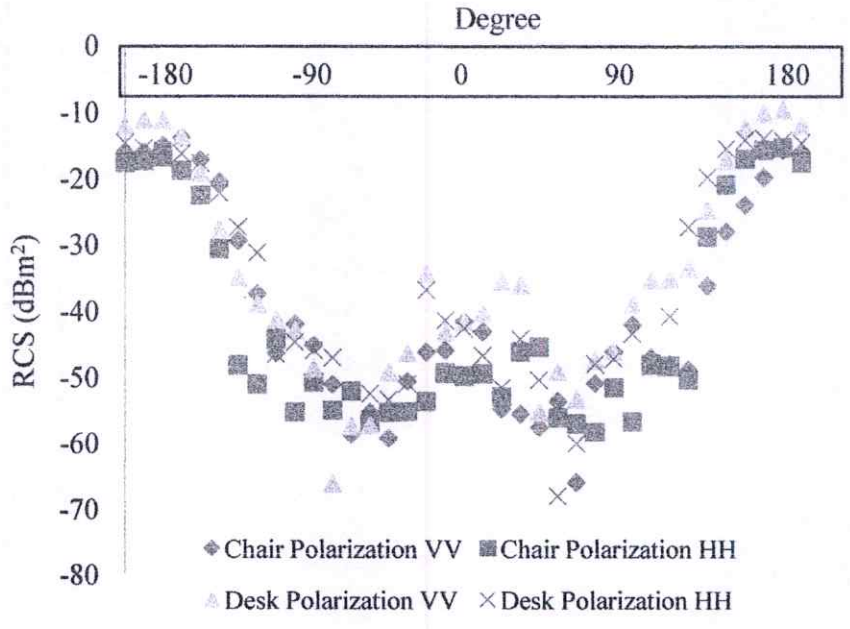

Figure 6.10 Summary in scatter plots of RCS measured results with time gating at 7 GHz.

6.2 Recommendation for Improvement

The results and observed actual measurements are presented. However, the measurements have some distinct problem areas, and so give suggestions on possible improvements.

First is the problem of the accuracy of the data. This is particularly true in the case of an object whose return is not easily predictable theoretically. Some requirements must be met to minimize measurement errors.

6.2.1 Measurement Errors

There may be some disagreement on the required degree of accuracy in RCS measurements because of moving by manually. Most of RCS measurements are examined using anechoic chamber. In considering the present program many users would be satisfied with the accuracy of the data obtained for targets if the far field

data were excluded. It is difficult to assign because no theoretical analysis is available for complex targets.

Adequate equipment and facilities, the use of proven measurement procedures and careful, experienced and well-motivated operating personnel are required to insure accurate measurements.

6.2.2 Equipment and Facilities

The performance of the equipment and facilities used in these tests that accurate measurements can be made and shown also that no major deficiency exists in the equipment and facilities except for the cases.

6.2.3 Near Field Measurement

One recommended for the near field problem is quite straightforward: namely, design the equipment and range, so that the target can always be in the far field. The RCS ranges measured at the generally accepted distance $R > \frac{2D^2}{\lambda}$.

6.3 Future Works

This thesis proposed the extension of radar equation using time gating method for RCS of complex objects. In this work, frequency domain measurement is utilized for experimental. There are many possibilities to build on this work for further investigations.

By introducing the complex radar cross section, multi-shape geometry can be investigated in ray tracing.

The channel measurement with multiple scattering will be considered as a target co-located in an indoor environment.

Far-field ranges can be tested and measured by channel propagation.

The time domain measurement system can be used in future and compared with frequency domain measurement.

Position of object or rotation of the object can be changed and analyzed. One consideration for the future is incorporating apedestal for the rotation of targets. The ability to rotate the target in precise angle increments and correcting coherent data at different aspect angles allows the generation of two-dimensional scattering images of the target using inverse synthetic aperture radar (ISAR) techniques.

Predictive simulation software such as XFDTD, CST, HFSS can be used to predict and analyze the RCS of the complex targets.

The cross polarization for the antenna is more considered for RCS and RCS matrix.

Finally, the multiple diffraction interpretation can be verified or rejected by measuring multiple polarizations, object of different sizes, and different types of materials.

REFERENCES

[1] G. Durgin, "Advanced Site-specific Propagation Prediction Techniques," Master Thesis, Virginia Polytechnic Institute and State University, 1998.

[2] Y. Kishiki and J. Takada, "Improvement of 3D ray tracing simulation in microcell environment by introducing the complex radar cross section," International Symposium on Antennas and Propagation (ISAP 2008), Oct. 2008.

[3] Y. Kishiki, J. Takada, G. S. Ching, N. Lertsirisopon, M. Kawamura, H. Takao, Y. Sugihara, S. Matsunaga, and F. Uesaka, "Application of reflection on curved surfaces and roughness on surface in ray tracing for tunnel propagation," Fourth European Conference on Antennas and Propagation (EuCAP 2010), Apr. 2010.

[4] C. Lim, J. Volakis, K. Sertel, R. Kindt, and A. Anastasopoulos, "Indoor propagation models based on rigorous methods for site-specific multipath environments," IEEE Transactions on Antennas and Propagation, vol. 54, no. 6, pp. 1718–1725, June 2006.

[5] T. S. Rappaport, "Wireless Communications: Principles and Practice," Prentice Hall, 2002.

[6] A. Goldsmith, "Wireless Communications," Cambridge University Press, 2005.

[7] H. Hashemi, "The Indoor radio propagation channel," Proceeding of the IEEE, vol. 81, no. 7, pp. 943-968, July 1993.

[8] V. Kostylev, M. Cherniakov, "Bistatic Radar: Principles and Practice," John Wiley & Sons, 2007.

[9] E. Knott, J. Shaeffer, and M. Tuley, "Radar Cross Section: Its Prediction, Measurement and Reduction," Artech House, Norwood, Massachusetts, 1985.

[10] P. C. Dowdy, "RCS probability distribution function modeling of a fluctuating target," IEEE Radar Conference, pp. 164-168, 1991.

[11] W. Shi, X-W. Shi and L. Xu, "RCS characterization of stealth target using χ^2 distribution and lognormal distribution," Progress In Electromagnetics Research M, vol. 27, pp. 1-10, 2012.

[12] W. Shi, X-W. Shi and L. Xu, "Radar cross section (RCS) statistical characterization using Weibull distribution," Microwave and Optical Technology Letters, vol. 55, no. 6, June 2013.

[13] A. D. Maio, A. Farina, and G. oglia, "Target fluctuation models and their experimental validation," IEEE Radar Conference, pp. 272-277, USA, 2005.

[14] F. J. Massey, Jr., "The Kolmogorov-Smirnov test for goodness of fit," Journal of the American Statistical Association, vol. 46, no. 253, pp. 68–78, 1951.

[15] M. ,A. S. Miacci, E. L. Nohara, I. M. Martin, G. G. Peixoto, and M. C. Rezende, "Indoor radar cross section measurement of simple targets," Journal of Aerospace Technology and Management (JATM), vol. 4, no. 1, pp. 25-32, Mar. 2012.

[16] I. Nicolaescu, and G. Iubu, "Simple and collected targets radar cross section," International Conference on Electromagnetics in Advanced Applications (ICEAA), pp. 295-298, 2007.

[17] D. E. Bocanegra, D. P. Martinez, R. F. Recio., A. J. Lucena, and I. M. Sanchez, "New benchmark radar targets for scattering analysis and electromagnetic software validation," Progress In Electromagnetics Research (PIER), pp. 39-52, 2008.

[18] Y. Bennani, F. Comblet, and A. Khenchaf, "RCS of complex targets: original representation validated by measurements—application to ISAR imagery," IEEE Transactions on Geoscience and Remote Sensing, Vol. 50, no. 10, Oct., 2012.

[19] V. D. Esposti, F. Fuschini, E. M. Vitucci, and G. Falciasecca, "Measurement and modelling of scattering from buildings," IEEE transactions on Antennas and Propagation, vol. 55, no. 1, pp. 143-153, 2007.

[20] P. Pongsilamanee, and H. L. Bertoni, "Specular and nonspecular scattering from building facades," IEEE transactions on Antennas and Propagation, vol 52. no. 7, pp. 1879-1889, 2004.

[21] Y. L. C. Jong, and M. H. A. J. Herben, "A Tree-scattering model for improved propagation prediction in Urban microcells," IEEE Transactions on Vehicular Technology, vol. 53, no. 2, pp. 503-513, 2004.

[22] M. Ghoraisti, J. Takada, and T. Imai, "Radio wave scattering from lamposts in microcell Urban mobile propagation channel," ECTI Transactions on

Electrical Engineering, Electronics, and Communications, vol. 7, no. 1, pp. 14-20, Feb. 2009.

[23] H. Tsuchiya, N. Lertsirisopon, J. Takada., and T. Kobayashi, "Effects of bragg scattering on ultra-wideband signal transmission from periodic surfaces," IEICE Transactions on Communications, vol. E91-B, no. 2, pp. 536-542, Feb. 2008.

[24] C-P. Lim, J. L. Volakis, K. Sertel, R. W. Kindt, and A. Anastasopoulo, "Indoor propagation models based on rigorous methods for site-specific multipath environment," IEEE Transactions on Antennas and Propagation, vol. 54, no. 6, pp. 1718-1725, 2006.

[25] Y. Kishiki, and J. Takada, "Improvement of 3D ray tracing simulation in microcell environment by introducing the complex radar cross section," International Symposium on Antennas and Propagation (ISAP), pp. 790-793, Oct. 2008.

[26] M. Cheffena, "Physical-statistical channel model for signal effect by moving human bodies," EURASIP Journal on Wireless Communications and Networking, pp. 1-13, 2012.

[27] A. A. M. Saleh and R. A. Valenzuela, "A statistical model for indoor multipath propagation," IEEE in Communications, vol. 5, no. 2, pp. 128-137, 1987.

[28] H. Budiarto, K. Horihata, K. Haneda, J. Takada, "Multipath characteristics of non-specular wave scattering from building surface roughness," Personal, Indoor and Mobile Radio Communications Conference, pp. 945 – 949, 2003.

[29] V. G. Borkar, A. Ghosh, R. K. Singh, and N. Chourasia, "Radar cross-section measurement techniques," Defence Science Journal, Vol. 60, No. 2, pp. 204-212, Mar. 2010,

[30] L. V. Blake, "Radar Range Performance Analysis," Artech House, Norwood, USA, 1986.

[31] M. I. Skolnik, "Introduction to Radar Systems," 3rd Edition, McGraw Hill, New York, 2001.

[32] A. K. Bhattacaryya, D. L. Sengupta, "Radar Cross Section Analysis and Control," Artech House, Norwood, USA, 1991.

[33] E. F. Knott, Shaeffer, F. John, Tuly, T. Michael, "Radar Cross Section," 2nd Edition, Boston, Artech House, 1993.

[34] I. Oppermann, M. Hamalainen and J. Iinatti, "UWB Theory and Applications," John Wiley & Sons, Ltd., 2004.

[35] K. Siwiak , D. McKeown, "Ultra-Wideband Radio Technology," John Wiley & Sons, Ltd., 2004.

[36] M. Dawood, "Ultrawideband Coherent Random Noise Radar Theory and Experiments," PhD thesis, University of Nebraska-Lincoln, 2001.

[37] I. J. Immoreev and J. D. Taylor, "Future of Radars," 2002 IEEE Conference on Ultra Wideband System and Technologies, pp.197-199, 2002.

[38] Federal Communications Commission, "Revision of Part 15 of The Commission's Rule Regarding UWB Transmission Systems," First Report, FCC 02-48, Apr. 2002.

[39] W. Hirt and M. Weisenhorn, "Overview and implications of the emerging global UWB radio regulatory frameworks," 2006 IEEE International Conference on Ultra-Wideband, pp. 581-586, Sept. 2006.

[40] M. P. Wylie-Green, P. A. Ranta and J. Salokannel, "Multi-band of OFDM UWB solution for IEEE 802.15.3a WPANs," Sarnoff Symposium on 2005 IEEE Advances in Wired and Wireless Communication, pp. 102-105, 2005.

[41] L. D. Nardis and M. D. Benedetto, "Overview of the IEEE 802.15.4/4a standards for low data rate Wireless Personal Data Networks," 4th Workshop on Positioning, Navigation and Communication (WPNC), pp. 285-289, 2007.

[42] K. S. Kwak, S. Ullah and N. Ullah, "An overview of IEEE 802.15.6 standard," 2010 3rd International Symposium on Applied Sciences in Biomedical and Communication Technologies (ISABEL), pp. 1-6, 2010.

[43] D. Iyengar, "Understanding Ultra Wideband Technology: Advantages, Applications, and Regulatory Policy," M.A. Thesis, Tufts University, May 2002.

[44] CA. Baianis, "Advanced Engineering Electromagnetics," John Wiley & Sons, Inc., New York, NY, 1989.

[45] C. A. Balanis, "Antenna Theory," John Wiley & Sons, Inc., New Jersey, 2005.

[46] R. G. Kouyoumjian, P. H. Pathak, "A uniform geometrical theory of diffraction for and edge in a perfectly conducting surface," Proceedings of the IEEE, vol. 62, no. 11, pp. 1448-1461, 1974.

[47] R. F. Harrington, "Field Computation by Moment Methods," IEEE Press, 1993.

[48] J. D. Kraus, R. J. Marhefka, A. S. Khan, "Antennas and Wave Propagation," 4th Edition, McGraw Hill, 2012.

[49] C. A. Balanis, "Antenna Theory Analysis and Design," 3rd Edition, John Wiley & Sons, Inc., Hoboken, New Jersey.

[50] A. Taflove, S. C. Hagness, "Computional Electrodynamics: The Finite Different Time Domain Method," 2nd Edition, Artech House, Boston, London, 2000.

[51] F. Chatzigeorgiadis, "Development of code for a Physical Optics Radar Cross Section Prediction and Analysis Application," Master's Thesis, Naval Postgraduate School, Monterey, California, Sept. 2004.

[52] L.Tan and J..Jiang, "Digital Signal Processing Fundamentals and Applications," Elsevier Inc., 2007.

[53] S. Kingsley and S. Quegan, "Understanding Radar Systems," McGraw-Hill, 1992.

[54] R. J. Sullivan, "Radar Foundations for Imaging and Advanced Concepts," Scitech Publishing, 2004.

[55] I. H. Woodhouse, "Introduction to Microwave Remote Sensing," Taylor & Francis, 2006.

[56] A. Technologies, "Agilent Technologies 8510C Network Analyzer System," 3rd Edition, USA, May, 2001.

[57] EMC Test Systems, "Model 3115 Double-Ridge Waveguide Horn," Mar., 2002.

[58] N. L. Johnson, S. Kotz, N. Balakrishnan, "Continuous Univariate Distributions," vol. 1. 2nd Edition, Wiley Series, 1994.

[59] F. Massey: "The Kolmogorov-Smirnov test for goodness of fit," J. Amer. Stat. Assoc., vol. 46, no. 253, pp. 68–78, 1951.

APPENDIX

List of Publications

International Journal

[1] M. M. Maw, P. Supanakoon, S. Promwong and J. Takada, "Measurement and evaluation of radar cross section for furniture in an indoor propagation channel," Advances in radio science, vol. 12, pp. 273-278, Nov., 2014.

International Conferences

[1] M. M. Maw, P. Supanakoon, S. Promwong and J. Takada, "Indoor propagation channel model with ray tracing for wireless communications," in Proceeding, Thailand-Japan Microwave (TJMW), KMITL, Bangkok, pp. 28-31, Aug., 2011.

[2] M. M. Maw, P. Supanakoon, S. Promwong and J. Takada, "Furniture effects in indoor propagation channel at 5.8 GHz," in Proceeding 2012 Asia - Pacific Symposium on Applied Electromagnetics & Mechanics Conference (APSAEM), Hochi Min, Vietnam, pp. 372-377, July, 2012.

[3] M. M. Maw, P. Supanakoon, S. Promwong and J. Takada, "Measuring and modeling of furniture effects in indoor propagation channel at 5.8 GHz," in Proceeding, Thailand-Japan Microwave (TJMW), Chulalongkorn University, Bangkok, Aug., 2012.

[4] M. M. Maw, P. Supanakoon, S. Promwong and J. Takada, "A comparison of indoor channel measurements and FDTD simulations at 5.8 GHz," in International Conference on Engineering Applied Sciences and Technology (ICEAST), Bangkok, pp. 547-551, Nov., 2012.

[5] M. M. Maw, P. Supanakoon, S. Promwong and J. Takada, "UWB reflection measurement for indoor WPANs," in Regional Conference on Computer and Information Engineering (RCCIE), Bangkok, pp 87-91, Aug., 2013.

[6] M. M. Maw, P. Supanakoon, S. Promwong and J. Takada, "Experimental evaluation of furniture radar cross section in indoor propagation channel," in Proceeding, Thailand-Japan Microwave (TJMW), Kasetsart University, Bangkok, Dec., 2013.

Adv. Radio Sci., 12, 273–278, 2014
www.adv-radio-sci.net/12/273/2014/
doi:10.5194/ars-12-273-2014

Advances in Radio Science
Open Access Proceedings

Measurement and evaluation of radar cross section for furniture in an indoor propagation channel

M. M. Maw[1], P. Supanakoon[1], S. Promwong[1], and J. Takada[2]

[1]Faculty of Engineering, King Mongkut's Institute of Technology Ladkrabang, Chalongkrung Road, Ladkrabang, Bangkok 10520, Thailand
[2]Graduate School of Science and Engineering, Tokyo Institute of Technology, S6-4, 2-12-1, O-okayama, Meguro-ku, Tokyo 152-8552, Japan

Correspondence to: M. M. Maw (myomyintmawphdit5@gmail.com)

Received: 9 January 2014 – Revised: 17 June 2014 – Accepted: 9 August 2014 – Published: 11 November 2014

Abstract. This paper has attempted to evaluate the radar cross section (RCS) of two furniture items in an indoor environment in a frequency range of 3–7 GHz of the ultra-wideband (UWB) range. The RCS evaluation is achieved through an extended version of the radar equation that incorporates the channel transfer function of scattering. The time-gating method was applied to remove the multipath effect, a phenomenon which typically occurs in the indoor environment. Two double-ridged waveguide horn antennas for both vertical and horizontal polarizations were used to obtain the transfer function of scattering of the furniture prior to analysis in order to derive their bistatic RCS. The RCS results validate the applicability of the proposed extended radar equation to the indoor propagation prediction.

1 Introduction

In an indoor environment, scattering targets, e.g., furniture items, walls, or even a human body, have an effect on the total received signal. In addition, the scatterers and their environment affect the radio wave propagation. Thus, the diverse effects of different scattering objects on the radio wave propagation warrant examination and analysis. In the case of furniture items, their multi-shape geometry necessitates special treatment to investigate and model their effects on the radio wave propagation.

Techniques have been proposed for the determination of the radar cross section (RCS) of various types of targets. Depending on the target size and selected frequency range, RCS can be investigated in either an outdoor environment, indoor environment, or inside an anechoic chamber. Miacci et al. (2012), Nicolaescu and Iubu (2007), and Bocanegra et al. (2008) examined the RCS of scattering objects in an anechoic chamber. Esposti et al. (2007) and Pongsilamanee and Bertoni (2004) analyzed the RCS of typical building walls, and Jong and Herben (2004) investigated the scattering of trees. Ghoraisti et al. (2009) studied the scattering from lampposts, traffic lights, and signboards. Tsuchiya et al. (2008) researched the Bragg scattering from periodic surfaces in an ultra-wideband (UWB) signal transmission. Lim et al. (2006) used the full wave simulation technique to investigate the scattering from multi-shape or porous objects, e.g., bricks, tables, and chairs. Kishiki and Takada (2008) studied the scattering of buildings in a street microcell environment, and Cheffena (2012) simulated the effect of a moving human body on the statistical channel.

This paper measures the channel transfer function of scattering from the furniture items in the indoor environment to obtain the magnitude and phase. The bistatic scattering measurements are analyzed by means of the extended radar equation and the Kaiser–Bessel window to derive the RCS of the furniture items. The organization of the paper is as follows: after this introduction, Sect. 2 details the underlying theory of RCS analysis in this paper. Section 3 deals with the experimental setup and procedure. Section 4 describes the RCS measurement results. The concluding remarks are provided in Sect. 5.

Published by Copernicus Publications on behalf of the URSI Landesausschuss in der Bundesrepublik Deutschland e.V.

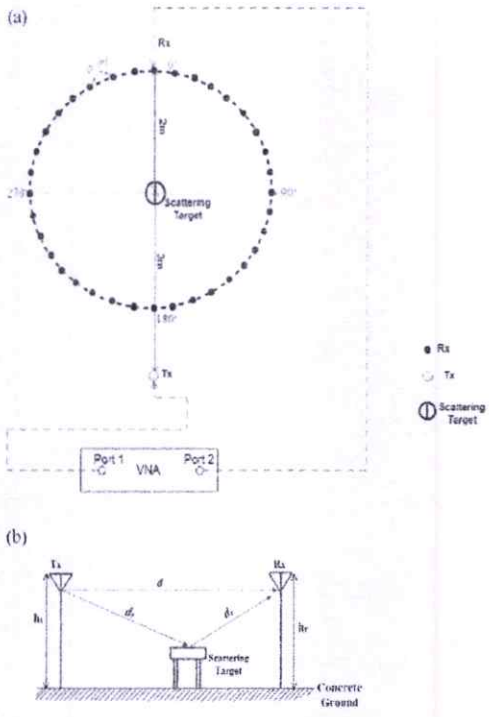

Figure 1. Top view and side view of the bistatic RCS.

2 Theory of RCS evaluation

The radar equation (Knott et al., 1985) is commonly used to describe the relationship between the received power and a target. For the radar link from a transmitter antenna (Tx) to a receiver antenna (Rx), and with the polarizations of both antennas pointing to a scattering target, the received power $P_r(f, \theta_i, \varphi_i, \theta_s, \varphi_s)$ can be calculated from

$$P_r(f, \theta_i, \varphi_i, \theta_s, \varphi_s) = \frac{c^2}{64\pi^3 f^2 d_t^2 d_r^2} \sigma(f, \theta_i, \varphi_i, \theta_s, \varphi_s) G_t(f) G_r(f) P_t(f). \quad (1)$$

where $P_t(f)$ is the transmitted power, $G_t(f)$ is the gain of Tx, $G_r(f)$ is the gain of Rx, d_t and d_r are the respective distances from the target to Tx and Rx, $\sigma(f, \theta_i, \varphi_i, \theta_s, \varphi_s)$ is the RCS of the target, c is the velocity of light, f is a carrier frequency, θ_i and φ_i are the elevation and azimuth incident angles to the target, and θ_s and φ_s are the elevation and azimuth scattering angles from the target.

This research work has adopted the extended version of the radar equation which incorporates the channel transfer function of scattering to evaluate RCS. The experimental targets are singly placed between Tx and Rx under a bistatic condition. The channel transfer function of scattering in frequency domain, $H_{sc}(f, \theta_i, \varphi_i, \theta_s, \varphi_s)$, can be written as

$$H_{sc}(f, \theta_i, \varphi_i, \theta_s, \varphi_s) = \left[\frac{c}{8(\pi)^{3/2} f d_t d_r} H_\sigma(f, \theta_i, \varphi_i, \theta_s, \varphi_s) e^{-j2\pi f (d_t + d_r)/c} + H_c(f, \theta_i, \varphi_i, \theta_s, \varphi_s) \right] H_t(f) H_r(f), \quad (2)$$

where $H_c(f, \theta_i, \varphi_i, \theta_s, \varphi_s)$ is the transfer function in the indoor environment without scattering targets, such as floor, walls, ceiling, and the mutual coupling between Tx and Rx; $H_t(f)$ is the transfer function of Tx; $H_r(f)$ is the transfer function of Rx; and $H_\sigma(f, \theta_i, \varphi_i, \theta_s, \varphi_s)$ is the channel transfer function of scattering, where σ can be determined from

$$\sigma(f, \theta_i, \varphi_i, \theta_s, \varphi_s) = |H_\sigma(f, \theta_i, \varphi_i, \theta_s, \varphi_s)|^2. \quad (3)$$

The experiments attempt to evaluate the indoor RCS of the furniture items, $H_\sigma(f, \varphi_s)$. However, the channel transfer function in an indoor environment without scattering, $H_c(f, \varphi_s)$, is inevitable in such measurement. The time-gating method is applied to remove $H_c(f, \varphi_s)$ using the Kaiser–Bessel window in time domain, $w(t, \theta_i, \varphi_i, \theta_s, \varphi_s)$ (Eq. 4), and the impulse response of scattering component, $h_{sc}(t, \theta_i, \varphi_i, \theta_s, \varphi_s)$ (Eq. 6). Then, the channel transfer function after time gating, $H_{tg}(f, \varphi_s)$ (Eq. 7), is scaled by the channel transfer function in free space, $H_{fs}(f)$ (Eq. 8), to remove $H_t(f)$ and $H_r(f)$. The final result is $H_\sigma(f, \varphi_s)$ (Eq. 9).

The Kaiser–Bessel window is used in the time domain to extract scattering from the target at a delay time of $(d_t + d_r)/c$. The Kaiser–Bessel window $w(t, \theta_i, \varphi_i, \theta_s, \varphi_s)$ is defined as

$$w(t, \theta_i, \varphi_i, \theta_s, \varphi_s) = \begin{cases} \dfrac{I_0\left(\pi\alpha\sqrt{1-\left\{\frac{2[t-t_p(\theta_i,\varphi_i,\theta_s,\varphi_s)]}{T}\right\}^2}\right)}{I_0(\pi\alpha)} & t_p - \frac{T}{2} \le t \le t_p + \frac{T}{2} \\ 0 & \text{otherwise,} \end{cases} \quad (4)$$

where T is the window width, α is a window shape parameter whose value is 4.8; $t_p(\theta_i, \varphi_i, \theta_s, \varphi_s)$ is set at the time around $(d_t + d_r)/c$ to capture the impulse response corresponding to the scattering component; and $I_0(x)$ is the zeroth-order modified Bessel function of the first kind, which can be expressed as

$$I_0(x) = \frac{1}{\pi} \int_0^\pi e^{x\cos(\theta)} d\theta. \quad (5)$$

The impulse response of the scattering component $h_{sc}(t, \theta_i, \varphi_i, \theta_s, \varphi_s)$ can be calculated from

$$h_{sc}(t, \theta_i, \varphi_i, \theta_s, \varphi_s) = \int_{-\infty}^{\infty} H_{sc}(f, \theta_i, \varphi_i, \theta_s, \varphi_s) e^{j2\pi f t} df. \quad (6)$$

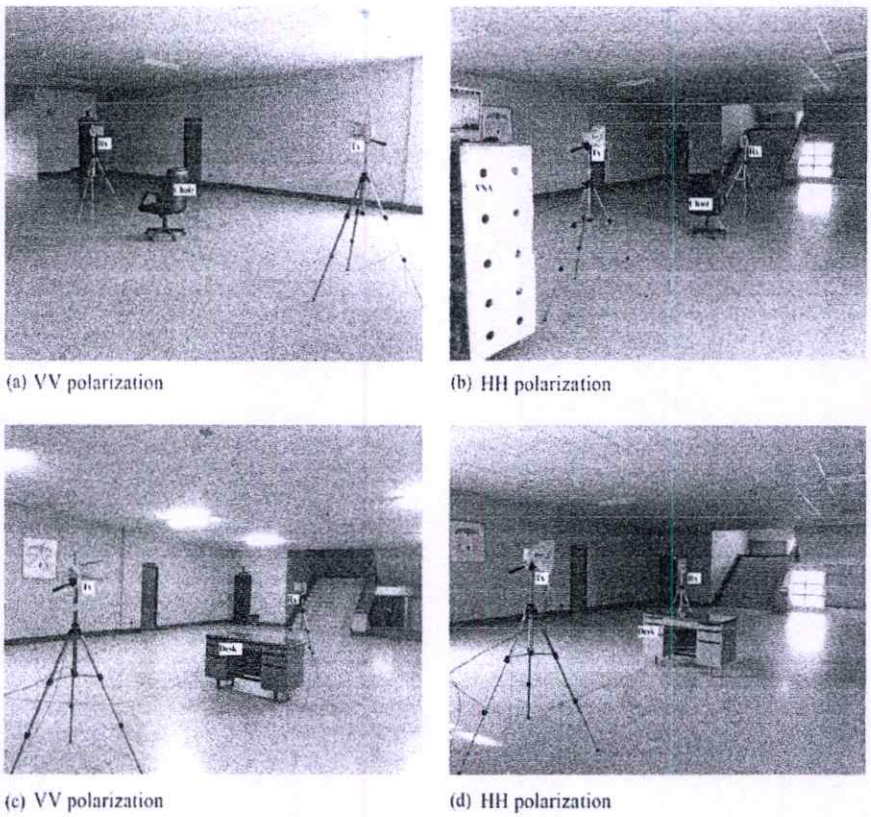

(a) VV polarization (b) HH polarization

(c) VV polarization (d) HH polarization

Figure 2. Bistatic measurement setups for an office chair and a steel desk with VV and HH polarizations.

The frequency transfer function after time gating $H_{\mathrm{ti}}(f,\varphi_{\mathrm{s}})$ can be estimated from

$$\begin{aligned} &H_{\mathrm{ti}}(f,\theta_{\mathrm{i}},\varphi_{\mathrm{i}},\theta_{\mathrm{s}},\varphi_{\mathrm{s}}) \\ &= \int_{-\infty}^{\infty} h_{\mathrm{sc}}(t,\theta_{\mathrm{i}},\varphi_{\mathrm{i}},\theta_{\mathrm{s}},\varphi_{\mathrm{s}})\, w(t,\theta_{\mathrm{i}},\varphi_{\mathrm{i}},\theta_{\mathrm{s}},\varphi_{\mathrm{s}})\, e^{-j2\pi ft}\, dt \\ &\approx \frac{c}{8(\pi)^{3/2} f d_{\mathrm{t}} d_{\mathrm{r}}} H_{\sigma}(f,\varphi_{\mathrm{s}})\, e^{-j2\pi f(d_{\mathrm{t}}+d_{\mathrm{r}})/c} H_{\mathrm{t}}(f)\, H_{\mathrm{r}}(f) \end{aligned} \quad (7)$$

The measurement of the channel transfer function of free space, $H_{\mathrm{fr}}(f)$, was carried out in an anechoic chamber prior to substituting in Eq. (9) to remove $H_{\mathrm{t}}(f)$ and $H_{\mathrm{r}}(f)$. The Tx and Rx antennas were aligned such that they pointed at each other to obtain a direct link. The channel transfer function of free space, $H_{\mathrm{fr}}(f)$, can be written as

$$H_{\mathrm{fr}}(f) = \frac{c}{4\pi f d_{\mathrm{f}}} e^{-j2\pi f d_{\mathrm{f}}/c} H_{\mathrm{t}}(f)\, H_{\mathrm{r}}(f), \quad (8)$$

where d_{f} is the distance from Tx to Rx.

The channel transfer function of scattering, or RCS, is finally derived and can be expressed as

$$H_{\sigma}(f,\varphi_{\mathrm{s}}) = \frac{\sqrt{4\pi} d_{\mathrm{t}} d_{\mathrm{r}}}{d_{\mathrm{f}}} e^{j2\pi f(d_{\mathrm{t}}+d_{\mathrm{r}}-d_{\mathrm{f}})/c} \frac{H_{\mathrm{ti}}(f,\theta_{\mathrm{i}},\varphi_{\mathrm{i}},\theta_{\mathrm{s}},\varphi_{\mathrm{s}})}{H_{\mathrm{fr}}(f)}. \quad (9)$$

3 Experimental evaluation of sample furniture

The location where the experiments were carried out was an indoor open area on the sixth floor of the E-Building, Faculty of Engineering, King Mongkut's Institute of Technology Ladkrabang. The measurements were taken on weekends to avoid interferences from the human body. A sequence of measurements were completely undertaken prior to analysis of the RCS of the experimental furniture items. The measurement setup and procedure are detailed next.

A vector network analyzer (VNA) (HP 8510C) was utilized to measure the magnitude and phase of the transmission coefficients. The VNA was operated in the response measurement mode, where port 1 and port 2 were the transmitter

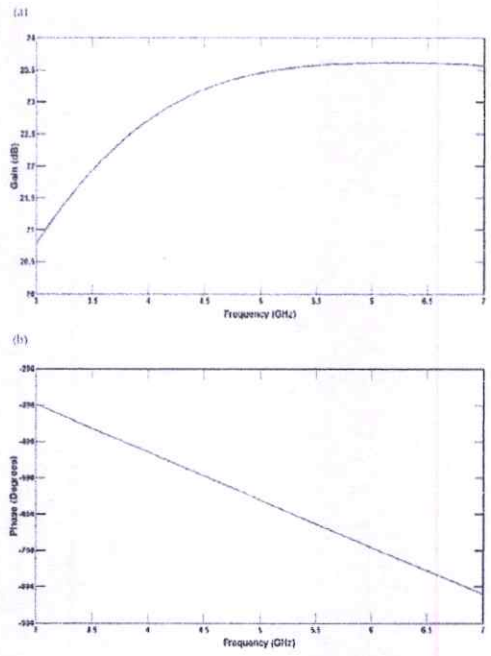

Figure 3. Gain and phase of horn antennas relative to frequency.

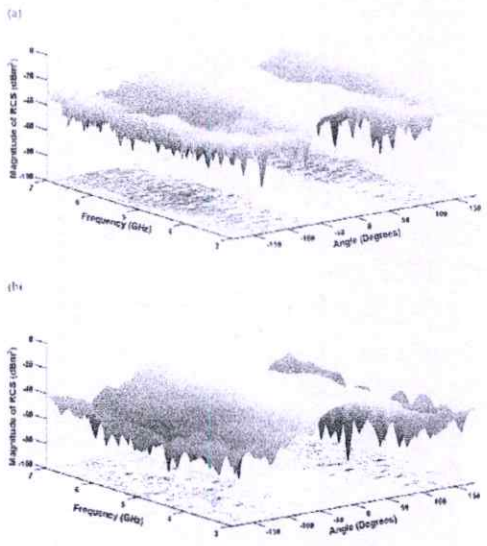

Figure 4. Comparison of RCS without and with time gating.

and receiver ports, respectively. The full two-port method was utilized to calibrate the analyzer to suppress the noise level and to improve the sensitivity and accuracy measurement. Two double-ridged waveguide horn antennas were used, one as Tx and the other as Rx, with an operating frequency range of 1–18 GHz for both vertical and horizontal polarizations. Two experimental scattering targets were an office chair of 1 m × 0.62 m × 0.44 m ($H \times W \times L$) and a steel desk of 0.76 m × 1.37 m × 0.66 m ($H \times W \times L$).

In general, an accurate RCS is achievable only in an anechoic chamber in which the effects of walls, floor, ceiling, and other background clutters are removed. Nevertheless, since the available anechoic chamber is too small to fit the two horn antennas and either of the scattering targets with sufficient space remaining for running the experiments, the experiments were thus carried out in two steps: (1) the evaluation of RCS with the existence of either target in the indoor open area on the sixth floor of the E-Building, and (2) the antenna calibration in the anechoic chamber.

For the setup, the frequency range is from 3 to 7 GHz with a total of 801 frequency points. The averaging factor was set at 4096 to reduce the noise level and improve the signal-to-noise ratio (SNR). The sweep time was 200 ms and the intermediate frequency bandwidth (IFBW) of the vector network analyzer was 10 kHz. The measurement at each angle required approximately 15 min. The maximum transmitted power of 10 dBm was selected to obtain the maximum system dynamic range, and the received impulse response of each receiver position was recorded. For the RCS in the presence of either of the scattering targets, the distance from Tx to the center of the target was 3 m, and the distance between the center of the target and the Rx antenna was 2 m. The experiments were conducted in the near-field (Fresnel) region due to space and power limitations. Both Tx and Rx were placed at a height of 1.5 m from the ground. The receiving antenna was rotated with a 10° increment around the scattering target for a total of 36 positions. The measurements were thus repeated by varying the angle of Rx, while that of Tx remained stationary to achieve the directional pattern of the bistatic RCS between Tx and Rx, assuming that $\theta_i = \theta_s = 90°$, $\varphi_i = 180°$, and $\sigma(f, \theta_i, \varphi_i, \theta_s, \varphi_s)$ is simplified to $\sigma(f, \theta_s)$. Figure 1 illustrates the top and side views of the bistatic RCS, while Fig. 2a–d are photographs of the measurement setups for the chair and desk for vertical–vertical (VV) and horizontal–horizontal (HH) polarizations.

In the calibration, the antenna measurement in the anechoic chamber was carried out to determine the channel transfer function of free space. The Tx and Rx antennas in the calibration were each 1.40 m in height from the ground and were placed at a distance of 2 m and aligned pointing at each other. Figure 3 shows the broadside–broadside (0°) gains and phases of the horn antennas relative to the frequency.

4 Experimental results

This section presents how the accuracy of the conventional ray tracing simulation technique can be improved upon with the proposed extended radar equation. The indoor RCS of

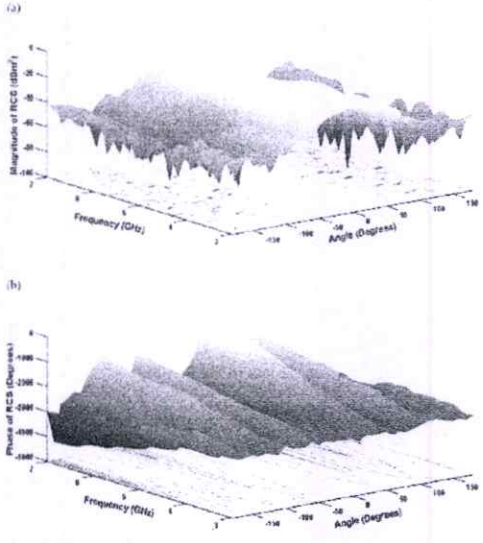

Figure 5. The RCS for the experimental office chair for VV polarization.

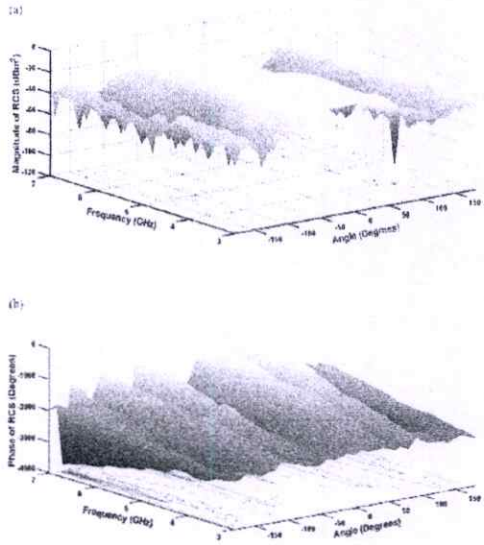

Figure 7. The RCS for the experimental steel desk for VV polarization.

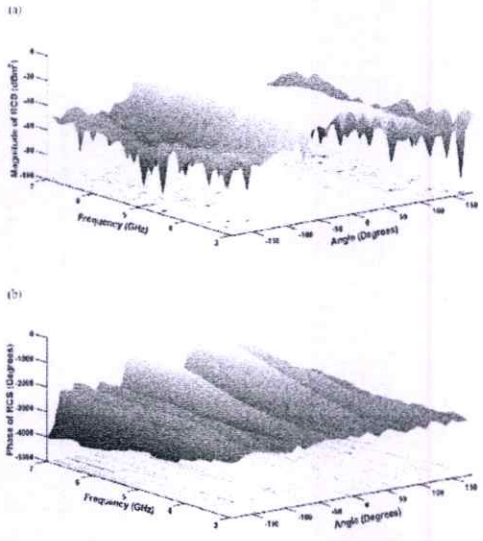

Figure 6. The RCS for the experimental office chair for HH polarization.

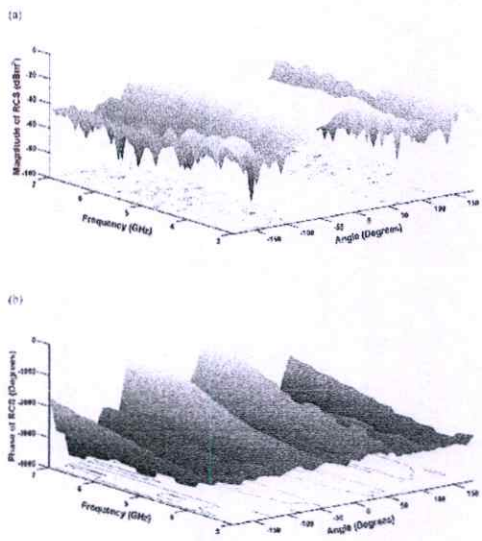

Figure 8. The RCS for the experimental steel desk for HH polarization.

the two scattering targets, i.e., the office chair and steel desk, were evaluated in the frequency range of 3–7 GHz in VV polarization and HH polarization. It is found that the VV and HH polarizations yielded different RCS.

This paper utilized time gating to remove the multipath effect in the received signals. The time-gating method transforms the frequency domain response into a time domain response and also filters out the late time pulses, which are attributable to the multipath effect. To demonstrate the effectiveness of time gating in removing the multipath effect, the comparison between the RCS of the chair without and with time gating is provided. Figure 4 compares the RCS without and with time gating along the frequency range of 3–7 GHz and with different incident angles. In Fig. 4a, without time

gating, the scattering from the chair induces the interferences and ripples in the RCS, while in Fig. 4b, the time gating reduces the ripples in the main beam. Moreover, the scattering lobes beyond 90 ° are reduced to below −20 dBm^2, resulting in a significant reduction in the edge diffraction effect, which in turn makes the scattering effect easier to extract. As shown in Fig. 4b, the multipath effects from 90 to 180 ° and −90 to −180 ° along the frequency range of 3–7 GHz are considerably removed. With time gating, more accurate RCS can be achieved.

The 3-D graphics of RCS with time gating of the experimental chair for VV and HH polarizations are illustrated in Figs. 5 and 6, respectively, while those of the desk for VV and HH polarizations are depicted in Figs. 7 and 8. It was observed that the RCS for HH polarization is larger than that of VV polarization for most observation angles. In addition, the RCS varies with changes in incident angle and frequency. For instance, the RCS at 0 ° of the chair for VV polarization at the frequencies of 3 and 5 GHz are −40 and −62 dBm^2, respectively; for HH polarization they are −36 and −53 dBm^2 at the same frequencies. In the case of the desk at 0 °, the RCS for VV polarization at 3 and 5 GHz are respectively −55 and −47 dBm^2, and they are −36 and −46 dBm^2 at the same frequencies for HH polarization. The findings indicate that the RCS is subject to types of scattering objects, angle, frequency, and polarization.

5 Conclusions

This paper has attempted to evaluate the RCS of two furniture items, i.e., an office chair and a steel desk, using the extended radar equation at the frequency range of 3–7 GHz. Time gating was utilized to remove the multipath effect, and its removal effectiveness is verified by the comparison between the RCS without and with time-gating method. This research paper has also investigated the scattering characteristics of the two furniture items for different frequencies, angles, and polarizations. The maximum RCS of the experimental office chair and steel desk are approximately −11 and −9 dBm^2, respectively. In both experimental scattering objects, the VV-polarization RCS is generally lower than that for HH polarization. This is possibly due to the diffraction at the side edge.

Acknowledgements. The authors gratefully acknowledge the anonymous reviewers and referees for their useful comments and constructive suggestions. The authors would like to extend deep gratitude to the Japan International Cooperation Agency (JICA) under the AUN/SEED-Net (ASEAN University Network, Southeast Asia Engineering Education Development Network) program. Sincere appreciation is also extended to the Wireless Communication Laboratory for the support with regard to the anechoic chamber. Special credit goes to S. Teawchim, S. Duanhsuwan, J. Sahakit, and W. Vinicchayakul for their assistance and contributions to this research.

Edited by: M. Chandra
Reviewed by: G. Wanielik and one anonymous referee

References

Bocanegra, D. E., Martinez, D. P., Recio, R. F., Lucena, A. J., and Sanchez, I. M.: New Benchmark Radar Targets for Scattering Analysis and Electromagnetic Software Validation, Prog. Electromagn. Res., 88, 39–52, 2008.

Cheffena, M.: Physical-Statistical Channel Model for Signal Effect by Moving Human Bodies, EURASIP J. Wirel. Comm., 77, 1–13, 2012.

Esposti, V. D., Fuschini, F., Vitucci, E. M., and Falciasecca, G.: Measurement and Modelling of Scattering from Buildings, IEEE T. Antenn. Propag., 55, 143–153, 2007.

Ghoraishi, M., Takada, J.-I., and Imai, T.: Radio Wave Scattering from Lamposts in Microcell Urban Mobile Propagation Channel, ECTI-EEC, 7, 14–20, 2009.

Jong, Y. L. C. and Herben, M. H. A. J.: A Tree-Scattering Model for Improved Propagation Prediction in Urban Microcells, IEEE T. Veh. Technol., 2, 503–513, 2004.

Kishiki, Y., and Takada, J.-I.: Improvement of 3D ray tracing simulation in microcell environment by introducing the complex radar cross section, The 2008 International Symposium on Antennas and Propagation (ISAP 2008), Taipei, Taiwan, 27–30 October 2008, 790–793, 2008.

Knott, E. F., Shaeffer, J. F., and Tuley, M. T.: Radar Cross Section, Artech House, New Jersey, 1985.

Lim, C.-P., Volakis, J. L., Sertel, K., Kindt, R. W., and Anastasopoulo, A.: Indoor Propagation models based on rigorous methods for site-specific multipath environment, IEEE T. Antenn. Prop., 54, 1718–1725, 2006.

Miacci, M. A. S., Nohara, E. L., Martin, I. M., Peixoto, G. G., and Rezende, M. C.: Indoor Radar Cross Section Measurement of Simple Targets, Journal of Aerospace Technology and Management (JATM), 4, 25–32, 2012.

Nicolaescu, I. and Iubu, G.: Simple and Collected Targets Radar Cross Section, International Conference on Electromagnetics in Advanced Applications (ICEAA 2007), Torino, 17–21 September 2007, 295–298, 2007.

Pongsilamanee, P. and Bertoni, H. L.: Specular and Nonspecular Scattering from Building Facades, IEEE T. Antenn. Prop., 52, 1879–1889, 2004.

Tsuchiya, H., Lertsirisopon, N., Takada, J.-I., and Kobayashi, T.: Effects of Bragg Scattering on Ultra-Wideband Signal Transmission from Periodic Surfaces, IEICE Transactions on Communications, E91-B, 536–542, 2008.

International Conference on Engineering, Applied Sciences, and Technology
November 21 – 24, 2012, Swissôtel Le Concorde, Bangkok, Thailand

A Comparison of Indoor Channel Measurements and FDTD Simulations at 5.8 GHz

Myo Myint Maw*, Pichaya Sunpankoon†, Sathaporn Promwong†and Jun-ichi Takada‡
*International College, King Mongkut's Institute of Technology Ladkrabang, Bangkok 10520, Thailand
Email: myomyintmawphdit5@gmail.com
†Department of Telecommunication Engineering, Faculty of Engineering
King Mongkut's Institute of Technology Ladkrabang, Bangkok 10520, Thailand
‡Department of International Development Engineering
Graduate School of Science and Engineering, Tokyo 152-8552, Japan

Abstract—**In this paper, the channel predicted by using a two-dimensional (2-D) transverse magnetic (TM) mode of finite difference time domain (FDTD) is presented and compared to measurement results performed in a typical lecture room. To get accurate predictions, a good description of the electromagnetic properties of the obstacles present in the environment is needed. After that, we evaluate the path loss effect with our proposed model in an indoor environment. Our proposed model is a class room structure, which consists of brick wall, wood door, and wood chairs. Furthermore, these obtained data model the path loss by using the regression model and cumulative distribution function (CDF) of fading are illustrated.**

I. Introduction

The performances of modern wireless communication systems strongly depend on the electromagnetic characteristics of the environment in which they operate. This aspect is particularly important for cellular phones, wireless local area networks (WLANs) and personal communication systems operating in complex environments (buildings, factories, hospitals, railway stations, airports, etc). Recently, ray tracing techniques (RT), associated to the UTD [1], have emerged as the dominant techniques to predict the wide-band channel behavior. Indeed, these asymptotic methods are fast and not limited in frequency. However, dealing with indoor propagation, this classical approach is not sufficient to model object of wavelength size or with complex forms. For these structures, rigorous methods like the FDTD, consisting in solving Maxwell's equations in discrete time domain, are well-suitable. In this paper, we present the FDTD methods, in order to enhance the propagation channel's modeling.

Wireless local-area networks are expanding rapidly as a result of the increasing demand on computer communications and the advances in digital radio systems. Several frequency bands have been proposed to be used by these systems, including the 100 MHz band around a centre frequency of 5.8 GHz [2], which is considered in this paper. The deployment of these networks requires the study of the propagation environment and the measurement of the reflection, transmission, and scattering of radio waves by the different obstacles, to obtain data that can then be used to develop and validate radio-planning tools.

A ray tracing technique has been demonstrated to be promising for indoor radio propagation. A finite difference time domain (FDTD) method [3], [4] is an alternative method for modeling the channel. Although the FDTD method requires more computer resources compared with the ray tracing technique, the simulation of indoor environment requires less computer resources than that of the outdoor environment. Furthermore, the FDTD method can compute the scattered fields more accurately compared with the ray tracing technique for complex lossy structures with finite dimensions encountered in the indoor environment. Therefore, the FDTD method is usually used to model a site-specific narrow band indoor channel [5], [6].

In this paper, the two-dimensional (2-D) transverse magnetic (TM) mode of the FDTD method, satisfying the numerical stability condition and with perfectly matched layer absorbing boundary condition (PML ABC) [5], is used to simulate the indoor radio wave propagation and path loss model. The modulated Gaussian pulse satisfying the signal definition and FCC indoor limit spectral mask [4] is used as the excitation signal. The free space path loss obtained from the FDTD method is shown. After that, we evaluate the path loss effect with our proposed model in the indoor environment. Our proposed model is a room structure (furnished room), which consists of door, 32 chairs and brick walls. Furthermore, these obtained data model the path loss by using the regression model. The cumulative distribution function (CDF) of fading is illustrated. This paper is organized as follows. In Section II, the FDTD method used in this paper is reviewed. The measurements presented in this paper are taken in lecture room environments that are the main field of applicability of WLAN in Section III. Next, the comparison of statistics from numerical simulation and measurement results are shown. Conclusions are given in Section V.

II. FDTD Method

The 2-D TM mode of finite difference equations are directly derived from Maxwell's curl equations in time domain. Maxwell's curl equation can be written as [11]

International Conference on Engineering, Applied Sciences, and Technology
November 21 – 24, 2012, Swissôtel Le Concorde, Bangkok, Thailand

$$\mu\frac{\partial\vec{H}}{\partial t} = -\nabla\times\vec{E} \quad (1)$$

$$\epsilon\frac{\partial\vec{E}}{\partial t} = \nabla\times\vec{H} \quad (2)$$

where H is the magnetic field, E is the electric field, is the magnetic permeability and is the electric permittivity.

To obtain discrete approximation of the continuous partial differential equations, the centered difference approximation is used on both the time and space first-order partial difference. The entire computation domain is the collection of all the unit cells. The dimensions of the unit cell along x and y directions are Δx and Δy, respectively. The node with subscripts indices i and j corresponds to node number x in and y directions. The time step is indicated with the superscript index n. The time interval of each time step is Δt. After simple arrangement, the 2-D TM mode of finite difference equations are described as [6], [7]

$$H_x|_{i,j}^{n+1/2} = H_x|_{i,j}^{n-1/2} + \left(\frac{\Delta t}{\mu_{i,j}}\right)\left(\frac{E_z|_{i,j-1/2}^{n} - E_z|_{i,j+1/2}^{n}}{\Delta y}\right) \quad (3)$$

$$H_y|_{i,j}^{n+1/2} = H_y|_{i,j}^{n-1/2} + \left(\frac{\Delta t}{\mu_{i,j}}\right)\left(\frac{E_z|_{i+1/2,j}^{n} - E_z|_{i-1/2,j}^{n}}{\Delta x}\right) \quad (4)$$

$$E_z|_{i,j}^{n+1} = C_a|_{i,j}E_z|_{i,j}^{n-1} + C_b|_{i,j}\left(\frac{H_y|_{i+1/2,j}^{n+1/2} - H_y|_{i-1/2,j}^{n+1/2}}{\Delta x} + \frac{H_x|_{i,j-1/2}^{n+1/2} - H_x|_{i,j+1/2}^{n+1/2}}{\Delta y}\right). \quad (5)$$

With the electric field updating coefficients at node (i, j) are given by

$$C_a|_{i,j} = \frac{1-\frac{\sigma_{i,j}\Delta t}{2\epsilon_{i,j}}}{1+\frac{\sigma_{i,j}\Delta t}{2\epsilon_{i,j}}}, \quad (6)$$

$$C_b|_{i,j} = \frac{\frac{\sigma_{i,j}\Delta t}{2\epsilon_{i,j}}}{1+\frac{\sigma_{i,j}\Delta t}{2\epsilon_{i,j}}}. \quad (7)$$

where the parameter σ is the electric conductivity.

The maximum time step is limited by the stability restriction of the finite difference equation. The numerical stability condition of 2-D FDTD is specified as [11]

$$\Delta t \le \frac{1}{c\sqrt{\frac{1}{\Delta x^2}+\frac{1}{\Delta y^2}}} \quad (8)$$

where c is the velocity of light in free space.

In this paper, the magic time step condition is used to obtain the minimum numerical error. The magic time step condition is defined as

$$\Delta t = \frac{1}{c\sqrt{\frac{1}{\Delta x^2}+\frac{1}{\Delta y^2}}} \quad (9)$$

The modulated Gaussian pulse satisfies the signal definition and the FCC indoor limit spectral mask is used as the excitation signal V_S. The expression of this pulse is [13]

$$V_S = Ae^{-[(n-n_0)\frac{\Delta t}{d}]^2}\cos[2\pi f_c(n-n_0)\Delta t] \quad (10)$$

where A is the maximum amplitude of the envelope signal, f_c is the carrier frequency, d is the $\frac{1}{c}$ characteristic decay time and n_0 is the delayed time step.

A. PML ABC Treatment

The tangential field components on the four mesh walls must be specified in such a way that outgoing waves are not reflected. The FDTD simulation in this paper uses the PML ABC [10]. The PML ABC can effectively absorb propagation wave by using nonphysical lossy media adjacent to the outer grid boundaries backed by perfectly conducting walls. The field components are split into two subcomponents. The electric and magnetic losses, σ_e and σ_h, inside the PML medium are specified by satisfying the PML impedance matching condition

$$\frac{\sigma_e}{\epsilon} = \frac{\sigma_h}{\mu} \quad (11)$$

After the specification of electric and magnetic losses, electromagnetic waves inside the PML medium are rapidly attenuated. The explicit exponentially difference file-updating equations are used to replace the conventional FDTD algorithm.

The electric loss inside the PML legion is assumed to increase with depth from zero at $\rho = 0$ to a maximum value of σ_{max} at $\rho = \delta$ by the quadratic ramping

$$\sigma_e = \sigma_{max}\left(\frac{\rho}{\delta}\right)^2 \quad (12)$$

where σ_{max} is chosen to bound the PML reflection coefficient, the PML reflection coefficient at normal incident has the following expression

$$R(0) = e^{\frac{-2\sigma_{max}\sigma}{3c}} \quad (13)$$

III. Measurement Setup and Environments

The indoor radio channel transfer function is measured in frequency domain. The measurement system consists of the VNA (HP-8510C), the S-parameter test set (HP-8514B), the frequency synthesized sweeper (HP-83620A), the biconical antenna pair and the personal computer. The VNA is operated in the response measurement mode, where port 1 is the Tx which is connected to Tx antenna and port 2 is the Rx which is connected to the Rx antennas and via the semi-rigid cable as shown in Figure 1. The measurement setup parameters is listed in Table I.

The biconical antennas with the maximum diameter of 65.3 mm and the length of 37 mm are used as the Tx and Rx antennas. The geometric and dimension of biconical antenna is shown in Figure 2. The biconical antenna typically has an omni-directional radiation pattern, with a linearly phase

Fig. 1. Overview of the Measurement setup

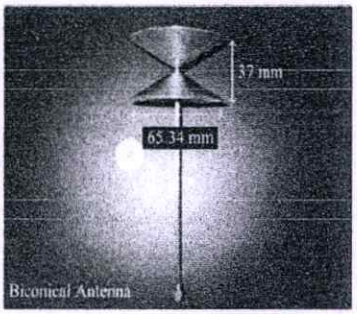

Fig. 2. Geometric and dimensions of Biconical antenna

TABLE I
MEASUREMENT SETUP PARAMETERS

Parameter	Value
Frequency range	5.7GHz 5.9GHz
Number of frequency points	801
Dynamic power Range	80
Tx antenna height	0.9m
Rx antenna height	0.9m
Distance from Point Model	0.6m
Antenna Type	Biconical
Polarization	Vertical

response. The measurement was done in Lecture room (E12-305) on 3rd floor Engineering Building at King Mongkut's Institute of Technology Ladkrabang (KMITL).

IV. Numerical Simulations and Measurement Results

We proceed now with the full-wave analysis of a classroom based on the two-dimensional transverse magnetic mode of finite difference time domain method. The examples of interest are the class room occupied with 32 chairs. The dimensions of the room and detailed floor plan are displayed in Figure 3. The room is of length 1237.5 cm, width 692 cm and height 300cm.

The electromagnetic properties of other materials such as

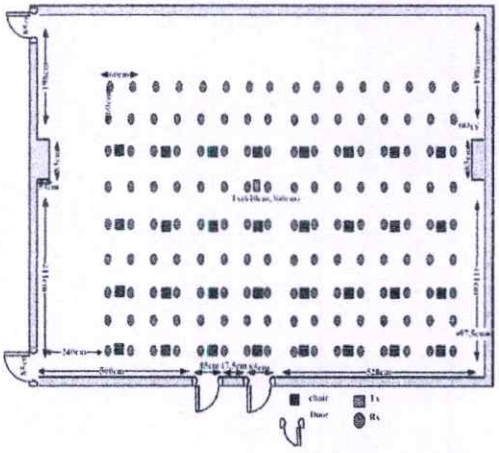

Fig. 3. Layout of a room indoor environment

TABLE II
ELECTROMAGNETIC PROPERTY OF DIFFERENT MATERIALS

Material	Electromagnetic property
Brick wall	$\sigma = 0.11, \epsilon_r = 3.58$
Wood door	$\sigma = 0.06, \epsilon_r = 5.84$
Wood chair	$\sigma = 0.20, \epsilon_r = 2.88$

brick wall with mean value (permittivity = 3.58 and conductivity = 0.11) and wooden door with mean value (permittivity=5.84 and conductivity = 0.06) at 5.8 GHz is shown in Table II [14]. The simulation was done in Lecture room (E12-305) on $3rd$ floor Engineering Building at King Mongkut's Institute of Technology Ladkrabang (KMITL). We evaluate the path loss effect with our proposed model in the indoor environment.

The 2-D TM mode of FDTD simulation is used to model this structure. The cell sizes in x and y directions are $\Delta x = \Delta y = 0.005m$. The PML ABC with 16 layers is used to reduce the reflection error at the edges of the simulation boundary. The dimension of total lattice is 2681 × 1484 cells. The time interval of each time step is $\Delta t = 11.79ps$, which satisfies the numerical stability condition. The total time steps of this simulation are N= 5000.

For the narrow band WLAN excitation signal, the parameters of modulated Gaussian signal satisfying the narrow band WLAN signal definition and FCC indoor limit spectral mask are $f_c = 5.8GHz$, $d = 0.11ns$, $n_0 = 25$ and $A = 3.76mV/m$, respectively. The excitation signal in the time domain and its radiated power spectral density (PSD) compared with Federal Communications Commission (FCC) indoor limit spectral mask are shown in Figure 4 and 5 , respectively.

For modeling the path loss, the linear regression model based on log-distance path loss model [14] is used. The model can be realized by curve fitting on a scatter plot of obtained

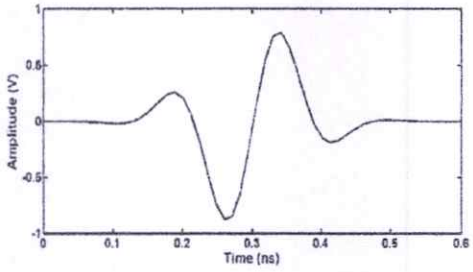

Fig. 4. Excitation signal in time domain

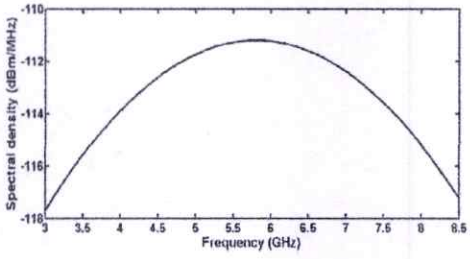

Fig. 5. Radiated PSD excitation Signal

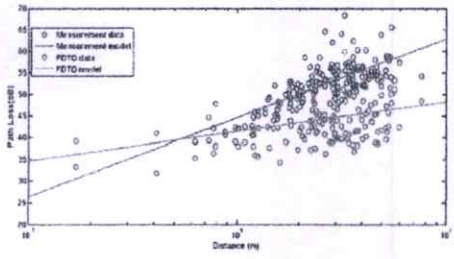

Fig. 6. The measured and predicted path loss for a 5.8 GHz propagation in room

path loss and then the path loss exponent n is derived from:

$$PL(d) = \overline{PL}(1) + 10n\log(d) + X_\sigma \qquad (14)$$

where PL(d) is the path loss in dB at the TR separation distance of d, is the average large-scale path loss at $1m$ TR separation distance, X_σ is the shadowing fading parameter with the standard deviation of σ in dB. When plotted on a log-distance graph, the path loss model is a straight line and can be determine from the slope of dB per decade. The value n and σ depend on the specific propagation environment. The main objective of this simulation is to determine $\overline{PL}(1)$, n and X_σ of the signal propagation in class room.

The scatter plot of path loss obtained from FDTD simulation and regression model and measurement are shown in Figure 6 for Lecture room. The 144 data points are used to model the path loss. For this area, the model parameters of simulation are dB and and dB and are from measurement. For considering

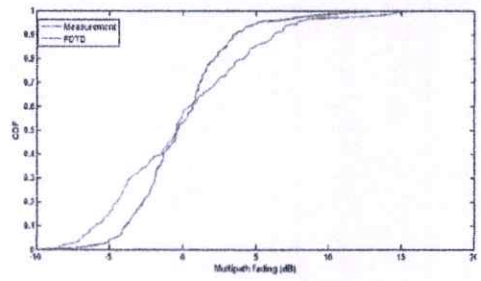

Fig. 7. CDF of fading in class room model

the fading parameter X_σ , the statistic model is used. The cumulative distribution function (CDF) of fading are evaluated. Figure 7 shows the CDF of fading in classroom with chairs. The statistic parameters of this area are the standard deviation of $\sigma = 4.97$ dB and zero mean.

V. Conclusion

In this paper, we presented an original approach of the 2-D TM mode of FDTD method is used to simulate the indoor radio wave propagation. It is flexible to model a narrow band channel of different environment according to the desired accuracy by setting the cell size. By using the FDTD method, numerous data points can be obtained for modeling the path loss. This simulation can be applied to arbitrary bandwidths or types of indoor signals. From the results, we can see that the FDTD simulation is convenient and flexible for the site specific and statistical models of the indoor radio wave propagation. Further, we want to extend this approach to the variety of small and complex structures in indoor model. A study will be done around parameters such as the dimensions, the form or the material of the structures. Globally, for wireless indoor applications, our goal with presented method is to evaluate the influence of small and complex structures on the channel modelling. The model accuracy was investigated through comparisons between measurements and simulated results.

References

[1] D. McNamara, C. Pistorius, and J. Malherbe, *Introduction to the Uniform Geometrical Theory of Diffraction*, Artech House, Inc., 1990.
[2] R. O. Lamaire, A. Krishna, and P. Bhagwat, "Wireless LAN's and mobile networking: Standards and future directions," IEEE Commun. Mag., pp.86 94, August 1996.
[3] G. Durgin, "Advanced site-specific propagation prediction techniques," master thesis, Virginia Polytechnic Institute and State University, 1998
[4] Y. Kishiki and J. Takada, "Improvement of 3d ray tracing simulation in microcell environment by introducing the complex radar cross section," in 2008 International Symposium on Antennas and Propagation (ISAP2008), Oct. 2008.
[5] C. Lim, J. Volakis, K. Sertel, R. Kindt, and A. Anastasopoulos, "Indoor propagation models based on rigorous methods for site-specific multipath environments," IEEE Transactions on Antennas and Propagation, vol. 54, no. 6, pp. 1718-1725, Jun. 2006.
[6] K.S. Yee, "Numerical Solution of Initial Boundary Value Problems Involving Maxwell's Equations in Istropic Media," IEEE Transactions on Antennas and Propagation, vol. 14, pp.302'307, 1966.

[7] Taflove, *Computational Electro-Dynamics: The Finite-Difference Time-Domain Method*, Norwood, MA: Artech House, 1995.
[8] P. Supanakoon, P. Rawiwan, P. Tangtisanon and J. Takada, "Indoor Radio Wave Propagation Modeling Using Modified FDTD Method," 2001 International SYmPosium on Communications and Information Technology (ISCIT 2001), pp. 441-444 Nov 2001.
[9] S. Reynaud, C. Guiffaut, A. Reineix1, Rodolphe .V, "Modeling indoor propagation using an indirect hybrid method combining the UTD and the FDTD methods," European Conference on Wireless Technology, Amsterdam, 2004
[10] J. Berenger, "A Perfectly Matched Layer for the Absorption of Electromagnetic Wave," Journal on Computational Physics, vol. 14,pp. 1 85-200, 1 994.
[11] BAlanis,*Advanced Engineering Electromagnetics*, John Wiely, 1989.
[12] Taflove and M. E. Brodwin, *Numerical Solution of Steady -State Electromagneric Scattering Prolbems Using The Time Dependent Maxwell's Equation*, IEEE Transactions on Microwave Theory and Techniques, vol.23, pp. 623-630, 1975.
[13] P. Supanakoon,T . Subson,M . Chamchoy, P. Rawiwan, S. Promwong and P. Tangtisanon,"FDTD Simulation for Site Specific Modeling of Indoor Radio Wave Propagation", 24th Electrical Engineering Conference (EECON-24), pp. 874-879, Nov.2001.
[14] I?igo Cui?as, David Mart?nez, Manuel Garc?a S?nchez, Ana V?zquez Alejos, "Modelling and measuring reflection due to flat dielectric surfaces at 5.8 GHz", IEEE Transactions on Antennas and Propagation, vol.55, no.4, April 2007.
[15] T. S. Rappaport, *Wireless Communication Principles and Practice*, Prentice Hall PTR, 2nd Edition, 2002.

Thailand-Japan MicroWave 2013

Experimental Evaluation of Furniture Radar Cross Section in Indoor Propagation Channel

Myo Myint Maw†, Sathaporn PROMWONG† and Jun-ichi TAKADA‡

† Faculty of Engineering, King Mongkut's Institute of Technology, Bangkok, Thailand

‡Department of International Development Engineering,Graduate School of Science and Engineering, Tokyo 152-8552, Japan

E-mail: †s3601051@kmitl.ac.th, †kpsathap@kmitl.ac.th ‡takada@ide.titech.ac.jp

Abstract For the propagation prediction model, the complex furniture such as table and chair are typical objects that cannot be accurately modeled in the ray tracing simulation. Therefore, the effects of scattering on ultra wideband (UWB) signal from furniture are discussed in this paper. The extension of the radar equation in the complex transfer function to evaluate the radar cross section (RCS) is introduced. The time gating method is applied to remove the effect of multipath, which occurred in indoor environments. The RCS results of example furniture with vertical and horizontal polarizations using horn antennas are shown. These results are useful to apply for indoor propagation prediction using ray tracing techniques.

Keyword Scattering, Radar Cross Section, Furniture, Indoor Propagation Channel

1. Introduction

The determination of channel characteristics in indoor applications is dominated by scattering considerations. In the indoor environments, the effect of all scattering targets such as furniture will contribute to the total received field. Due to the complex and random geometry, their effects on the radio wave propagation are become to be difficult to investigate and model. Several researches were accomplished with typical building walls [1] and a scattering of trees [2]. Moreover, the effect of scattering from objects such as lampposts, traffic lights and signboards have been analyzed [3] and then the effects of Bragg scattering on ultra wideband (UWB) signal transmission from periodic surfaces were reported [4]. However, the scattering from complex and canonical scattering targets such as table and chair, shelf, cabinet and human body are typical objects that cannot be accurately modeled in ray tracing simulation and have not been analyzed or modeled [5], even though their contribution to channel propagation have already been addressed.

In this paper, the experimental evaluation of furniture radar cross section (RCS) in indoor propagation channel is discussed. The extension of the radar equation in the complex transfer function to evaluate the RCS is introduced. The time gating method is applied to remove the effect of multipath. The RCS results of example furniture using horn antennas are shown. These results are useful to apply for indoor propagation prediction using ray tracing techniques.

2. Theory of RCS Evaluation

The radar equation [6] is widely used for the general radar link budget. The extension of radar equation in the complex form is developed and used with UWB signal. The frequency transfer function of this channel $H_{ss}(f.\theta_i.\phi_i.\theta_s.\phi_s)$ can be written as

$$H_{ss}(f.\theta_i.\phi_i.\theta_s.\phi_s) = \left[\frac{c}{8\pi\sqrt{\pi}d_t d_r|f|} H_\sigma(f.\theta_i.\phi_i.\theta_s.\phi_s) e^{-j2\pi f(d_t+d_r)/c} + H_c(f.\theta_i.\phi_i.\theta_s.\phi_s)\right] H_t(f) H_r(f) \quad (1)$$

where $H_c(f.\theta_i.\phi_i.\theta_s.\phi_s)$ is the transfer function of indoor environment without target scatter such as floor, wall and ceiling including the mutual coupling between TX and RX antennas. $H_t(f)$ and $H_r(f)$ are the transfer function of TX and RX antennas, respectively. $H_\sigma(f.\theta_i.\phi_i.\theta_s.\phi_s)$ is the complex notation of the target RCS. d_t and d_r are distances from target to TX and RX antennas. c is velocity of light, f is frequency, θ_i and ϕ_i are the elevation and azimuth incident angles to target, and θ_s and ϕ_s are the elevation and azimuth scattering angles from target.

For removing term $H_c(f.\theta_i.\phi_i.\theta_s.\phi_s)$, the time gating is used. The Kaiser-Bessel window is used in the time domain to extract the scattering from the target at the delay time of $(d_t+d_r)/c$. The frequency transfer function after time gating process $H_{tg}(f.\theta_i.\phi_i.\theta_s.\phi_s)$ can be estimated to

$$H_{tg}(f.\theta_i.\phi_i.\theta_s.\phi_s) = \frac{1}{4\pi d_t d_r} H_\sigma(f.\theta_i.\phi_i.\theta_s.\phi_s) e^{-j2\pi f(d_t+d_r)/c} H_t(f) H_r(f) \quad (2)$$

Finally, the complex transfer function of radar cross section is derived and can be written as

$$H_o(f,\theta_i,\phi_i,\theta_s,\phi_s)=\frac{\sqrt{4\pi}d_t d_r}{d_t}e^{j2\pi(d_t+d_r-d_t)/c}\cdot\frac{H_o(f,\theta_i,\phi_i,\theta_s,\phi_s)}{H_s(f)} \quad (3)$$

where $H_s(f)$ is transfer function of free space channel and d_t is distance from TX to Rx antennas in free space channel.

This evaluation scheme does not need to calibrate with the transfer function of the known RCS target.

3. Measurement Setup

The measurement system consists of the VNA (HP-8510C), the S-parameter test set (HP-8514B), the frequency synthesized sweeper (HP-83620A), the double-ridged horn antenna pair and the personal computer. The measurement was done indoor lobby place on 6th floor E Building at King Mongkut's Institute of Technology Ladkrabang (KMITL). The office chair was used as the example target. The measurement setup parameters are listed in Table 1.

Table 1. Measurement setup parameters

Parameter	Value
Frequency range	3GHz~7GHz
Number of frequency points	801
Tx and Rx antenna height	0.93 m
Distance from TX to target	3 m
Distance from target to RX	2 m
Antenna type	Horn
Polarization	Vertical

4. Results

Magnitude of RCS along frequency from 3 GHz to 7 GHz is shown in Fig. For focusing at single frequency, magnitude of RCS at frequency of 5 GHz with and with out time gating is shown in Fig. 2.

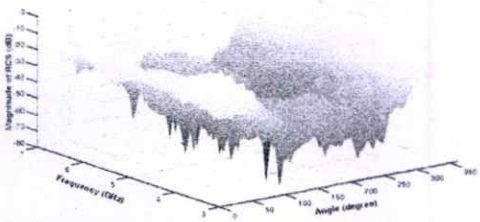

Fig. 1. Magnitude of RCS at frequency 3-7 GHz

5. Conclusion

These results presented a simple setup built in an indoor environment, proper to measure RCS of chair was characterized by measuring the backscattered radiation patterns in different aspect angles, in the frequency range of 3 GHz to 7 GHz. Obviously, the strength of any object's effect depends on target properties or materials, frequency, its shape and size. Finally, we can conclude the results that the time gating process can remove the mutual coupling between TX and RX antennas and multi-path effect from the side and backside.

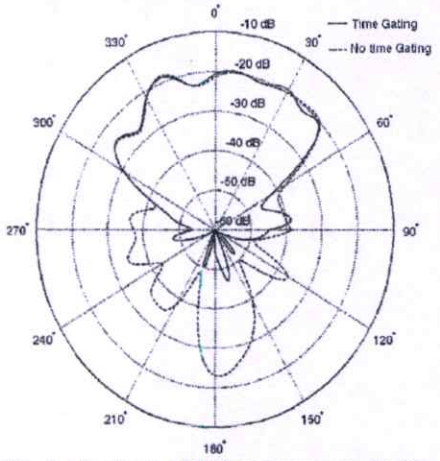

Fig. 2. Magnitude of RCS at frequency of 5 GHz

References

[1] V. D.-Esposti, F. Fuschini, E. M. Vitucci and G. Falciasecca, "Measurement and Modelling of Scattering from Buildings," IEEE transactions on Antennas and Propagation, vol. 55, no. 1, pp. 143-153, 2007.

[2] Y. L. C. de Jong, and M. H. A. J. Herben, "A Tree-Scattering Model for Improved Propagation Prediction in Urban Microcells," IEEE Transactions on Vehicular Technology, vol. 53, no. 2, pp. 503-513, 2004.

[3] M. Ghoraishi, J. Takada and T. Imai, "Radio Wave Scattering from Lamposts in Microcell Urban Mobile Propagation Channel," ECTI Transactions on Electrical Engineering, Electronics, and Communications, vol. 7, no. 1, pp. 14-20, Feb. 2009.

[4] H. Tsuchiya, N. Lertsirisopon, J. Takada and T. Kobayashi, "Effects of Bragg Scattering on Ultra-Wideband Signal Transmission from Periodic Surfaces, IEICE Transactions on Communications, vol. E91-B, no. 2, pp. 536-542, Feb. 2008.

[5] C.-P. Lim, J. L. Volakis, K. Sertel, R. W. Kindt and A. Anastasopoulos, "Indoor Propagation models based on rigorous methods for site-specific multipath environment," IEEE Transactions on Antennas and Propagation, vol. 54, no. 6, pp. 1718-1725, 2006.

[6] E.F.Knott, J.F.Shaeffer, and M.T.Tuley, Radar Cross Section, Artech House, New Jersey, 1985.

AUTHOR BIOGRAPHY

Myo Myint Maw was born in Mongyine Village, Pale Township, Sagaing Division, Myanmar. Her major subject is Information Technology (IT). She received B.E. from Technological University, Monywa in 2005 and M.E. from Mandalay Technological University (MTU), Mandalay, in 2007 in Myanmar, respectively. She is an Assistant Lecturer at Ministry of Science and Technology (MOST) in Myanmar. In 2010, she entered King Mongkut's Institute of Technology Ladkrabang (KMITL), Bangkok, Thailand for Doctoral Degree as a student. Her current interesting researches are wireless propagation and channel modeling, radar communication.